Gold in the historic copper deposits at Flatschach, Styria

Master thesis

Thomas Leitner BSc

Supervisor:

Prof. Dr. Johann G. Raith

Department of Applied Geosciences and Geophysics;

Chair of Resource Mineralogy

Montanuniversitaet Leoben, Austria

Leoben, March 2013

AFFIDAVIT

I declare in lieu of oath, that I wrote this thesis and
performed the associated research myself,
using only literature cited in this volume.

Leoben, 06. March 2013 Leitner Thomas

Zusammenfassung

Gold in den historischen Kupferlagerstätten bei Flatschach, Steiermark

Das Projektgebiet befindet sich nördlich von Knittelfeld im Bereich des Schönbergs und des Tremmelbergs im Bezirk Murtal. In diesem Gebiet wurden gangförmige Kupferlagerstätten, die an NNE-SSW bis NE-SW streichende und steilstehende Gangsysteme in mittelgradig metmorphen Serien des ostalpinen Kristallins gebunden sind, abgebaut. Diese Vererzungen werden derzeit hinsichtlich ihrer Goldführung von Noricum Gold Ltd. neu untersucht.

Im Sommer 2011 erfolgte eine mehrwöchige geologische Aufschlusskartierung im Maßstab 1:10000 und die Lithologien und geologischen Strukturen wurden aufgenommen. Anschließend folgten die petrographische Untersuchung der Hauptlithologien (Polarisationsmikroskopie im Durchlicht) und die erzmikroskopische und mineralchemische Analyse von Erzproben (Auflichtmikroskopie, EMPA Analysen). Dazu wurden 52 Erzanschliffe von historischem Material des Universalmuseums Joanneum und aus der Sammlung von Prof. W. Paar und untergeordnet neu aufgesammeltes Material von Halden untersucht.

Es werden drei paragenetische Phasen ausgewiesen, welche alle goldführend sind.

Phase 1 entspricht dem primären hydrothermalen Vererzungsstadium im dem Gold mit den eisenreichen Sulfiden Chalkopyrit, Arsenopyrit und Pyrit assoziiert ist.

Phase 2 umfasst Cu-reiche und Fe-arme Sulfide wie Digenit, Anilit, „blaubleibenden“ Covellin etc. Als seltenere Cu-Arsenide treten Domeykit und Koutekit auf. Gold der paragenetischen Phasen 1 und 2 zeigt ähnliche Zusammensetzung von fast reinem Gold (95% Au) bis zu Elektrum (~70% Au, ~30% Ag).

Phase 3 ist durch eine sehr starke Oxidation charakterisiert und beinhaltet Hämatit, Cuprit, sowie nicht näher bestimmte Fe- und Cu-Hydroxide und -Karbonate. Gold der Phase 3 weist höhere Ag- und Hg-Gehalte auf.

Die untersuchten Cu-(Au)-Lagerstätten zeigen gewisse Ähnlichkeiten mit orogenen gangförmigen Goldlagerstätten (orogenic lode gold deposits) in metamorphen Gebieten, die allerdings eine nachträgliche untypische Alteration erfahren haben. Die Bildung ungewöhlicher Cu-Arsenide mit Cu-Sulfiden (Phase 2), die Oxidation (Phase 3) und die jeweilige Mobilisation von Gold sind das Ergebnis dieser späteren Alteration, an der sowohl niedrig temperierte hydrothermale als auch supergene Prozesse maßgeblich beteiligt gewesen sein könnten.

Abstract

The project area is located north of Knittelfeld (Bezirk Murtal, Styria), at Schönberg and Tremmelberg. In this historic mining district copper was mined from vein type copper deposits in medium-grade metamorphic rocks of the Austroalpine basement. These deposits are currently re-investigated by Noricum Gold Ltd for their gold contents. During extensive fieldwork in summer 2011 a new geological map (1:10,000 scale) was prepared and the lithologies and geological structures were analysed. In a next step a microscopic study of the main lithologies (thin sections) was made and ore samples (polished sections) were investigated using reflected light microscopy and an EMPA analyser. Most sections are from archive material from Universalmuseum Joanneum and Prof. W. Paar's private collection; a few new samples collected from dumps were included.

Three paragenetic Stages can be distinguished. All three Stages are gold bearing.
Stage 1 includes the primary hydrothermal ore mineralisation of the veins. Gold of this Stage is typically associated with the Fe-rich sulfides chalcopyrite, pyrite and arsenopyrite.
Stage 2 includes Cu-rich Fe-poor sulfides like digenite, anilite, covellite etc. and the rare Cu arsenides domeykite and koutekite. Gold of Stages 1 and 2 has similar chemical composition ranging from pure gold (95% Au) to electrum (~70% Au, ~30% Ag).
Stage 3 is characterized by a strongly oxidised alteration assemblage with hematite, cuprite, and various (not determined in detail) Cu- and Fe-hydroxide and carbonate minerals. Gold of Stage 3 is Ag-rich electrum and has higher Hg contents.
The Cu-(Au) deposits in the Flatschach area show some similarities to orogenic lode gold deposits, however they show an unusual subsequent alteration overprint (e.g. Cu arsenides of Stage 2; oxides of Stage 3). Low temperature hydrothermal as well as supergene processes are possible causes of this later alteration, which both mobilised gold.

Contents

1 Introduction

This MSc project was done in close cooperation of Montanuniversitaet Leoben with Noricum Gold Ltd, a junior stock-exchange noted company, which is involved in gold exploration in the Eastern Alps (http://www.noricumgold.com). At present Noricum Gold Ltd is holding 54 licenses in the Schönberg - Tremmelberg area in the former (historic) Flatschach mining district. The current Master thesis is part of an ongoing exploration program of this company in this area.

The aims of this thesis were:

- Preparation of a geological and structural map of the Schönberg – Tremmelberg area, based on new fieldwork and compilation of available geological data.
- Microscopic investigation of thin sections of rocks and polished sections of ore samples (mostly historic samples); the latter includes samples collected by Prof. W. Paar and W. Jarlowsky / Universalmuseum Joanneum and few self collected samples (Barbara adit dump site).
- Mineral chemical analyses of gold and ore minerals using EMPA techniques.
- To provide basic geological and mineralogical data for planning the next steps of exploration.

The thesis completes three previous unpublished reports to Noricum Gold Ltd:

- Geology of the Schönberg and Tremmelberg area (Leitner, 2011)
- Ore microscopy and microprobe analyses on samples from the Flatschach Cu-(Au) mine - project Schönberg, Austria (Leitner and Raith 2012a)
- Ore microscopy and microprobe analyses of the Jarlowsky (1951) samples - project Schönberg, Austria (Leitner and Raith 2012b)

2 Location of the study area

The project area is located NW of Knittelfeld (WGS 84 – N 14° 45,36' E 47° 14,21') in the province of Styria in Austria (Fig. 1). It is situated in five communities in the political district Murtal (formerly Knittelfeld and Judenburg): Flatschach, Spielberg, Fohnsdorf, Seckau, Gaal. It covers approximately 18 km² (Fig. 2). Schönberg and Tremmelberg are the two main mountains in the study area geographically belonging to the southern Seckauer Tauern. The Fohnsdorfer basin is bordering the study area in the south. The mountains Schönberg and Tremmelberg are separated by the Hämmergraben / Gaalgraben valley. The area is mountainous with elevation between 760m and 1360m above sea level. The whole area is

covered by forest and minor grassland. Hence, most outcrops are found along forest roads. The outcrops are often overgrown by vegetation and weathered. In densely vegetated areas geological information mostly comes from rubblestones.

The accessibility to the historic mining sites in the Flatschach mining district along existing forest roads is good. There exists a dense network of forest roads, which would allow transport of most drilling equipment to drilling sites of possible interest.

Fig. 1: Location of the project area in the province of Styria, Austria (red point)

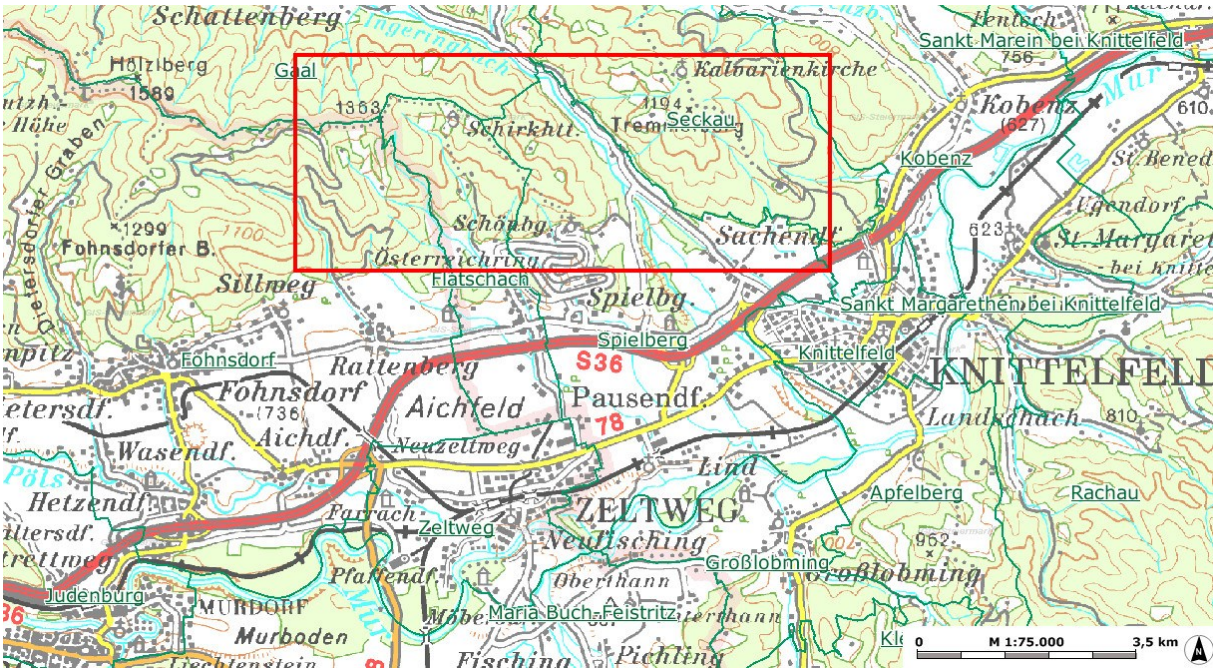

Fig. 2: Location of the project area in the communities Flatschach, Fohnsdorf, Spielberg, Seckau and Gaal; dark green lines show community borders

3 Methods

3.1 Geological mapping

The geological survey included lithological mapping and recording of the structural data and of the former mining activities in the Flatschach mining district.

The area was mapped on a scale 1:10,000 using the topographic map enlarged from the 1:50,000 ÖK map (sheet 161 Knittelfeld; Appendix A: Geological map (map and pdf file)). To be shown on the map the minimum size of a geological object must be >10m. Because most outcrops are smaller, they are only shown as points on the map. In this way 330 outcrops have been recorded. Waypoints were recorded with a Garmin portable GPS and drawn on a topographic map on a scale 1:10,000 (www.gis.steiermark.at).

The 2D geological map was constructed through contouring of the outcrop points and digitized using the Esri® ArcGis software (www.arcgis.com). In addition to the collection of lithological information the structural data were measured in the field using a CLAR – compass (planes: azimuth of dip direction / dip angle; lineations: azimuth of trend / plunge angle).

The names of the lithologies distinguished on the map are based on macroscopic identification of the modal mineralogy in the field and through later microscopic petrographic investigation. The locations of the old mine workings and dumps, as shown on the geological map, are based on own field observations and the old survey map by Boos and Spannraft (1949).

For the preparation of the digital geological map the coordinate system outlined in Table 1 was used.

Table 1: Coordinate system

Projected Coordinate System:	MGI Austria GK Central
Projection:	Transverse Mercator
False easting:	0
False northing:	-5,000,000 m
Central meridian:	13.33333333
Scale factor:	1
Latitude of origin:	0
Linear unit:	Meter
Geographic coordinate system:	GCS_MGI
Datum:	D MGI
Prime meridian:	Greenwich
Angular unit:	Degree

3.2 Samples

For petrographic and mineralogical investigations 51 polished sections and 16 thin sections were investigated.

During fieldwork 43 hand specimens were collected
In total 16 thin sections were investigated for a detailed petrographic description of the lithologies. The samples were collected in the whole mapping area (see Appendix B).

Samples of Prof. W. Paar
In the first project phase a total 22 polished sections were investigated (Leitner and Raith, 2012a). Most of theses samples are from archive material of University of Salzburg and were provided by Prof. W. Paar. The material investigated is mainly from the "Weissenbach" mining district in the Flatschach area. Samples from other mining districts are under-represented.

Samples of W. Jarlowsky / Universalmuseum Joanneum and self collected material
In the second project phase a total 29 polished sections and one polished thin section were investigated. 27 of these samples are from the original material of the PhD thesis by Jarlowsky (1951) and were provided by Universalmuseum Joanneum Graz where this material is archived (so called "Friedrich Archiv"). Three new samples (two polished sections and one thin section) collected during sampling of dumps at Barbara adit in April 2012 were added to this sample set. The total material investigated is from all three mining districts in the Flatschach area; i.e. Adlitzgraben, Weissenbach and Brunngraben. Hence, this sample set extends the set of previously investigated ore samples, which mainly are from the Weissenbach district Leitner & Raith (2012b).

3.3 Microscopy

Polished sections Ø 40mm (sample set Jarlowsky (1951)) and new samples) and Ø 30mm (samples Prof. W. Paar) were used for reflected light microscopy. 52 polished sections were studied in total. Two of them were self collected (T.01 and T.02), and 5 sections were prepared from hand specimens (J.01 - J.05), collected by Jarlowsky in the year 1949. The remaining 45 samples already existed as polished blocks. They were only repolished.

16 new thin sections were prepared (28 x 48 mm, sample thickness ~30 μm). 15 of these were collected at geological outcrops and only one was from the Barbara adit dumpsite.

A Zeiss AXIO Scope.A1 polarization microscope equipped with a Zeiss AXIO Cam ERc 5s digital camera and AxioVision Rel.4.8.2.0 software was used for transmitted and reflected light microscopy.

3.4 EMPA analyses

The electron microprobe analyses were made at the Eugen Stumpfl Electron Microprobe Laboratory of the Universitätszentrum Angewandte Geowissenschaften Steiermark (UZAG) at Montanuniversitaet Leoben. The analyses were made by wavelength dispersive spectrometry (WDS) using a JEOL JXA 8200 Superprobe. The analytical conditions and detection limits (ppm) are summarized in Table 2. Some analyses of small grains (<10 μm) may show effects of the surrounding matrix and give too low totals.

The detection limit (D.L.) is calculated with the formula:

$$D.L. = \frac{z}{m}\sqrt{2 \cdot \frac{I_{bg}}{t_{bg}}}$$

z … Factor for confidence levels; 99% → 2,3, 95 % → 1.6

m … Factor of the calculation in mass% (standard)

I_{bg} ... Intensity of back ground (cps)

t_{bg} … Time of back ground counting (s)

Table 2: Analytical conditions and detection limits (2σ) of EMPA analyses; acceleration voltage 25 kV, probe current 15 nA

	X-ray line	Crystal	Channel/ Spectro-meter	Peak pos. (nm)	Detection limit (ppm)	Peak (s)	Background (s)	Standard
Fe	Kα	LIFH	5	134.728	80	15	10	ChpNWM
Cu	Kα	LIFH	5	107.094	110	15	10	CuS_N20
Ag	Lα	PETH	4	132.862	180	20	10	AgBiSe2
Au	Lα	LIFH	5	88.371	~800	20	5	AuAgTecabri16
Sb	Lα	PETJ	3	110.032	1680	15	10	PdSbcabri29720K
Hg	Mα	PETJ	3	180.859	~1900	15	5	Pd3HgTe3cabri
Pb	Mα	PETJ	2	169.095	1690	15	5	PbSCZ25KvLB
Bi	Mα	PETH	4	163.870	1780	15	5	AgBiSe2
S	Kα	LIFH	3	172.123	110	15	5	42spiZnS
As	Lα	TAP	1	105.156	500	20	10	19Skutt

3.5 Raman spectroscopy

The Raman spectra were measured with an ISA JobinYvon LABRAM confocal Raman spectrometer, using a frequency-doubled 120 mW Nd-YAG laser with an excitation wavelength of 532.2 nm. Silicon and polyethylene were used for calibration. The spectra were collected between 180 and 2000 cm^{-1} with a resolution of approximately ± 2cm^{-1}. The

measured spectra were compared with spectra reported in the RRUFF database (www.rruff.info) for interpretation and phase identification.

4 Geology

4.1 Geological overview

The Alps are one of the best studied orogens in the world. They formed due to collision of the European with the African plate. They can be subdivided into the Western, Southern and Eastern Alps. The latter two largely consist of Austroalpine tectonic units that were thrust on Penninic units plus the European continental margin, during the Alpine orogeny (Fig. 3).

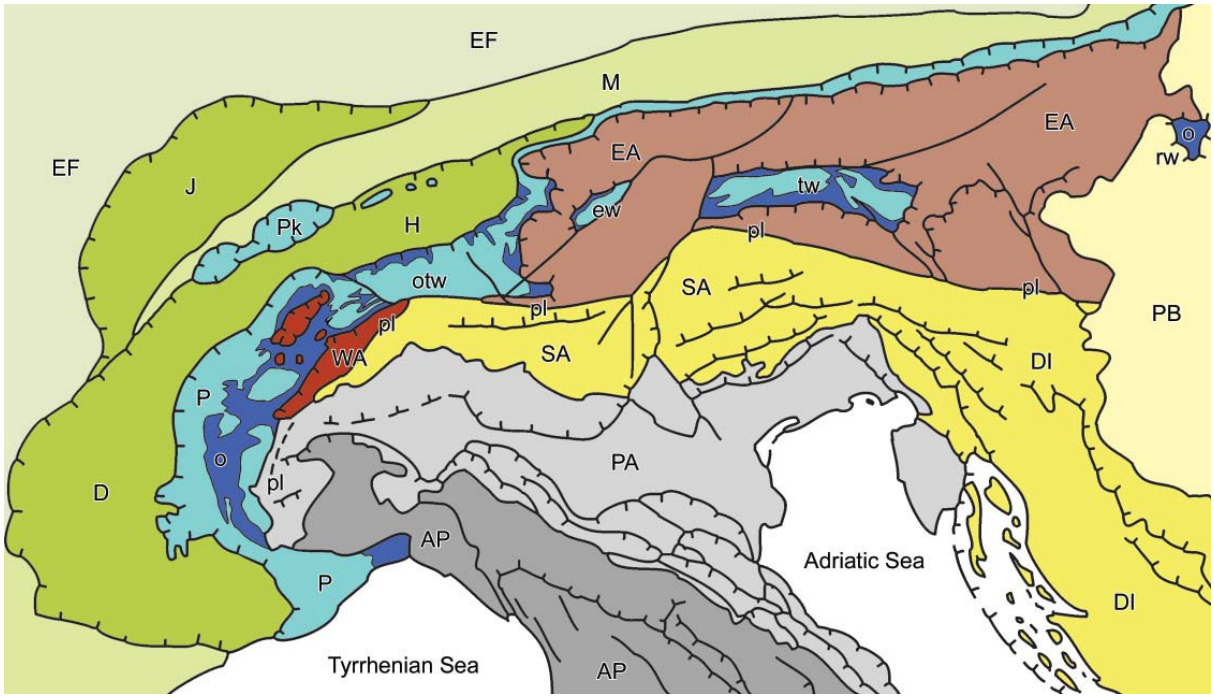

Fig. 3: Geological and tectonic overview of the alps (Dal Piaz et al., 2003); (1) Europe-vergent collisional belt: i) Western (WA) and Eastern (EA) Austroalpine; ii) Penninic domain: continental and ophiolitic (o) nappes in western Alpine arc (P) and tectonic windows (otw: Ossola-Ticino, ew: Engadine, tw: Tauern, rw: Rechnitz); Prealpine klippen (Pk); iii) Helvetic-Dauphinois (H-D) domain; iv) Molasse foredeep (M); v) Jura belt (J). (2) Southern Alps (SA), bounded to the north by the Periadriatic lineament (pl). Pannonian basin (PB), European (EF) and Po Valley Adriatic (PA) forelands, Dinaric (DI) and Apenninic (AP) thrust-and-fold belts.

The Eastern Alps can be subdivided in to several main tectonic units (Schmid et al., 2004): Austroalpine nappes, Penninic and Sub-Penninic nappes, Northern Alpine foreland and Helvetic nappes.

The Austroalpine is further subdivided into (Fig. 4):

1. Northern Calcareous Alps and Greywacke Zone (Upper Austroalpine).

2. Upper Austroalpine basement nappes consisting of:

   Mesozoic cover, Drauzug – Gurktal nappe system, Ötztal – Bundschuh nappe system, Koralm – Wölz nappe system and Silvretta – Seckau nappe system.
3. Lower Austroalpine nappes.

Following this classification the study area is located in the Silvretta – Seckau nappe system (Bösenstein-Pletzen-nappe and Gaaler Schuppenzone) and the Koralm – Wölz nappe system (Wölz-Complex). The Neogene pull-apart Fohnsdorf basin and the correlated strike slip fault system are the youngest geological units / structures.

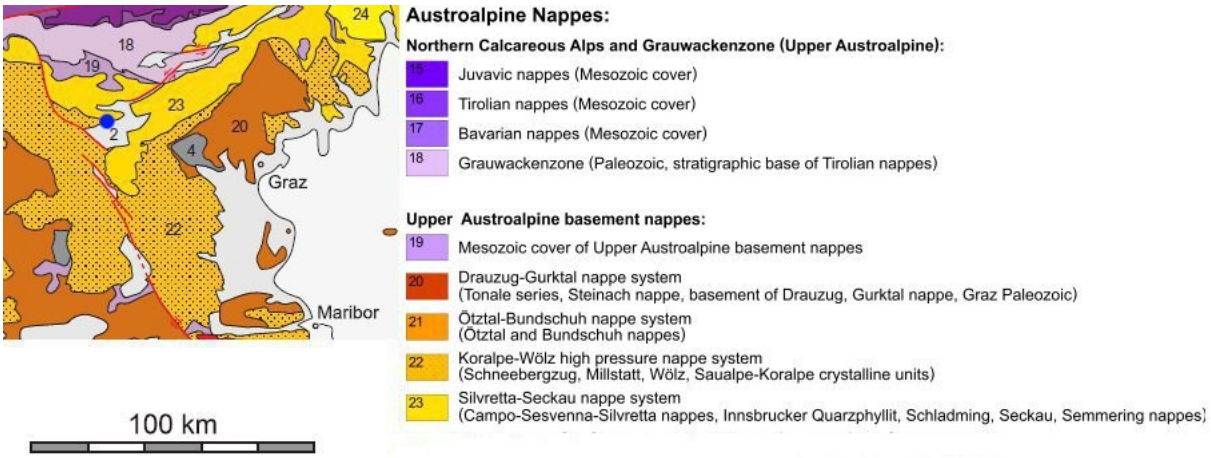

Fig. 4: Tectonic map of eastern part of the Eastern Alps (after Schmidt et al. 2004). Blue point shows location of project area. 2 … (light gray) shows Fohnsdorf basin; major geological faults are shown in red.

4.2 Austroalpine basement

4.2.1 Silvretta-Seckau nappe system (SSNS)

The following summary is based on Schuster (2011a). For the original references the reader is referred to this paper.

The Silvretta-Seckau nappe system is the deepest Upper Austroalpine tectonic unit and overlay the Lower Austroalpine tectonic unit. The nappes of this system are composed of metamorphic rocks (up to few km thick) which are covered by post-Variscan sediments. The dominant metamorphic rocks of this nappe system are prevalent biotite-plagioclase gneisses (sometimes hornblende bearing and migmatitic). Amphibolites occur in few sections of the nappe system in larger connected areas. They are associated with metagabbro and ±serpentinized ultramafic rocks. Acid to intermediate plutonitic rocks occur as metagranites

to metagranodiorites, locally developed as augen gneisses (Becker, 1979; Neubauer, 1988). In the project area, the Silvretta-Seckau nappe system is represented by the Bösenstein-Pletzen nappe and the Gaaler Schuppenzone.

Bösenstein-Pletzen nappe

This is the deepest nappe in the SSNS and is composed of the Seckau complex and the Ranach complex (not exposed in the project area). Both complexes are connected by a transgressive contact. The nappe is cut by the Miocene Palten fault. Rb-Sr-dating of muscovite gave a Variscan age of about 330 Ma. In contrast the Rb-Sr age of biotite is Eoalpine, yielding about 75 Ma. A K-Ar age of 105±4 Ma is interpreted as nearly totally reset Variscan metamorphic age; resetting is related to Eoalpine metamorphic overprint of these pre-Alpine crystalline rocks. This indicates Eoalpine temperatures between 350°C and 500°C (Scharbert, 1981)

Seckau complex

The Seckau complex is composed of various orthogneisses, minor paragneisses, hornblende gneisses and amphibolites. The paragneisses are mostly migmatitic biotite-plagioclase gneisses and minor chlorite-epidote gneisses, hornblende gneisses and amphibolites. The orthogneisses show sharp contacts to the surrounding rocks. The majority of this orthogneisses derived from I-type granodiorites and tonalites with calc-alkaline signature (Schermaier et al., 1997). In addition granitic intrusions with A-type affinity as well as leucocratic granite gneisses and augen gneisses with S-type are known. Two Rb-Sr-whole rock isochrons ages yielding 354±16 and 432±16 Ma respectively were interpreted as emplacement ages. These ages indicates that the protholiths formed during the Caledonian orogeny or even in Early Variscan times.

Gaaler Schuppenzone

The Gaaler Schuppenzone is the continuation of the Speik complex towards NW. It is a zone where rocks of the Speik complex are tectonically intermixed with rocks of the deeper series and relicts of the Permo-Triassic cover (Rannach complex). The latter is exposed to the east of the study area and indicates an Eoalpine age of the tectonics. Metamorphic conditions of the Eoalpine metamorphism of the Rannach Formation were estimates at 530-550°C, 0.8 - 0.9GPa (Faryad et al., 2002). In the Hochgrössen area eclogites of pre - Alpine age are associated with a lager ultramafic body within the Speik complex. P-T conditions of high-P metamorphism are 700°C, 1.8-2.2 GPa and an Ar-Ar ages of the high - P amphiboles yielded an age of ~400 Ma (Faryad et al., 2002).

Speik complex

The Speik complex is mainly composed of amphibolites, serpentinites and ultramafic rocks. The ultramafic rocks are primarily found toward the basis of the complex below the amphibolite dominated part. In the hanging wall of the amphibolites marbles, carbonate-silicate rocks and micaschists become more common. The bulk of the amphibolites occur as banded amphibolite characterized by the alternation of light plagioclase and quartz-rich and dark amphibole-rich layers. Garnet-bearing and feldspar-poor amphibolite varieties are also known. The whole complex is interpreted as a pre-Silurian back arc basin- ophiolite Neubauer et al (1989). Melcher et al. (2002) propose ophiolite formation in a supra subduction regime in the Late Proterozoic (~750 Ma). The Rb-Sr whole rock errorchron age of 331±25 Ma for an augengneiss (Frank et al., 1981), is related to the Variscan events.

4.2.2 Koralm-Wölz nappe system (KWNS)

The following summary is based on Schuster (2011b). For the original references the reader is referred to this paper.

The Koralm-Wölz nappe system is tectonically overlaying the Silvretta-Seckau nappe system. It consists of different metamorphic units, which are tectonically separated nappes. All units record the same Eoalpine deformation and metamorphic history. The metamorphic gradient of the units increases from the northern (greenschist facies) to the southern central units (eclogite facies) and decreases from the basal central units to the hanging wall (too greenschist facies). The rocks record polymetamorphic regional metamorphism. In addition to Eoalpine medium to high-pressure Barrovian metamorphism some units preserve evidence of Permian low-pressure metamorphism. A Permo-Mesozoic cover is missing in the KWNS.

The dominant lithologies are metapelites, which occur as pyhillites, garnet-micaschists or alumosilicate-bearing gneisses. In some units marbles, amphibolites and quartzites are intercalated. Metagranitoids and metapegmatites are widespread. In the project area, the KWNS is represented by metapelites of the Wölz complex in the southernmost field area (near Rattenberg and Flatschach).

Wölz Complex

The Wölz Complex mainly consists of garnet-micaschists with intercalations of marbles, amphibolites and quartzites. Pegmatite gneisses occur in few areas. Other felsic metamorphic rocks are missing. The light colored garnet-micaschists contain white mica, quartz and minor albite, chlorite as well as biotite. Quartz mobilisates are found in form of folded layers or irregular aggregates. The rocks show evidence for polyphase deformation. Several varieties can be distinguished from north to south. Micaschists with no or only few

garnets (<3mm) are found in the north. The frequency of occurrence and size of the garnet porphyroclasts increases towards south. The mostly euhedral garnet crystals can reach sizes more than 1 cm, in some areas up to 5 cm. Staurolite and kyanite occur as other metamorphic index minerals.

Marbles (both calcite and dolomite marble) in the Wölz complex occur as lenses with a maximum thickness of 100m. Their texture is fine-grained with mostly bright gray to yellowish colors, in few cases they are gray banded. Amphibolites and hornblende bearing micaschists also occur in banded layers.

The oldest garnet generation in metapelites of the Wölz Complex formed during the low-P regional metamorphic event in the Permian (~270 Ma) (Schuster et al., 2001). The P-T conditions of this event are 0.4 GPa and 550°C (Bestel et al., 2009). The garnet rims and the smaller garnets in the northern micaschists crystallized in the Upper Cretaceous (~90 Ma) (Schuster et al., 2001) under P-T conditions of 0.75 GPa and 560°C (Bestel et al., 2009). The K-Ar muscovite ages are between 90 and 86 Ma and the Rb-Sr biotite ages are up to 80 Ma. All these age data confirm that the dominant metamorphic overprint under amphibolite facies conditions and accompanying deformation is of Eoalpine age. The exhumation of the Niederen Tauern can be dated with apatite fission-tracks between 20 and 14 Ma.

4.2.3 Older classifications

Accoding to the classification of Tollmann (1977) the Austroalpine tectonic units in the Eastern Alps are subdivided into the Lower, Middle and Upper Austroalpine. Following this scheme the study area is positioned in the Middle Austroalpine Unit.

The following tectono-stratigraphic classification of the Middle Austroalpine crystalline basement units was proposed by Flügel and Neubauer (1984). They distinguished (from bottom to top): the basal Gneiss complex, the Volcanogenic complex, the Speik complex (a sequence of various metabasites, meta-ultrabasites, gneisses and micaschists), the Micaschist complex and the Marble complex (Fig. 5). The mapped lithologies in the study area are best comparable with those of the Volcanogenic and Speik complexes for which a late Proterozoic to Early Paleozoic age is assumed. These complexes are polymetamorphic. The dominant regional metamorphism is Early Cretaceous (~90 Ma) and reached amphibolite facies conditions.

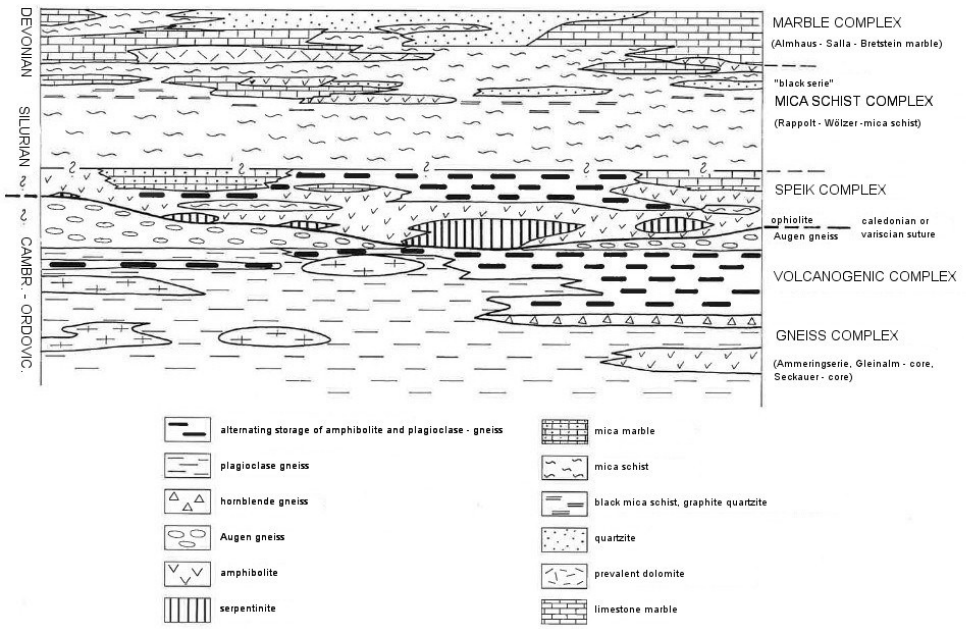

Fig. 5 Tectono-stratigraphic and lithological classification of the metamorphic complexes in the Austroalpine basement (modified from (Flügel and Neubauer, 1984)

4.3 The Neogene Fohnsdorf-Seckau basin

The following summary is based on Strauss et al. (2001). For the original references the reader is referred to this paper.

The Neogene Fohnsdorf basin comprises an area of about 120km² and is filled with Tertiary sediments of maximum 2000m thickness. It formed in the Miocene as result of orogen-parallel extension and lateral extrusion of central parts of the Eastern Alps to the east. The basin developed between major sinistral and dextral wrench faults and it is one of several en-echelon basins along the Mur-Mürz fault (MMF). It is located at the junction of the sinistral ENE-trending MMF and the Pöls-Lavanttal Fault (PLF), a dextral NW-trending fault system. The Neogene sediments are widely coverd by Quaternary deposits.

Three main lithostratigraphic units can be distinguished in the Neogene (Fig. 6): the lowermost Fohnsdorf Formation (breccias, sandstones and a coal seam at the top); the middle Ingering Formation (lacustrine-deltaic deposits) and the unconformably overlaying Apfelberg Formation (conglomerates including boulder beds). An age of Late Karpatian to Early Badenian is assumed for the Fohnsdorf and Ingering Formation; Middle to Late Badenian age is supposed for the Apfelberg Formation.

Four regional tectonic phases are distinguished in this area. In pre- Miocene time a NW-SE trending strike-slip fault was formed (e.g., the Ingering fault, IG). Similar brittle structures of Late Eocene to Oligocene age are known from the Northern Calcareous Alps. The other three phases are related to Miocene basin evolution. The first phase is the pull-apart phase

related to sinistral strike-slip faulting. The second phase represents subsequent fault reactivation and half-graben formation. The third phase is a post-sedimentary compressional event.

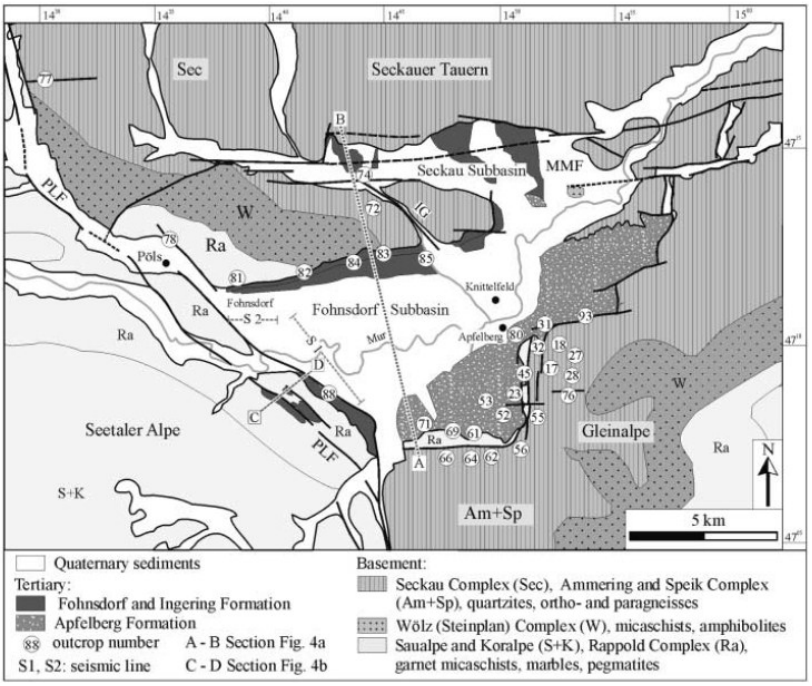

Fig. 6: Geological map of Fohnsdorf-Seckau basin; PLF Pöls-Lavanttal fault system, MMF … Mur-Murz fault system, IG … Ingering fault (from Strauss et al.(2001)

5 Historic mining and previous exploration

5.1 Historic mining activities

The following timeline is mainly based on Jarlowsky (1951) and includes the report by Rücker (1906)

Time line of historic mining activities

15th century: Mining activities at the western slope of Tremmelberg. Today no signs of former mining activities are detectable.

1670 to 1680 End of mining at Tremmelberg as a consequence the of counter-reformation and exodus of the protestant miners.

1716 Restart of mining in the Weissenbach mining district by the monks of Seckau abbey, especially by provost Franz Poiz.

1730 Start of mining in the Adlitz mining district. In 1747 there existed two adits but with low grade ore only.

1741 Beginning problems with mine water managment and death of the mine manager provost F. Poiz. During 1716 and 1741, 3939.63 metric tons (mt) of copper ore were mined and smelted to 290.736 mt of copper. This gives a calculated copper grade of 7.38 mass% for the mined ore.

1746 Finishing of first mining map. It shows 32 adits in total.

1747 Finishing the 900m long Fortuna Unterbau adit after 10 years of construction. The Urbani Unterbau adit in the Adlitz mining district reached a length of 223m without any sign of profitable ore. For the following two decades no records of exist mining activities.

1769 to 1782 In these years 5058 "wr. Zentner[1]" (~283.25 mt) of ore were mined with a grade of 4.94 mass% copper.

1789 End of mining activities.

1864 Reopening of the mines at the mining districts Brunngraben, Weissenbach and Adlitz under the supervision of Anton Nappey and the Vienna merchant Ludwig Kuschel. Mining data from this time are not known but the mining ended shortly after the reopening.

1906 - 1907 The owner Ludwig Apfelbeck reopened the Urbani - Unterbau adit and extended it for another 53m without success. From this period (Rücker, 1906) compiled a report about the metal grades based on an assay of 22 samples. The reported average metal contents are listed in Table 3. In 1907 all mining stopped in the districts.

Table 3: Reported contents of copper and precious metals according to Rücker (1906):

Copper	3.1 mass%
Gold	3.5 ppm
Silver	37.5 ppm
Extractable gold	3.2 ppm

Studies on economic geology and ore mineralogy in 20th century

An estimation of the ore resources (with great inaccuracy) was made by Petroff (1943). He estimated the ore resource of all 3 mining districts with 280,325 mt (estimated ore density of 3,800 kg/m³). The estimates for the individual mining districts are listed in Table 4.

Table 4: Ore resources calculated by Petroff (1943)

Mining district	Ore resource (mt)
Brunngraben	171,000
Weissenbach	72,929
Adlitzgraben	36,500

[1] old weight unit 1 wr. Zentner ~ 56kg

The ore to gangue ratio was given at approximately 1:3 to 1:5 .This old report is also interesting from another perspective. It contains a detailed sketch of a mineralized zone from one of the Brunngraben adits (Fig. 7). It shows a composite ore vein, which is ~70cm thick and composed of alternating veins and gangue.

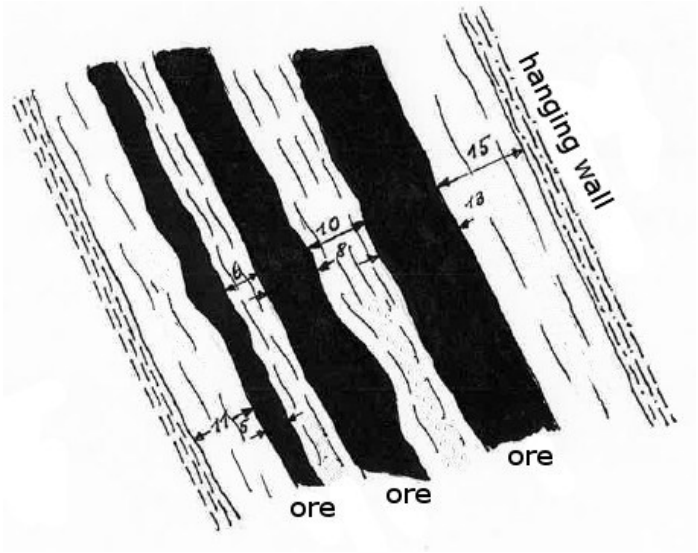

Fig. 7: Ore adit of the western slope of the Brunngraben with a thickness of 68 cm after (Petroff, 1943); three ore bands with a total thickness of 26 cm are to be seen; selvage total thickness is 42 cm.

About 40 years after the closure of the last mine an unpublished theses was made by Jarlowsky (1951). In this thesis Jarlowsky not only reported details about the ore mineralogy of the various ore districts in the Flatschach area but also compiled a lot of field informations. These are especially valuable today because several, now inaccessible, old underground workings were then still accessible.

According Jarlowsky (1951), the mineralization primarily occurs in the paragneisses and amphibolites. Eight ore veins are known in the whole area (Fig. 8). Three of them can be described as main ore veins. All veins have a strike of 30 - 45° NE - SW. The veins show a dip of 70 - 80° to NW in the western area (Brunngraben, Weissenbach). In the Brunngraben mining district, almost all veins change their direction to NNE - SSW. The veins in the Adlitzgraben mining district show a dip of 72 - 76° to SE. The vein thickness is almost ~1m and the veins are partly filled with alteration products of the surrounding rock. The mineralization occurs disseminated, in nests or massive. The gangue minerals are quartz and carbonates. The higher mine levels should be richer in arsenopyrite and pyrite. Chalcopyrite is increasing to the depth.

The mineralized ore veins are crosscutting the penetrative fabrics in the metamorphic rocks but coal-bearing sediments of the Neogene Fohnsdorfer basin cover the ore veins in the area of the Fortuna Unterbau gallery. The mineralization was interpreted as hydrothermal with starting temperatures of 350 to 400°C. The mineralization processes were still active to lower temperature conditions.

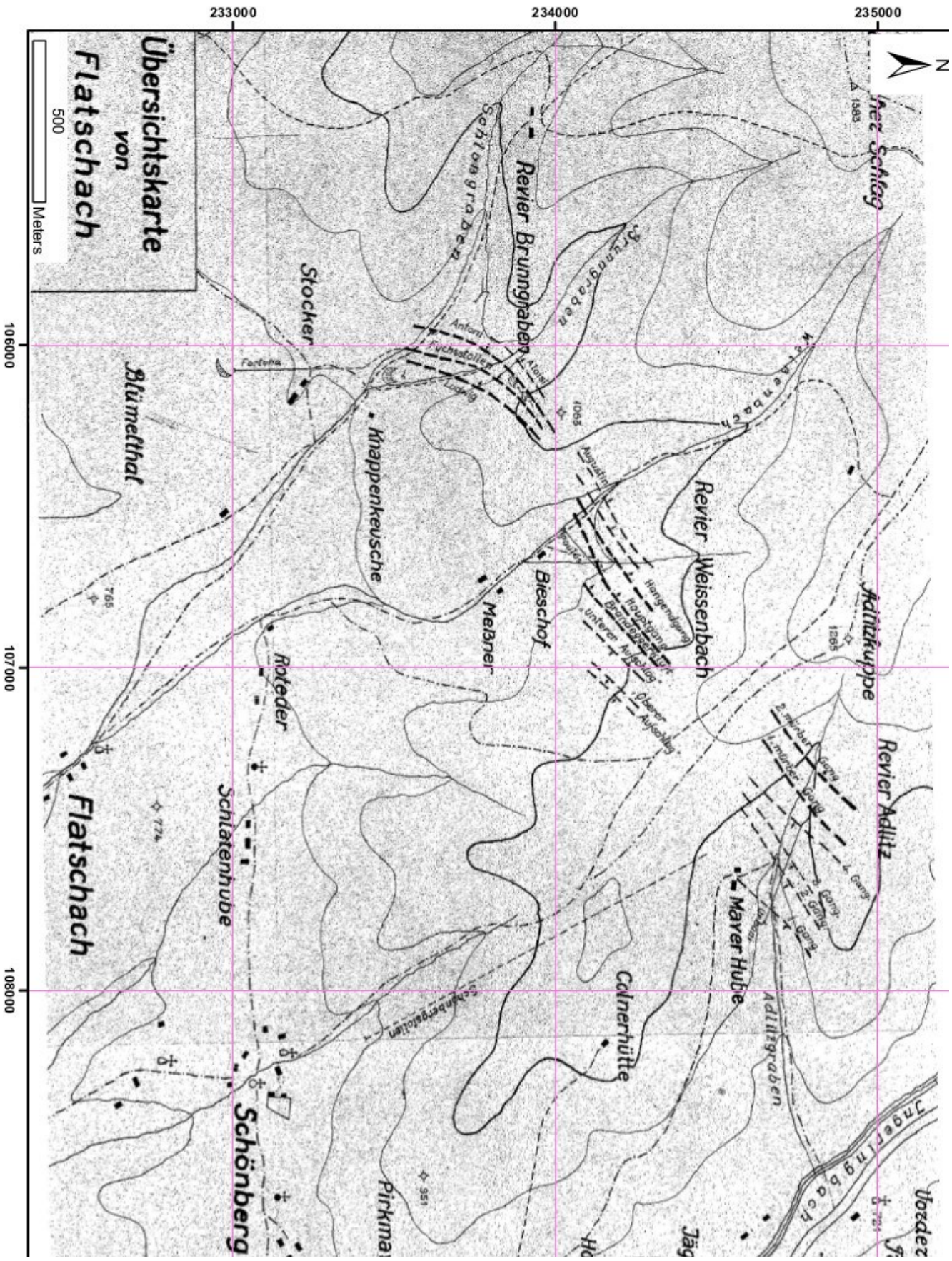

Fig. 8: Overview of the ore veins in the Flatschacher area. The map also show the location of the three main mining historic districts (“Revier”); i.e. Brunngraben, Weissenbach, Adlitzgraben. (after Jarlowsky (1951))

In 1964 O. Friedrich published Jarlowsky's results in the journal "Archiv für Lagerstättenforschung in den Ostalpen". The short summary below is mostly based on descriptions of the ore deposit by these authors (Friedrich, 1964; Jarlowsky, 1951).

In total eight veins are known, almost parallel to each other usually with a strike of 30 to 45 ° NE to SW and a dip of 70 to 80 ° to NW. Individual veins are up to 1m wide. They are mainly filled with fault gouge material derived from the surrounding host rocks; these are often hydrothermally altered and converted into argillaceous material. The ores are associated with the fault gouges and occur as disseminated nests or as massive ore. In addition, quartz and calcite are common gangue minerals. In the footwall and the hanging wall of the veins alteration selvages with clay minerals have been reported.

A more recent publication on the ore mineralogy and paragenesis was published by Paar and Meixner (1979). They studied samples of a ~12cm thick ore vein from the Brandeggerkluft in the Weissenbach mining district. According to this study gold occurs as native gold in association with various Cu - Fe sulfides and arsenides etc. in the primary paragenesis. The major reported minerals are chalcocite, digenite, covellite, domeykite, native bismuth and native copper. Limonite, malachite and azurite are common secondary minerals reported from the supergene zone. Material of this study was reanalyzed in this thesis (i.e. W. Paar sample set).

In 1977 a stream sediment survey was made by Punzengruber et al. (1977). 71 stream sediment samples were taken in the areas of Flatschach, Tremmelberg und Gaal-Ingering (~1 sample per km²). The locations of the sample points are shown in Fig. 9. About 500g of anorganic fine sediment was taken per sampling spot (~5m in size). The fine fraction (-80 mesh; ~0.177 mm) was then analyzed with atomic absorption spectroscopy (AAS) for the elements Cu, Ni, Pb, Zn and Au. The results of these analyses are shown in Fig. 10. The fine fraction in all 3 areas shows elevated gold concentrations between 1-3 ppm Au.

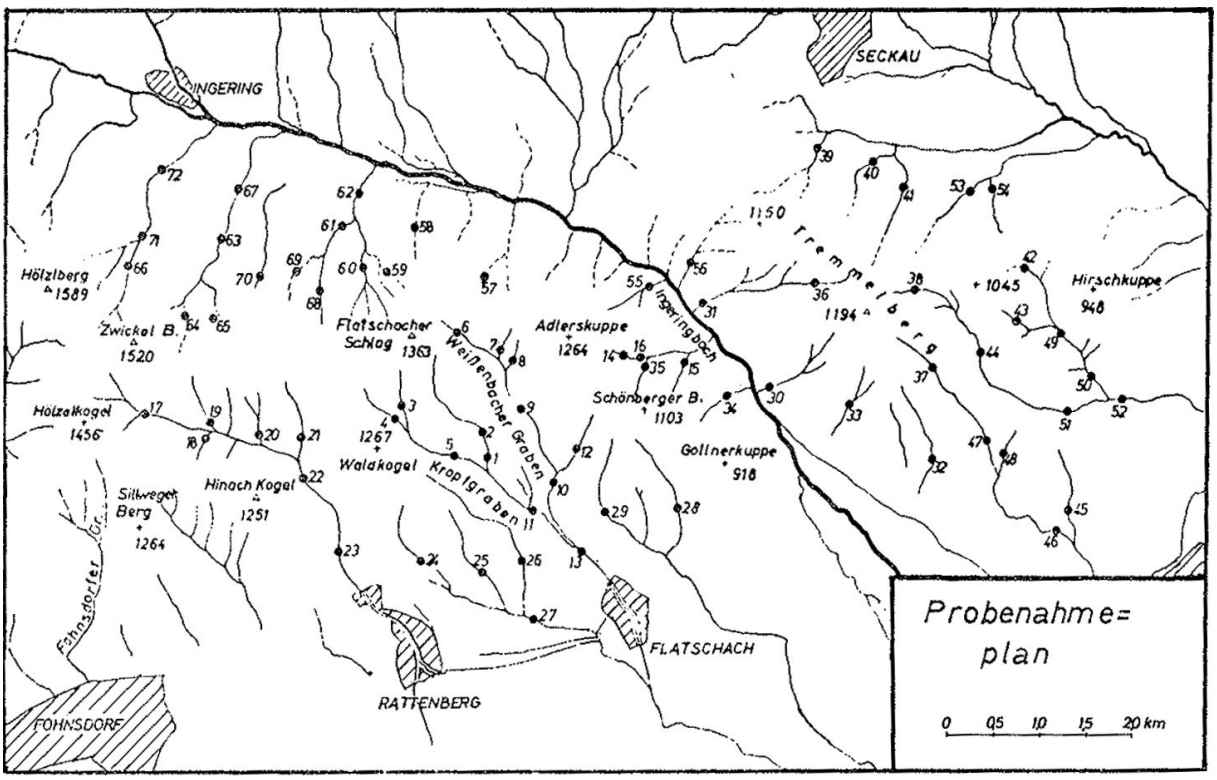

Fig. 9: Location oft the sample points of a stream sediment survey (Punzengruber et al., 1977)

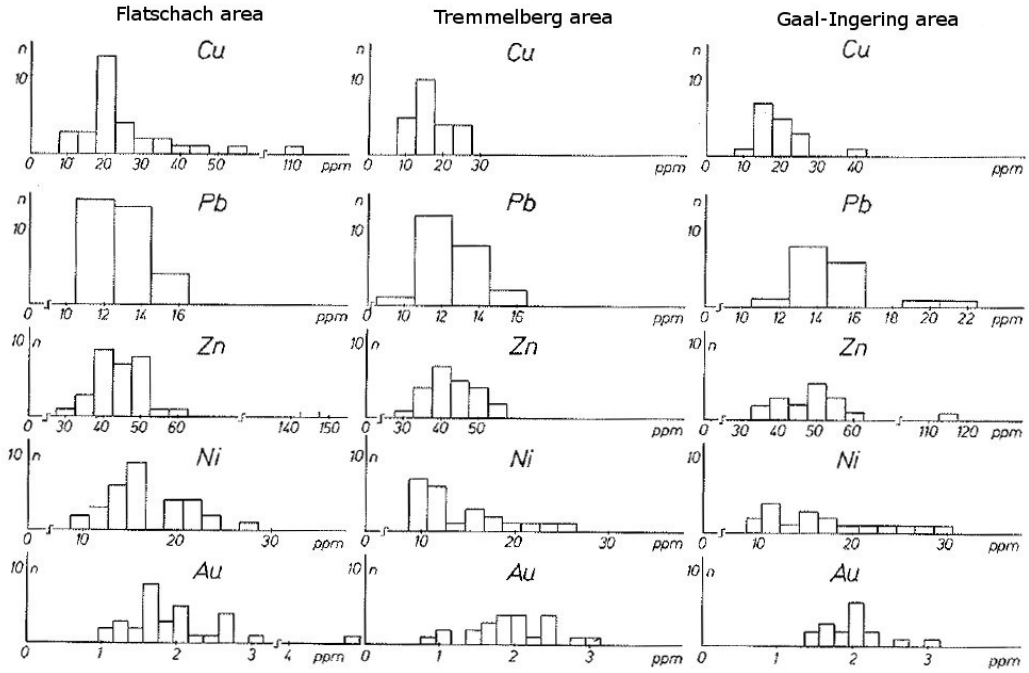

Fig. 10: Results of the analyses of (Punzengruber et al., 1977); Histograms for Cu, Pb, Zn, Ni and Au are shown for the 3 areas studied.

5.2 Exploration by MINEREX in 1985

In 1985 the Austrian exploration company MINERX Mineral - Explorationsgesellschaft m.b.H. did mineral exploration in the area of Flatschach / Schönberg and Tremmelberg (Göd, 1985). Below, the main results of these exploration campaign are summarized.

- Stream sediment analyses

130 heavy mineral concentrates, concentrated from 10 liter stream sediment material, were microscopically investigated. Chemical multi-element analysis was made on the fine fraction (≤0,15mm) of these 130 samples. From 87 additional samples taken during a second systematic sampling campaign only gold was analysed.
Unfortunately the original analytical data are not included in the Göd (1985) MINEREX report[2].
14 out of 130 samples contain free gold. Gold more frequently occurred in samples from the Tremmelberg area. Pyrite is a relatively common heavy mineral, especially in the old mining areas. Chalcopyrite, azurite, malachite, ankerite, barite and scheelite have been found as well and to a lesser extent sphalerite, cinnabar and molybdenite.
The non-ore heavy minerals were garnet, amphiboles, staurolite, sillimanite, epidote and rutile.
The multi - element chemical analyses revealed erratic single high gold values and a strong variation of the gold contents, even in the same river / rivulet.

- Soil geochemistry

Soil samples were taken along two profiles at Tremmelberg (for location of profiles see Appendix C). 246 samples, approximately 2.5 kg per sample, were taken and the fine fraction ≤ 0.18mm was analyzed for gold. The sample to sample grid distance on a profile line was 20m, the distance between the profiles 100m.
54 out of 246 samples were gold bearing with concentrations from 2 to 280 ppb gold. In the soil samples gold seems to be positively correlated with arsenic.

- Whole rock - geochemistry

Whole rock analyses were only made on few samples from Tremmelberg area and included dump samples from Jägerwirt and samples from selected outcrops.
The samples from the dump are pale quartzitic gneiss, dark hornblende-biotite gneiss, amphibolites and massive limonitic quartz. No gold was detected in any of these samples.

[2] When writing up the thesis the author learn that these data are still avaible at GBA Vienna in analogue form.

27 trench samples were taken from 9 selected outcrops. Five of these samples proved to be gold bearing with Au contents from 10 to 180 ppb. The samples also had increased zinc (up to 148 ppm) and copper (up to 161ppm) contents.

6 Geological mapping

6.1 Outcrop situation

The whole mapping area is covered with forest and grassland only few natural exposures could be located in the forest. Most outcrops are found along forest roads. One reason for this situation is the strong vegetation cover. Commonly the vegetation on forest glades is waist-high. On meadows it reaches a length of up to 30 cm. Because the outcrop situation is much better on forest roads they build the main framework of the geological map (Appendix A). The outcrop sizes are between <1m up to 70 meter (e.g. WP 86 - 90; along a new forest road). Most of the outcrops are slightly to strongly weathered.

There are few still accessible underground mining sites in the area, though they were not visited due to safety restrictions. Open tunnels existed in summer 2011 at two locations in the Weissenbach mining district (Table 5).
The best indicators of former mining activities are dumps. Major dumpsites are preserved at the locations listed in (Table 5).

Table 5 Locations of still accessible adits and major dumpsites (coordinate system: MGI Austria GK Central)

Easting (m)	Northing (m)	Mining district
Adits		
106304	234583	Weissenbach
106262	234583	Weissenbach
Dumps		
107305	234608	Adlitzgraben
107324	234557	Adlitzgraben
107292	234528	Adlitzgraben
107376	234675	Adlitzgraben
107469	234672	Adlitzgraben
107730	234623	Adlitzgraben
107782	234641	Adlitzgraben
107578	234675	Adlitzgraben
107296	234702	Adlitzgraben
106106	232944	Brunngraben
106128	233008	Brunngraben
106072	233493	Brunngraben
106132	233802	Brunngraben
106162	233838	Brunngraben
106216	233915	Brunngraben
106217	233855	Brunngraben
106241	233907	Brunngraben
106238	233896	Brunngraben
106219	233890	Brunngraben
106130	233876	Brunngraben
106133	233865	Brunngraben
106523	233358	Brunngraben
106655	234093	Weissenbach
106751	234247	Weissenbach
106752	234218	Weissenbach
106718	234169	Weissenbach

6.2 Lithological description

In this chapter a brief description of the lithologies as deduced from field observations and macroscopic study of hand specimens is given. For location of waypoints the reader is referred to Appendix C.

6.2.1 Garnet micaschist

The color of these rocks varies from silver-gray to light brown reflecting the predominance of white mica and the variable degree of weathering (Fig. 11). These rocks show a well developed main foliation (schistosity). Often a second foliation crosscutting the main foliation at a high angle is recognized. It is correlated with mm to cm scale crenulation and dm to m scale asymmetric folds and it is developed as a crenulation cleavage.
The rocks show a typical porphyroblastic fabric, the garnets forming up to ~1cm large subhedral porphyroblasts (Fig. 12).

Modal composition - major: muscovite, garnet
- minor: quartz, biotite, chlorite, ± plagioclase and potassium feldspar

This rock type is mainly exposed in the southernmost parts of the Flatschach area (Schlossberg and near Roteder). It is interpreted as a member of the tectonically higher Koralm – Wölz nappe system. In the SW of the mapped area a feldspar-bearing variety is exposed at the waypoints 97 to 109.

Fig. 11: Garnet micaschist outcrop at WP 7

Fig. 12: Porphyroplastic fabric of garnet micaschist at WP 10

6.2.2 Phyllonitic micaschist

This rock type has silvery gray to gray-brown color. The foliation is well developed and is crenulated. Besides muscovite biotite is a major mineral. In contrast to the above described micaschists garnet occurs less frequently. This lithology is limited to only two outcrops in the Tremmelberg area. This lithology is a strongly tectonized type of a metapelite or schist.

Modal composition - major: muscovite, biotite
- minor: quartz, garnet, chlorite

6.2.3 Banded amphibolite and Banded biotite gneiss

This unit is characterized by the alternation of amphibolites and biotite gneisses showing typical metamorphic banding / layering on the decimeter to meter scale. Outcrops with a higher content of amphibolite were mapped as banded amphibolite, those with a predominance of biotite as banded biotite gneiss (Fig. 13). However, it has to be noted that gradual transitions between these two lithologies are very common. Rocks of these two units are generally darker in rock exposures and hand specimens compared to the other gneisses. These rocks represent the two major lithologies in the study area.

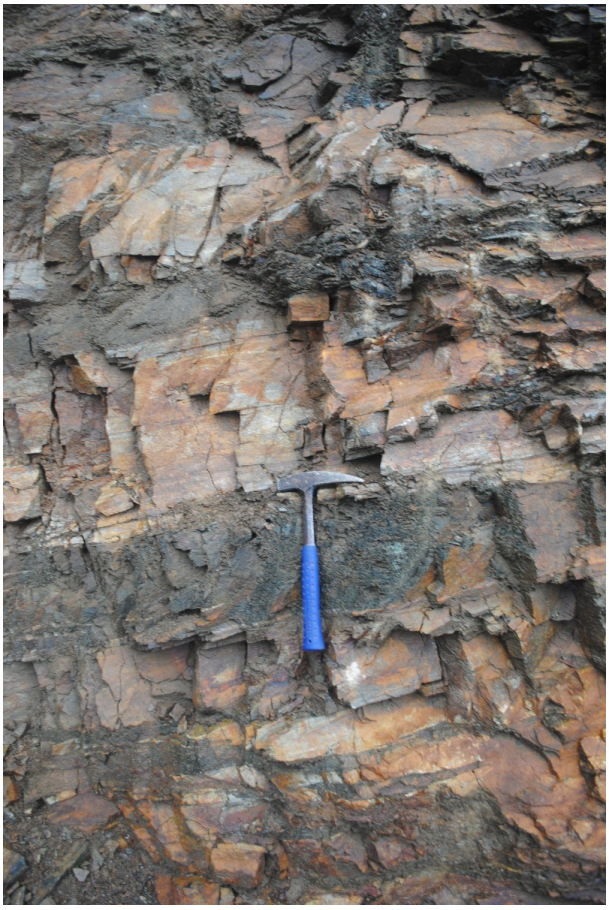

Fig. 13: Alternating sequence of lighter biotite gneiss and darker amphibolite; 1km E of Stadloberhütte WP 88

Amphibolite

These dark rocks show a greenish to black greenish color on fresh surfaces and brownish weathering colors (Fig. 13, Fig. 14). Massive to well foliated types have been observed. Decimeter to meter scale ductile folds are common. These metabasites are fine to medium grained and they show a well developed foliation. Biotite is often aligned parallel to the foliation planes. The amount of feldspar varies. Darker and lighter varieties are therefore distinguished. The darker more massive amphibolites usually form meter-sized lenses.

Modal composition - major: hornblende, feldspar (plagioclase)
- minor: quartz, biotite, ± garnet, ± muscovite

Fig. 14: Outcrop of more massive (brownish) to foliated amphibolite, 1km E of Stadloberhütte WP 90

Biotite gneiss

These rocks are of dark gray color and fine grained. These well foliated rocks show even fracturing, which is controlled by foliation planes and joints. Biotite ± muscovite is often enriched in the foliation planes (Fig. 15). Some gneisses contain hornblende. Intercalations of biotite schist, up to few meters thick, occur as intercalations in the biotite gneiss e.g. ~500m WNW Brandkuppe (waypoint 78).

Modal composition - major: feldspar (plagioclase, potassium feldspar), quartz, biotite
- minor: garnet, ±muscovite

Fig. 15: Hand specimen of biotite gneiss showing mm-scale metamorphic layering and foliation

6.2.4 Orthogneiss

These rocks have a light color, varying from light gray to pale yellowish brown. They have a typical gneiss fabric (Fig. 16). The grain size is medium to coarse grained. Locally, finer grained mylonitic varieties occur. In the Adlitzgraben area there is a gray variety characterized by a higher content of biotite. Rarely, thin greenish amphibolite layers occur as cm thick intercalations in the orthogneiss. In mica-rich layers a crenulation overprints the main foliation which is defined by elongate quartz-feldspar and aligned muscovite aggregates.

Modal composition - major: potassium feldspar, plagioclase, quartz
- minor: muscovite, biotite, tourmaline

Fig. 16: Light orthogneiss with typical gneiss fabric at Gnollerkuppe WP 150

6.2.5 Granite gneiss

These rocks usually have a light brownish-gray to white color and are rather homogenous in composition. The fabric is massive with a weak foliation. These rocks are coarse grained and in contrast to the orthogneiss contain larger up to 10mm feldspar porhyroclasts (potassium feldspar); these show a weak deflection in the foliation direction. The larger feldspar porphyroclasts are interpreted as relict feldspars from an igneous intrusive protolith.
This lithology occurs mainly on the eastern slope of the Schönberger Berg area near to the Adlitzgraben.

Modal composition - major: potassium feldspar, plagioclase, quartz
- minor: muscovite, ± biotite

6.2.6 Serpentinite

Serpentinite occurs in the project only are in few outcrops. Only one outcrop is at most several tens of meters thick. It is located in the area at the Hinter Tremmel farm. Another small (<10m) outcrop of this type is found at waypoint 189 (Appendix A). These meta-altramafic rocks show a dark greenish to greenish-brown color and are well foliated. A microscopic description is shown in chapter 8.1.4. This sections given a large amount of serpentine-group minerals and olivine. Magnetite is also common in grain sizes up to few mm.

Modal composition - major: serpentine-group minerals, olivine and pyroxenes (?)
- minor: chlorite, magnetite

6.2.7 Vein rocks

a. Deformed quartz veins and quartz segregations have been observed in all lithologies. These quartz veins are concordant to the main foliation and often lens shaped. They only reach thicknesses of several cm, are never mineralized and do not show any alteration around them. They are interpreted as early- to syn-metamorphic quartz veins / segregations unrelated to Cu – Au mineralization.

b. Tourmaline-bearing quartz veins were found in the granite gneiss ~400m SE of Schönberger Berg (Fig. 17). These veins are few cm thick and exposed over ~2m. They do not contain any sulfides.

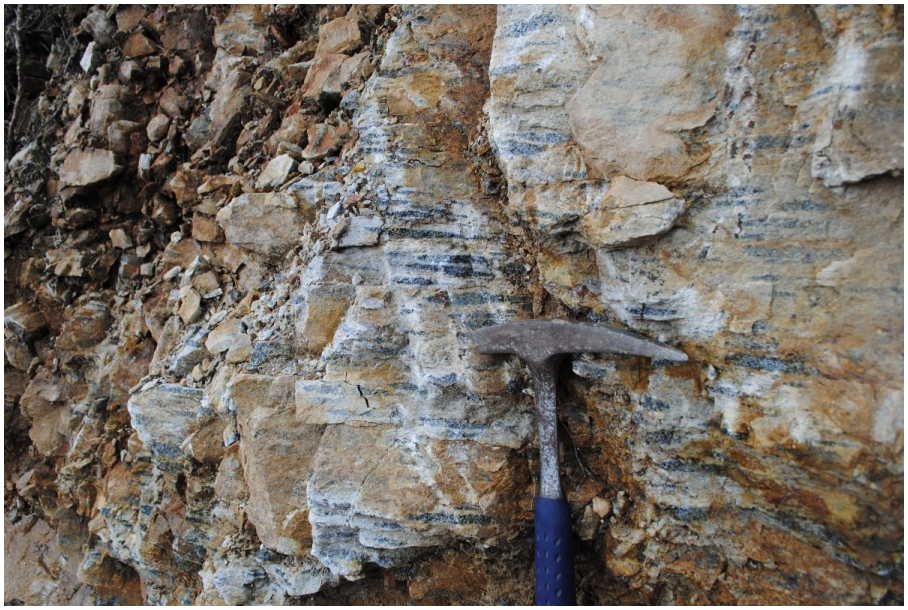

Fig. 17 Tourmaline bearing quartz veins in granite gneiss

c. Fault related cataclastic rocks were found in the westernmost part of the mapping area in the Kropfgraben. There, metabasites with hydrothermal carbonate-chlorite veinlets (~5mm thick) occur in an up to ~1.5m thick fault zone crosscutting the main foliation (Fig. 18). The wall rock around the veinlets shows carbonate-chlorite alteration.

The orientation of this late structure is ~NW-SE. It corresponds to the second minor set of joint planes (Fig. 21). The clear evidence of alteration indicates that this vein formed after the main deformation and peak metamorphism. At present it is unclear if these rocks are related with Cu-Au mineralization.

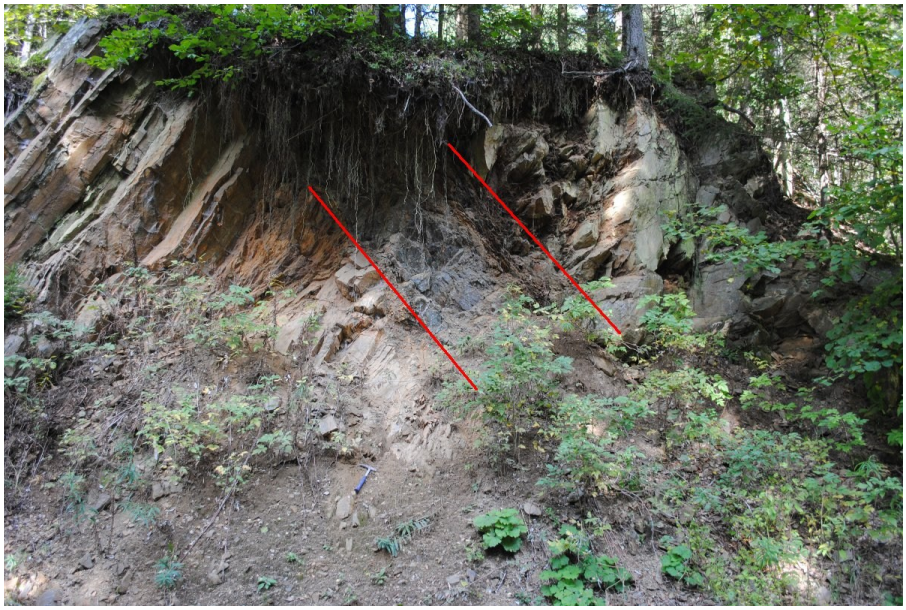

Fig. 18 Hydrothermally altered fault zone in metabasite; fault zone is between the red lines ~1.5m (WP 118)

7 Structural geology

In the following diagrams (Fig. 19 to Fig. 24) a summary of the structural measurements in the field is given (see Appendix D). Fig. 19 shows the poles of the foliation planes in a Schmidt projection. The poles are distributed along a ~N-S trending girdle. The π - circle (098/70), shown as red great circle, gives the axial surface. It was calculated and drawn by the eigenvectors of all foliation planes (using tectonicsFP; http://www.tectonicsfp.com). The π - point (1; 278/20) gives the calculated fold axis point. It fits well with the maximum of measured fold axes and lineations in the mapping area (Fig. 20). The majority of the lineations are oriented WNW – ESE with a predominant flat plunge to WNW.

The joint planes that formed during brittle deformation are compiled in Fig. 21 and Fig. 22. The two major directions are NNW – SSW and WNW – ESE; these sleepy dipping joint planes belong to a conjugate joint system.

The measured fault planes show a quite similar distribution, however, with a larger scatter of the data (Fig. 23 and Fig. 24). The main direction is between NNW to NW - SSW to SW with a dip of 70 to 90. This direction corresponds to the main directions of the ore veins.

A second set of fault planes is oriented NW - SE correlates with the Ingering fault system (see chapter 4.3).

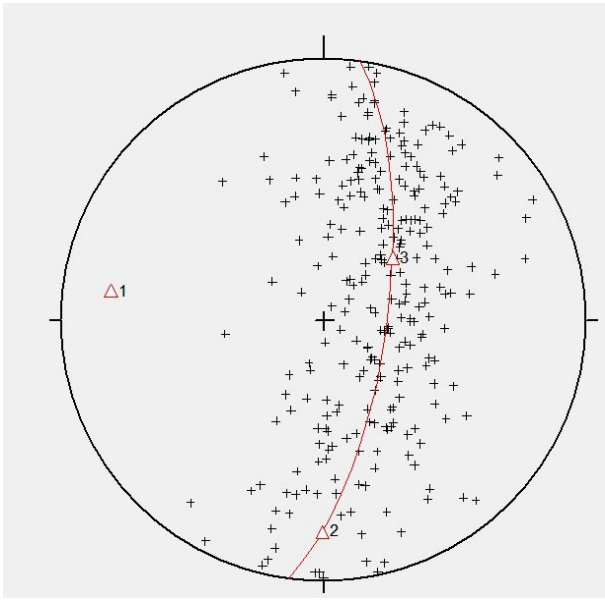

Fig. 19: Pole point plot of the foliation plane poles; the red line shows the constructed π - circle of the fold. Point 1 defines the constructed fold-axis. Points 2 and 3 defined the great circle.

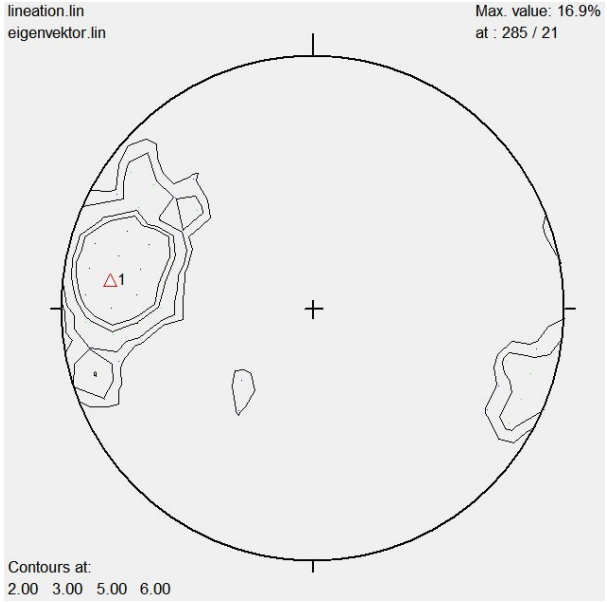

Fig. 20: Contour plot of lineations. The red triangle shows the calculated fold axis of the foliation planes from Fig. 19.

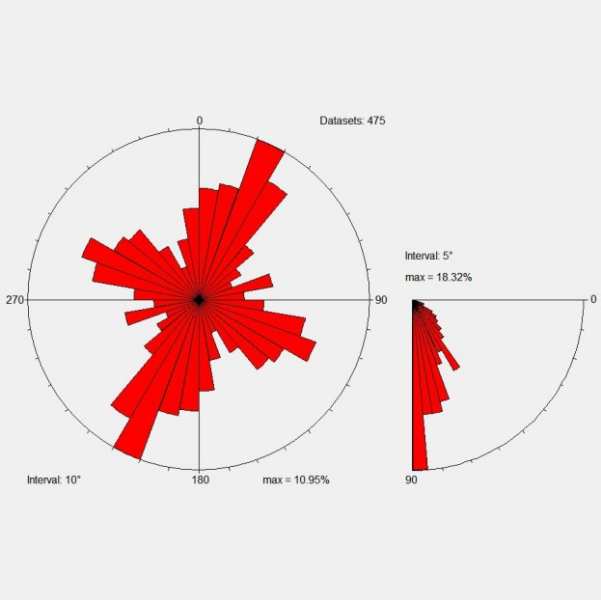

Fig. 21: Rose diagram of the joint planes. Two main directions are visible (NNW – SSW and WNW – ESE)

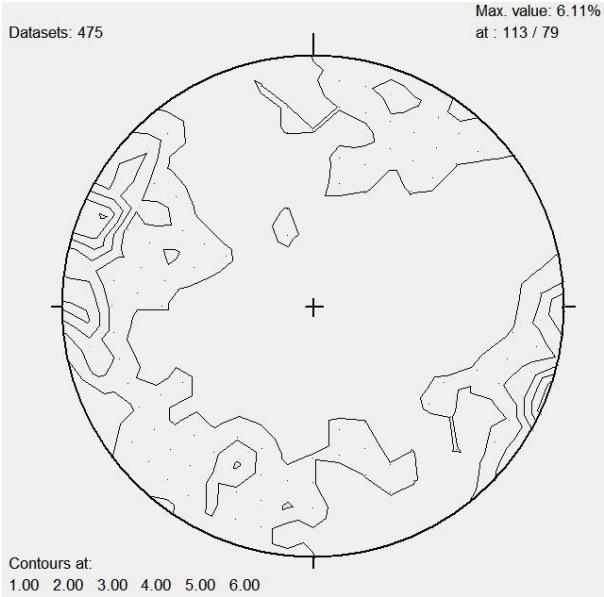

Fig. 22: Contour plot of the joint planes.

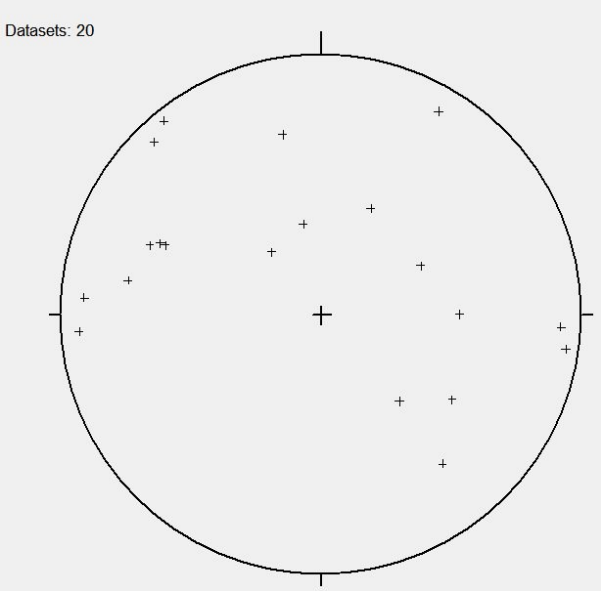

Fig. 24: Pole point plot of the fault planes.

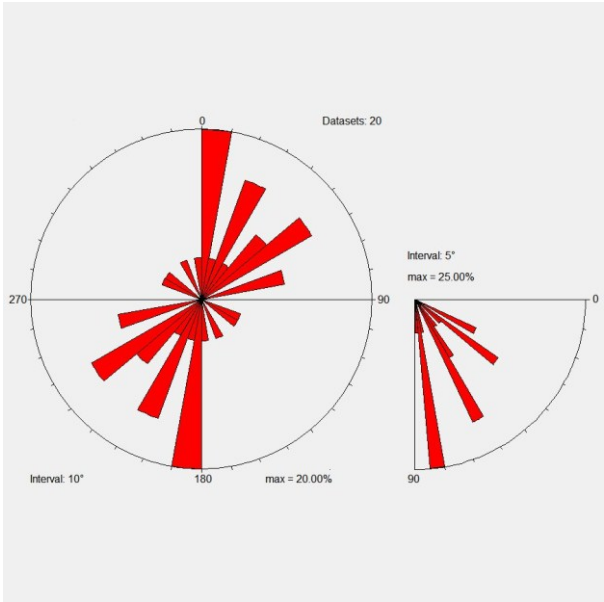

Fig. 23: Rose diagram of the measured fault planes

8 Petrography

8.1 Thin section microscopy

The studied thin sections are from the mapping area at Flatschach. 16 samples were investigated (Table 6). Most of them are non-mineralized host rocks; one sample is an ore-bearing sample from the dump site at Barbara adit.

Locations with waypoints are listed in Table 6 (also see Appendix B). The lithological formations / units in which the samples occur and the correct petrographic names are also given in this table.

Table 6: Waypoints and lithologies of the studied thin sections (see Appendix B)

Waypoint	Sample Nr.	Formation	Petrographic name
9	11Sch10	Garnet micaschist	Garnet-muscovite schist
107	11Sch19	Garnet micaschist	Garnet-chlorite-muscovite schist
22	11Sch05	Banded amphibolite and biotite gneiss	Amphibolite
23	11Sch06	Banded amphibolite and biotite gneiss	Garnet-bearing amphibolite
114	11Sch20	Banded amphibolite and biotite gneiss	Biotite-plagioclase-epidote gneiss, garnet-bearing
118	11Sch22	Banded amphibolite and biotite gneiss	Potassium feldspar-bearing plagioclase amphibolite
45	11Sch08	Banded amphibolite and biotite gneiss	Muscovite-biotite gneiss
80	11Sch15	Banded amphibolite and biotite gneiss	Garnet-bearing biotite-muscovite schist
83	11Sch17	Banded amphibolite and biotite gneiss	Biotite-bearing gneiss
134	11Sch24	Banded amphibolite and biotite gneiss	Magnetite-bearing serpentinite
182	11Sch29	Banded amphibolite and biotite gneiss	Garnet-biotite gneiss
189	11Sch31	Banded amphibolite and biotite gneiss	Epidote-hornblende gneiss
122	11Sch21	Orthogneiss	Muscovite gneiss
142	11Sch26	Orthogneiss	Tourmaline-bearing gneiss
118	11Sch22a	Vein rocks	Altered amphibolite with chlorite-calcite veins
	T.03	Barbara adit, ore sample	Altered host rock, with Cu-mineralization

8.1.1 Garnet micaschist

Sample: 11Sch10

Petrographic name: Garnet-muscovite schist

General remarks: This rock is from the garnet micaschist unit (waypoint 9, Appendix B) in the Schönberg area. The field relations of this outcrop are documented in chapter 6.2.1.

Modal mineralogy:

An overview of the section is shown in Fig. 25. There, it two large garnet porphyroblasts can be seen in a matrix of muscovite and biotite. The biotite rich parts are also rich in opaque phases.

Fig. 25: Overview of thin section 11Sch10

Muscovite, quartz and garnet are the major minerals. Biotite, chlorite, are minor, tourmaline, rutile, magnetite, ilmenite and Fe-hydroxides are accessory phases.
White micas occur as large muscovite crystals and as fine-grained sericite. Muscovite defines the predominant schistosity of the rock. Quartz forms lenses (size ~2 x 6mm) and coronas (mm-wide) around the garnet porphyroblasts (Fig. 26). Quartz usually shows evidence of recrystallization and undulatory extinction.
The euhedral garnet porphyroblasts reach a size up to ~7mm. They show micro-fractures which are often filled with red to brownish Fe-hydroxides. Inclusions of ilmenite and rutile are preserved in the garnets. Biotite occurs mainly in specific layers with Fe-hydroxides, magnetite and ilmenite. It commonly shows beginning chloritization. Some individual flakes of biotite occur in the matrix together with muscovite.

Fabric: This rock shows two foliations. The first fabric (S1) is overprinted by the dominant second crenulation (S2) at an angle of ~30°. Segregation quartz lenses are aligned in the S2 foliation.

Metamorphism and alteration: The metamorphic peak assemblage is garnet + biotite + muscovite + quartz. It is overprinted by a retrograde metamorphism (greenschist facies), shown by the alteration of biotite to chlorite and sericite.

Protolith: The protolith of these rocks may have been pelites with some psammitic material.

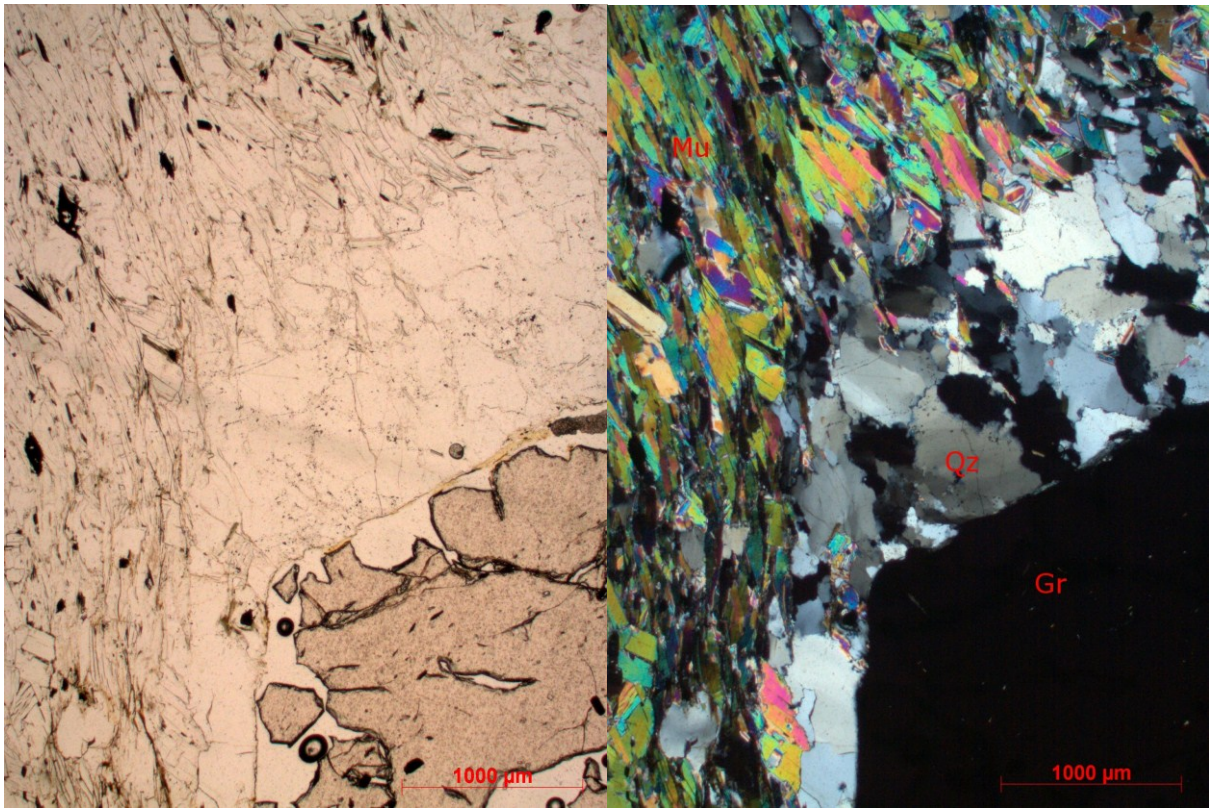

Fig. 26: Rim of larger garnet crystal separated by the muscovite-dominated matrix (well foliated) by a ~1mm thick quartz corona. Opaque phases are magnetite and ilmenite. Sample 11Sch10, left uncrossed- right crossed-nicols

Sample: 11Sch19

Petrographic name: Garnet-chlorite-muscovite schist

General remarks: This rock is from the garnet micaschist unit (waypoint 107, Appendix B) in the Schlossberg area. The field relations of this outcrop are documented in chapter 6.2.1.

Modal mineralogy:

An overview of the section is shown in Fig. 27. There, large garnet crystals and fold quartz segregations can be seen in a matrix of muscovite, chlorite and biotite.

Fig. 27: Overview of the section 11Sch19

In this sample the major minerals are muscovite, quartz, chlorite and garnet. Minor plagioclase and biotite are common. Accessory minerals are rutile, apatite, zircon (in biotite and in the matrix) and opaque phases like magnetite and ilmenite.

Muscovite, predominantly crenulated along the main schistosity and refolded by micro-folds, is the dominant main mineral. Quartz occurs as segregation in coarse-grained lenses, which are deformed and folded. Quartz also crystallized in small layers with muscovite and plagioclase. Garnet forms porphyroblasts, up to ~6 mm in size. The garnet crystals contain sigmoidal inclusion trails of quartz and opaque phases (rutile and ilmenite). Their growth seems to be mono-phase. The garnets are fractured, similar to sample 11Sch10, and the fractures are filled with Fe-hydroxides. Fine-grained plagioclase occurs in layers together with quartz. These layers show a granoblastic fabric with grain sizes of about ~ 0.3 mm. Plagioclase is weakly altered to sericite and shows simple twinning and in few grains a typical cleavage. Biotite shows a brownish to greenish pleochroism. It occurs around the garnet and in the matrix together with muscovite. The greenish color is due to the beginning alteration to chlorite. Small inclusions of zircon are found in the biotite (radioactive halos).

Fabric: The porphyroblastic fabric of this rock is well foliated and folded. A second foliation, like in the sample 11Sch10, is not visible

Metamorphism and alteration: The metamorphic peak assemblage of this section is garnet + biotite + muscovite + quartz + plagioclase. This assemblage is overprinted by a weak

retrograde metamorphism (greenschist facies), shown by the beginning alteration of biotite to chlorite.

Protolith: Similar to the section 11Sch10, the protolith of these rocks may have been a pelite with some psammitic material.

8.1.2 Banded amphibolite and biotite gneiss

Sample: 11Sch05

Petrographic name: Amphibolite

General remarks: This rock is from the banded amphibolite unit (waypoint 22, Appendix B) in the Adlerkuppe area. The field relations of this outcrop are documented in chapter 6.2.3.

Modal mineralogy:

An overview of the section is shown in Fig. 37. There, the foliation defined by the alternation of the green hornblende and white quartz-plagioclase layers can be seen.

Fig. 28: Overview of the section 11Sch05

The main minerals are green hornblende (≥60 vol.%). Quartz is the main mineral; plagioclase and ilmenite are minor minerals. Accessory minerals include clinozoisite, apatite, sericite and the sulfides minerals like pyrite, chalcopyrite and covellite.

Hornblende crystals have a size of up to 2mm and define the well developed foliation. Quartz and plagioclase occur as recrystallized fine-grained aggregates and as large crystals (up to 1mm in size). Plagioclase is usually altered to sericite and shows polysynthetic twins. The quartz crystals show undulatory extinction. The dominant sulfide in the section is pyrite. Chalcopyrite is partly intergrown with pyrite or occurs as single crystals in the matrix or in small cracks, respectively. Few chalcopyrite crystals are altered to covellite.

Fabric: This rock shows a well foliated, nematoblastic fabric.

Metamorphism and alteration: The metamorphic peak assemblage of this section is hornblende + plagioclase + quartz + ilmenite.

Protolith*:* The protolith of this rock may have been a mafic volcanic rock.

Sample 11Sch06

Petrographic name: Garnet-bearing amphibolite

General remarks: This rock is from the banded amphibolite unit (waypoint 23, Appendix B) in the Adlerkuppe area. The field relations of this outcrop are documented in chapter 6.2.3.

Modal mineralogy:

An overview of the section is shown in Fig. 29. Green hornblende-rich micro-areas and white to brownish quartz and plagioclase rich micro-areas can be distinguished. A weak foliation is visible in both domains.

Fig. 29: Overview of thin section 11Sch06

In this sample the major minerals are hornblende, quartz and plagioclase. The minor minerals are garnet, chlorite, clinozoisite and carbonate. Accessory minerals are sericite, biotite, apatite, titanite, rutile and opaque phases. The opaque phases are ilmenite and sulfides (chalcopyrite and pyrrhotite).

Hornblende forms very large, deformed poikiloblastic aggregates pointing to pre-kinematic crystallization. Some hornblende crystals have more bluish colors. Quartz and plagioclase are recrystallized. Plagioclase is strongly altered to sericite. Titanite occurs as flattened wedge-shaped crystals or as corona around ilmenite and rutile. The opaque phases are mainly dominated by ilmenite and rutile. Chalcopyrite is for the most part intergrown with pyrrhotite. Two different micro-areas are distinguished within the section (Fig. 30). The first one is rich in hornblende with lower content of quartz and plagioclase. Opaque phases are mainly associated with this micro-area. The second micro area is richer in quartz / plagioclase and garnet.

Fabric: The fabric of this rock varies with the amount of hornblende. The lighter micro-areas show a granoblastic fabric with porphyroblasts of small garnets. The hornblende rich micro-areas are better foliated and weakly folded.

Metamorphism and alteration: The metamorphic peak assemblage of this section is hornblende + plagioclase + garnet + quartz ± clinozoisite (?) ± calcite. No retrograde alteration is present in this thin section.

Protolith*:* The texture of this rock could reflect primary modal layering of the protolith; i.e. an alternation of mafic and felsic layers. The coarse hornblende could indicate a coarse grained mafic volcanic or even plutonic (gabbroic) protholith.

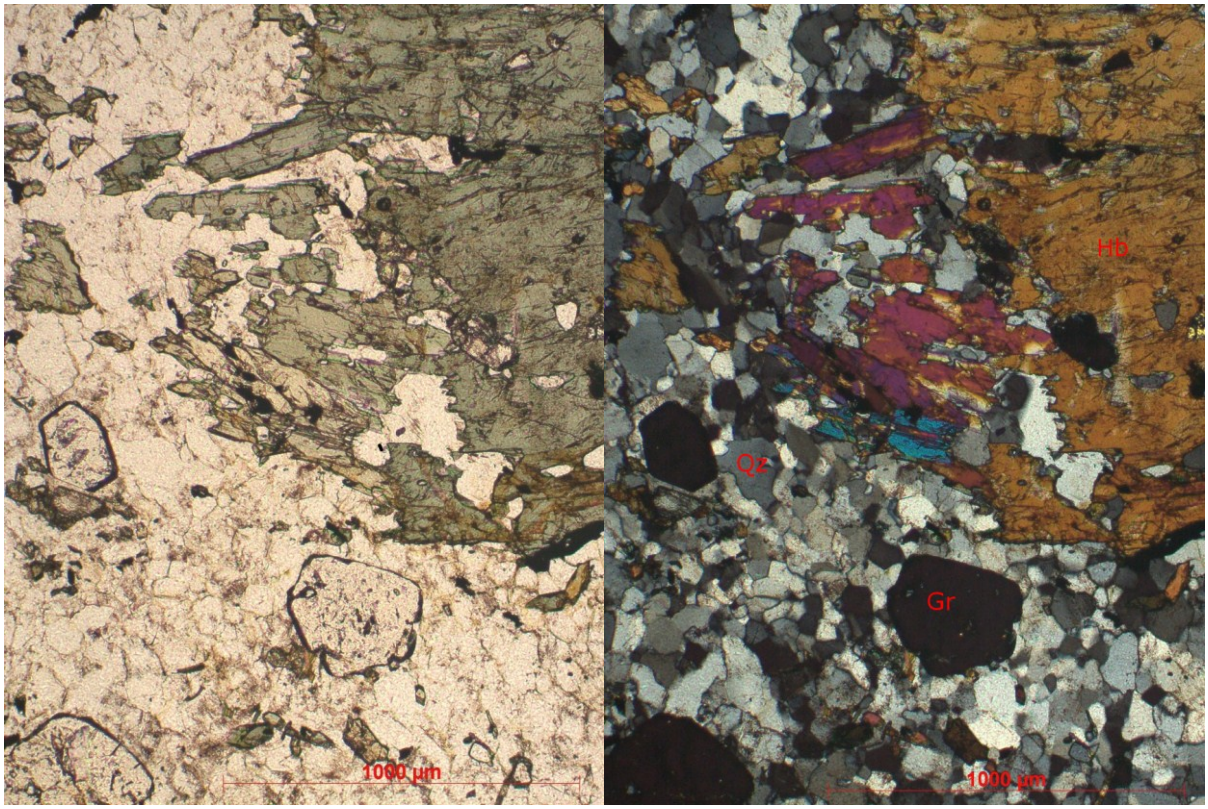

Fig. 30: Contact of the hornblende-rich and quartz/feldspar-rich micro-domains. Garnet mainly occurs in the granoblastic light colored parts. Sample 11Sch06; left uncrossed- right crossed-nicols

Sample: 11Sch20

Petrographic name: Biotite-epidote-plagioclase gneiss, garnet bearing

General remarks*:* This rock is from the banded amphibolite unit (waypoint 114, Appendix B) in the Kropfgraben area. The field relations of this outcrop are documented in chapter 6.2.3. This section represents a gneissic layer in the banded amphibolite unit.

Modal mineralogy:

An overview of the section is shown in Fig. 31. There, the weak foliation and folding of the rock are to be seen. A mm-thick segregated quartz vein crosscuts the section.

Fig. 31: Overview of thin section 11Sch20

Quartz, plagioclase, biotite and chlorite are major minerals in this section. Epidote / clinozoisite, garnet, potassium feldspar and muscovite (sericite) occur as minor minerals. Accessory minerals are rutile, zircon and opaque phases (ilmenite and magnetite).

Quartz occurs in two different modes; i.e. as few large quartz grains in segregations and as fine ±recrystallized aggregates with plagioclase and potassium feldspar (Fig. 32). Plagioclase is present as larger relict grains with a strong alteration and in the fine matrix with quartz. Plagioclase is usually altered to epidote and sericite. Biotite is characterized by brownish to greenish colors, due the variable degree of alteration to chlorite. Chlorite is common in the section and often forms by replacement of biotite. Garnet has a rounded subhedral shape, is locally fractured and partly altered. Epidote / clinozoisite occur throughout the whole section.

Fabric: The fabric of this medium-grained rock is granoblastic with few relicts of plagioclase and potassium feldspar. It is only weakly foliated.

Metamorphism and alteration: The metamorphic peak assemblage of this section is plagioclase + potassium feldspar (?) + epidote + garnet + biotite + muscovite + quartz. It indicates amphibolite facies conditions. The common occurrence of chlorite as a retrograde phase must be related do a low-temperature overprint, what could either have been retrograde regional metamorphism under greenschist facies conditions or hydrothermal alteration.

Protolith: The protolith of these rock was an igneous potassium feldspar and plagioclase-rich volcanic rock of intermediate to felsic composition. The predominance of plagioclase over potassium feldspar could indicate a protholith of rhyodacitic do dacitic composition.

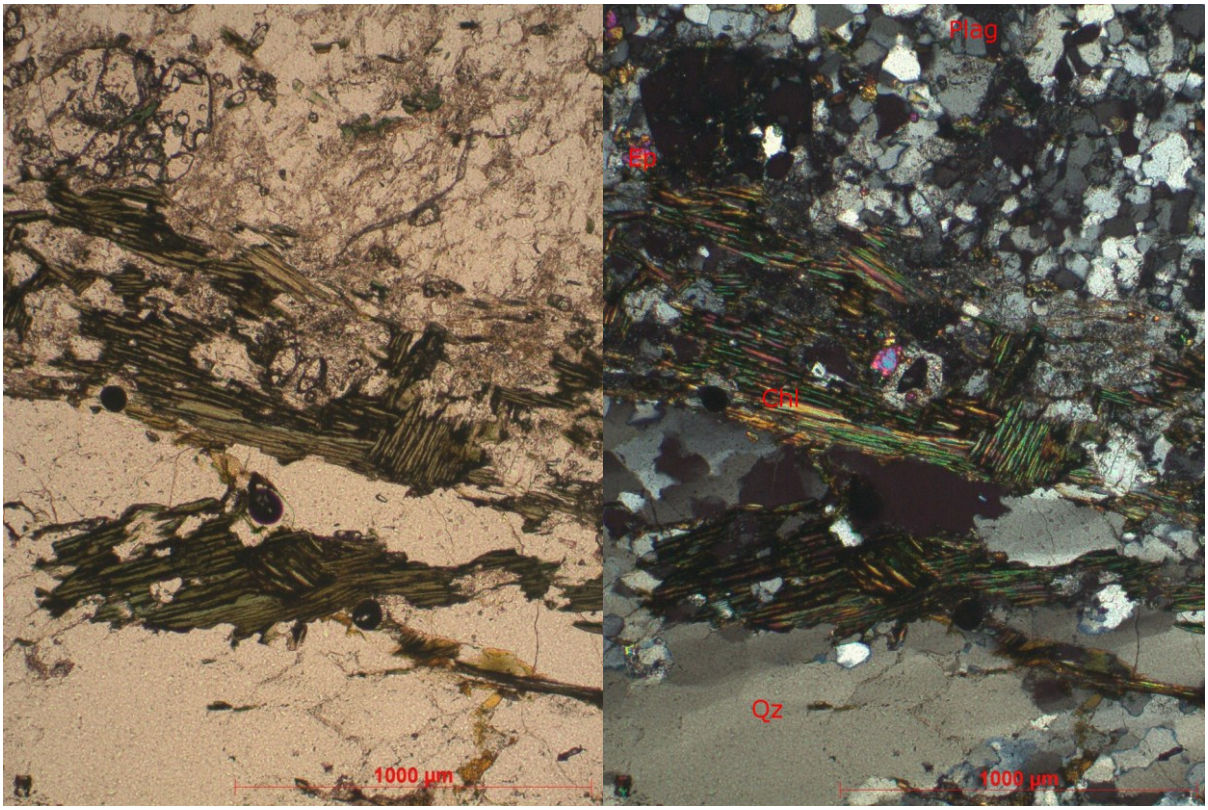

Fig. 32: Large chlorite formed by alteration of biotite, garnet and epidote in a quartz-feldspar matrix. Coarse-grained quartz is seen in the lower part of the photograph. Sample 11Sch20; left uncrossed- right crossed-nicols

Sample: 11Sch22

Petrographic name: Potassium feldspar- bearing amphibolite

General remarks*:* This rock is from the banded amphibolite unit (waypoint 118, Appendix B) in the Kropfgraben area. The field relations of this outcrop are documented in chapter 6.2.3.

Modal mineralogy:

An overview of the section is shown in Fig. 33. There are two distinct types of metamorphic layers / bands in the section (cm scale). Darker layers are rich in hornblende, lighter ones are richer in plagioclase and quartz. A pronounced foliation is visible in both layers.

Fig. 33: Overview of thin section 11Sch22

The major minerals in this section are hornblende, quartz and plagioclase. Biotite, potassium feldspar and titanite are minor phases. The accessory minerals are epidote, chlorite, zircon, Fe-hydroxides and pyrite.

The darker layers are hornblende - plagioclase rich, with the mineral assemblage hornblende, plagioclase titanite, ±biotite, ±pyrite. The hornblende is weakly weathered to Fe-hydroxides along the grain boundaries (Fig. 34). The biotite occurs as porphyroblasts mainly in the darker layers and reaches sizes up to 2 mm. It shows abnormal interference colors. Biotite crystals are not aligned in the major foliation, indicating a post-kinematic growth. Pyrite usually occurs in the hornblende rich layers and shows an alignment in the major schistosity. The grains are commonly fractured and altered to hematite / Fe-hydroxides.

The light layers are dominated by plagioclase, ±potassium feldspar and quartz. Biotite and hornblende are rare in these layers. Potassium feldspar occurs as porphyroclasts in the light layers. It is weakly altered to sericite.

Fabric: The rock shows a nematoblastic to granoblastic texture. The foliation is well developed in the dark hornblende rich parts, but is also visible in the light-colored parts.

Metamorphism and alteration: The peak metamorphic assemblage hornblende + plagioclase + quartz ± biotite ± epidote in the darker layers indicates amphibolite facies conditions.

Protolith: The layered texture of this rock could reflect primary modal layering of the protolith; i.e. an alternation of mafic and felsic layers. Such small scale variation in the mineralogy could be e.g. expected in pyroclastic protholiths.

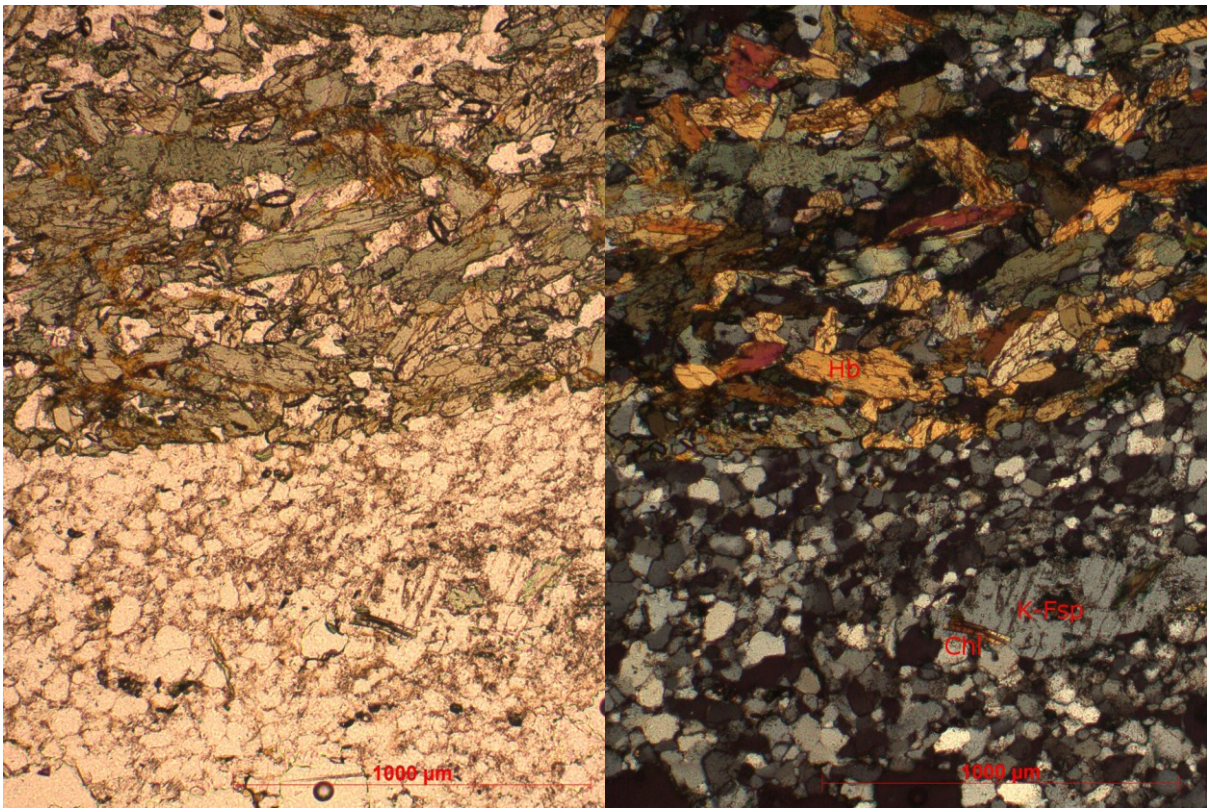

Fig. 34: Hornblende-rich and quartz-feldspar-rich layers with altered potassium feldspar porphyroblasts Sample 11Sch22; left uncrossed- right crossed-nicols

Sample: 11Sch08

Petrographic name: Muscovite-biotite gneiss

General remarks: This rock is from the banded biotite gneiss unit (waypoint 45, Appendix B) in the Flatschach Graben area. The field relations of this outcrop are documented in chapter 6.2.3.

Modal mineralogy:

An overview of the section is shown in Fig. 35. This light-colored rock shows a weak gneiss foliation on the mm-scale.

Fig. 35: Overview of thin section 11Sch08

This section has potassium feldspar, quartz, plagioclase, muscovite and biotite as major minerals. Apatite, rutile, garnet, chlorite, epidote and opaque phases (ilmenite, magnetite and Fe-hydroxides) are minor to accessory phases.

Potassium feldspar occurs in the medium-grained granoblastic matrix together with plagioclase and quartz. Potassium feldspar is also developed as large porphyroclasts up to 5mm in size and shows graphic intergrowths with quartz. Plagioclase occurs mostly in smaller grains; only few larger grains are visible in the section (~1mm, Fig. 36). Both feldspars show alteration to sericite and epidote. Quartz is partly recrystallized to finer grained aggregates. Larger quartz grains show undulatory extinction. Biotite is partly altered to chlorite, indicated by brownish to greenish pleochroism colors. Muscovite and biotite are aligned in the main foliation.

Fabric: The fabric is granoblastic to lepidoblastic depending on the mica to quartz content. The foliation can be described as a continuous schistosity on the mm scale.

Metamorphism and alteration: The peak metamorphic assemblage of this section is potassium feldspar + plagioclase + quartz + biotite ± garnet ±epidote.

Protolith: The protolith of this rock may have been an intermediate to felsic igneous rock because of the high content of potassium feldspar.

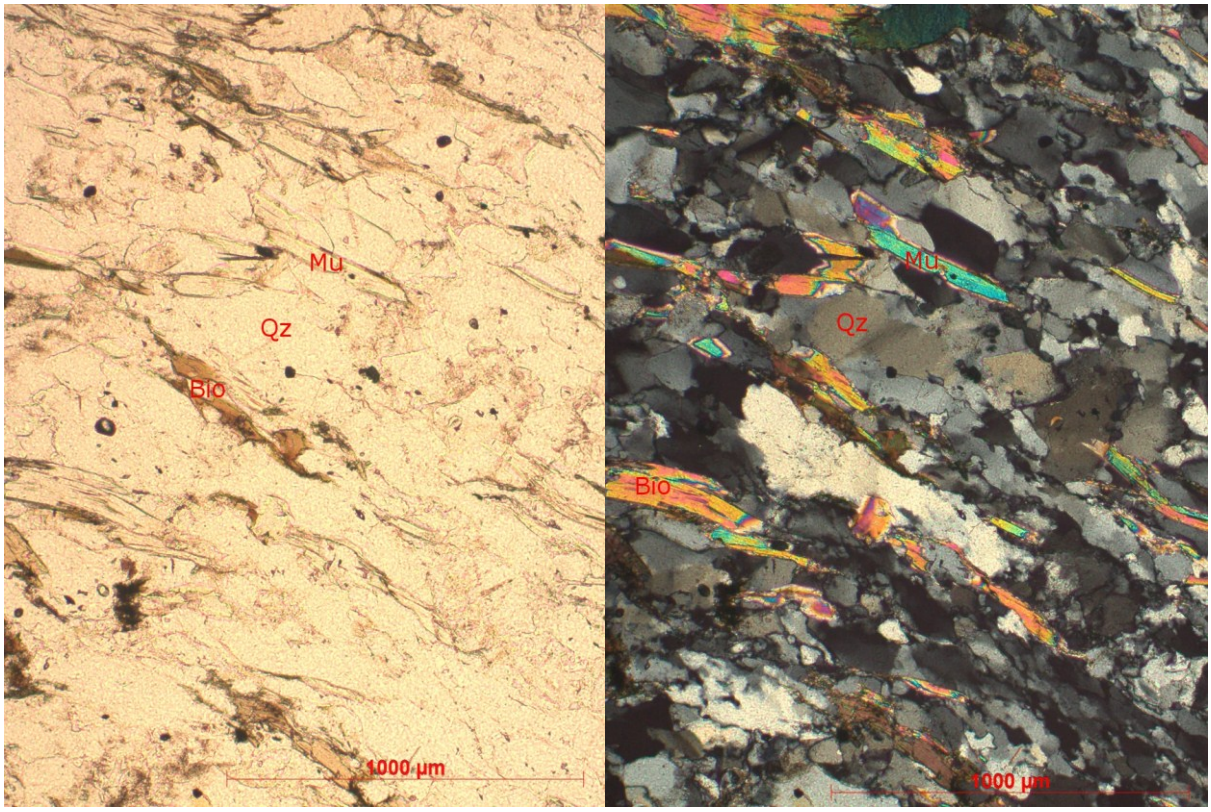

Fig. 36: Gneissic schistosity in quartz-rich gneiss. The schistosity is defined by aligned muscovite and biotite and elongated quartz. Sample 11Sch08; left uncrossed- right crossed-nicols

Sample: 11Sch15

Petrographic name: Garnet-bearing biotite-muscovite schist

General remarks: This rock is from the banded biotite gneiss unit (waypoint 80, Appendix B) in the western Brandkuppe area. The field relations of this outcrop are documented in chapter 6.2.3.

Modal mineralogy:

An overview of the section is shown in Fig. 37. There, larger parts can be seen which are rich in quartz. These quartz segregations are weakly folded and aligned in the main schistosity. Fe-hydroxide filled micro-cracks disect the whole section. The greenish to brownish color is due to a higher amount of chlorite and biotite.

Fig. 37: Overview of thin section 11Sch15

Quartz, biotite and muscovite are the main minerals of this section. Minor minerals are chlorite and garnet. Rutile, titanite, potassium feldspar, tourmaline and opaque are accessory phases. The opaque phases are ilmenite, magnetite and few pyrite.

Quarz occurs as fine-grained crystals in the whole matrix. It forms layers with plagioclase and muscovite and segregations. The micas (muscovite and biotite) mainly occur as larger crystals defining a good foliation. In the quartz rich layers, muscovite occurs in smaller aggregates with irregular orientation. Chlorite shows a weak pleochroism and anomalously low interference colors. It also tends to form larger crystals compared to the micas. *Garnet* and *tourmaline* occur as smaller porphyroblasts (Fig. 38). The garnet crystals appear in the muscovite richer parts in two different sizes. Small inclusions of pyrite are visible in garnet crystals. Tourmaline forms euhedral crystals with growth zoning. Fe-hydroxides fill micro-cracks.

Fabric: The rock has a good foliation and lepidoblastic fabric controlled by the alignment of muscovite and biotite. The quartz rich layers show a more granoblastic fabric.

Metamorphism and alteration*:* The metamorphic peak assemblage of this section is quartz + muscovite + biotite + garnet + tourmaline ±chlorite.

Protolith: The protolith of this rock may have been a psammo-pelitic clastic sediment with a higher amount of quartz

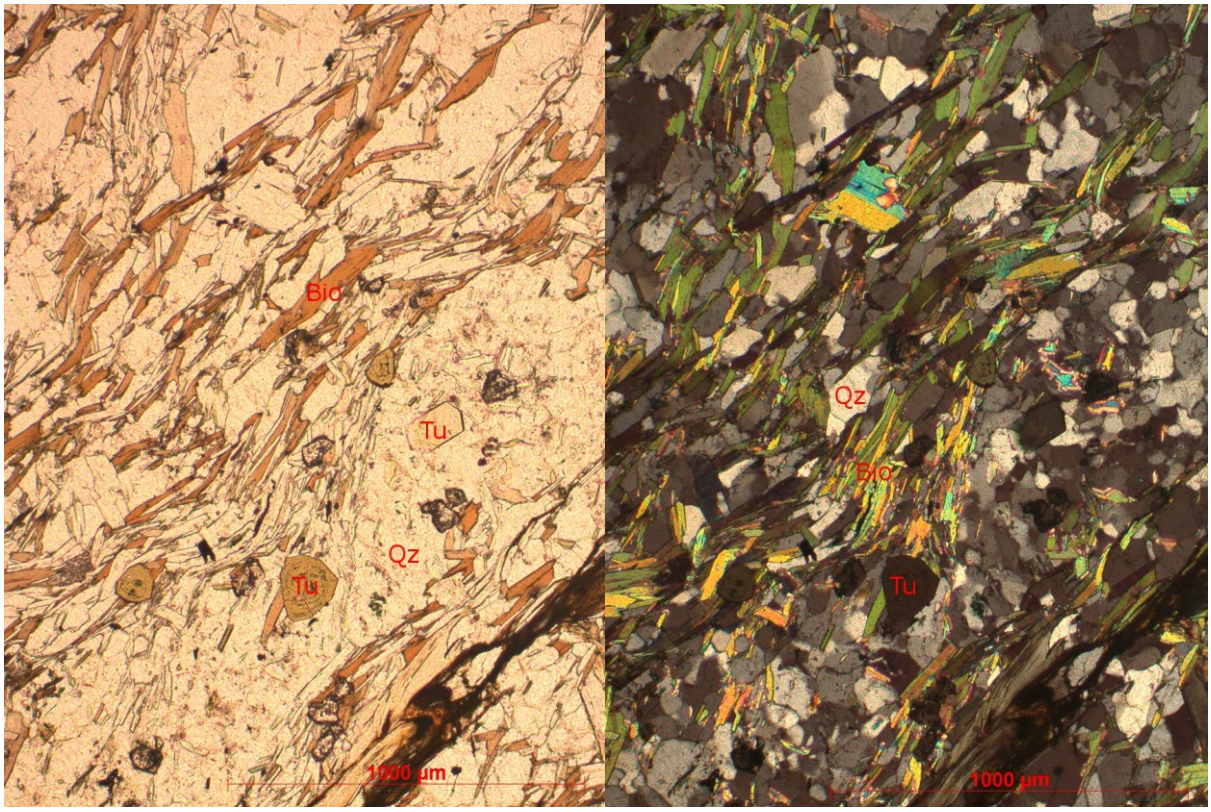

Fig. 38: Well foliated tourmaline bearing biotite schist from the biotite gneiss unit. Sample 11Sch15; left uncrossed- right crossed-nicols

Sample: 11Sch17

Petrographic name: Biotite gneiss

General remarks*:* This rock is from the banded biotite gneiss unit (waypoint 83, Appendix B) in the northern Brandkuppe area. The field relations of this outcrop are documented in chapter 6.2.3.

Modal mineralogy:

An overview of the section is shown on Fig. 35. This light-colored rock is only weakly foliated and folded. Few micro-cracks filled with Fe-hydroxides cross the section.

Fig. 39: Overview of thin section 11Sch17

Potassium feldspar, plagioclase and quartz are the dominant minerals in this section making up to 80 vol.%. Biotite is minor. Accessory minerals are the opaque phases ilmenite, pyrrhotite, chalcopyrite, pyrite, bornite, fahlore and Fe - hydroxides, as well as rutile, zircon and epidote.

Feldspars and quartz occur either as larger porphyroclasts or as fine ±recrystallized grains. Potassium feldspar is orthoclase with simple twinning and submicroscopic exsolution. The plagioclase is finer grained then potassium feldspar and mainly occurs with quartz in the matrix. The twinning lamellae are not always visible. Some biotites are altered to chlorite. Chalcopyrite occurs intergrown with pyrrhotite and fahlore. It is partly altered to bornite. Pyrrhotite shows weathering to Fe-hydroxides

Fabric: The fabric of this rock is equigranular granoblastic with some larger porphyroclastic potassium feldspars and weakly foliated.

Metamorphism and alteration: The peak metamorphic assemblage of this section is potassium feldspar + plagioclase + quartz + biotite + sulfides (?).

Protolith: The protolith of this gneiss may have been similar to 11Sch08 but more leucocratic as indicated by the lighter color due to the higher quartz and feldspar content.

Sample: 11Sch29

Petrographic name: Garnet - biotite gneiss

General remarks: This rock is a paragneiss intercalation from the orthogneiss unit (waypoint 182, Appendix B) in the north-east Adlerkuppe area. The field relations of this outcrop are documented in chapter 6.2.4.

Modal mineralogy:

An overview of the section is shown in Fig. 40. The section is rich in biotite (brownish color) with a poorly developed foliation. Larger domains enriched in feldspar and quartz can be distinguished. Few micro-cracks filled with Fe-hydroxides cut the section.

Fig. 40: Overview of thin section 11Sch29

The major minerals in this section are potassium feldspar, plagioclase, quartz, biotite and garnet. Minor phases are epidote, clinozoisite and muscovite. Accessory minerals include titanite, rutile, Fe-hydroxides, ilmenite, magnetite and pyrite.

Both feldspars occur in the matrix together with quartz as fine ±recrystallized grains and are ±altered to sericite and epidote. Garnet occurs at least in two different sizes. Larger garnet grains are associated with biotite, clinozoisite and quartz; these minerals form reaction products around them. The second garnet generation is smaller in size and tends to form euhedral crystals. The garnet grains may contain inclusions of pyrite and magnetite. Clinozoisite also occurs in the matrix of feldspar and quartz. Fe-hydroxides occur in micro-cracks and in fractures of the larger garnets.

Fabric: The fabric is porphyroblastic to granoblastic and shows layers of biotite and garnet. The schistosity is poorly developed and recognizable through the weak alignment of mica.

Metamorphism and alteration: The peak metamorphic assemblage of this section is potassium feldspar + plagioclase + quartz + garnet + biotite + muscovite. The retrograde metamorphic assemblage includes quartz + clinozoisite + sericite.

Protolith: This rock is best interpreted as a paragneiss. It derived from less aluminous and feldspar-quartz richer clastic sediments.

Sample: 11Sch31

Petrographic name: Epidote-hornblende gneiss

General remarks: This rock is from the orthogneiss unit (waypoint 189, Appendix) in the eastern Adlerkuppe area. The field relations of this outcrop are documented in chapter 6.2.4. This rock was collected at a small outcrop in the Adlitzgraben

Modal mineralogy:
An overview of the section is shown in Fig. 41. There, it can be seen green hornblende and epidote rich areas alternating with lighter feldspar-quartz rich domains.

The major minerals in this sample are quartz, plagioclase, potassium feldspar, epidote and hornblende. Carbonate and chlorite are minor minerals. Sericite and Fe-hydroxides, pyrite and magnetite are accessory phases.

Feldspars, quartz and carbonate occur as large grains with sizes up to 3mm as well as fine recrystallized grains in the matrix. The potassium feldspar shows domains with microcline twinning domains and perithitic exsolution. Graphic intergrowths are also visible in larger potassium feldspar grains. Plagioclase shows typical polysynthetic twinning. Epidote occurs in larger crystals and as small grains in the matrix. The opaque phases are rare and occur only as fine grains of magnetite and pyrite.

Fig. 41: Overview of thin section 11Sch31

Fabric: This rock shows a banded texture. Discontinuous darker layers are richer in epidote and hornblende; the lighter layers are mainly quartz and feldspar dominated. Carbonates occur in both layers. The lighter layers have a distinct granoblastic texture with larger porphyroclasts of feldspar and quartz. The epidote-hornblende-rich layers have a better foliation.

Metamorphism and alteration: The mineral assemblage consists of two feldspars + quartz + epidote + hornblende + calcite.

Protolith: The protolith of these rocks may have been a intermediate to mafic igneous rock.

8.1.3 Orthogneiss

Sample: 11Sch21

Petrographic name: Muscovite gneiss

General remarks: This rock is from the orthogneiss unit (waypoint 122, Appendix B) in the northern Kropfgraben area. The field relations of this outcrop are documented in chapter 6.2.4.

Modal mineralogy:

An overview of the section is shown on Fig. 42.

Fig. 42: Overview of thin section 11Sch21

Plagioclase, potassium feldspar, quartz and muscovite are the major minerals (~80 - 90 %,) in this light colored rock. Accessory minerals are garnet, epidote, biotite, chlorite, zircon, magnetite, apatite and Fe-hydroxides.

Both feldspars occur in large relict grains, with sizes up to 3mm and also as ±recrystallized grains in the finer matrix. The finer grained feldspar grains look quite fresh; the relicts show some alteration to muscovite and epidote. Quartz occurs in the fine grained matrix and shows undulatory extinction. Muscovite occurs as thin bands / layers in the section and as alteration mineral in feldspar. Biotite is altered to chlorite as indicated by brownish to greenish pleochroism colors and by its irregular interference colors. Magnetite has a subhedral habit and is strongly weathered to Fe-hydroxides.

Fabric: The texture is strained to granoblastic with large feldspar porphyroclasts. Muscovite is mainly aligned along the discontinuous schistosity, which gives the rock a typical gneiss fabric..

Metamorphism and alteration: The peak metamorphic assemblage of this section is potassium feldspar + plagioclase + quartz + muscovite ± biotite. It shows a low retrograde overprint indicated by the chloritization of the biotite and alteration of feldspars.

Protolith: The protolith of this gneiss may have been a quartz-rich leucocratic plutonic rock; i. e. a granodiorite.

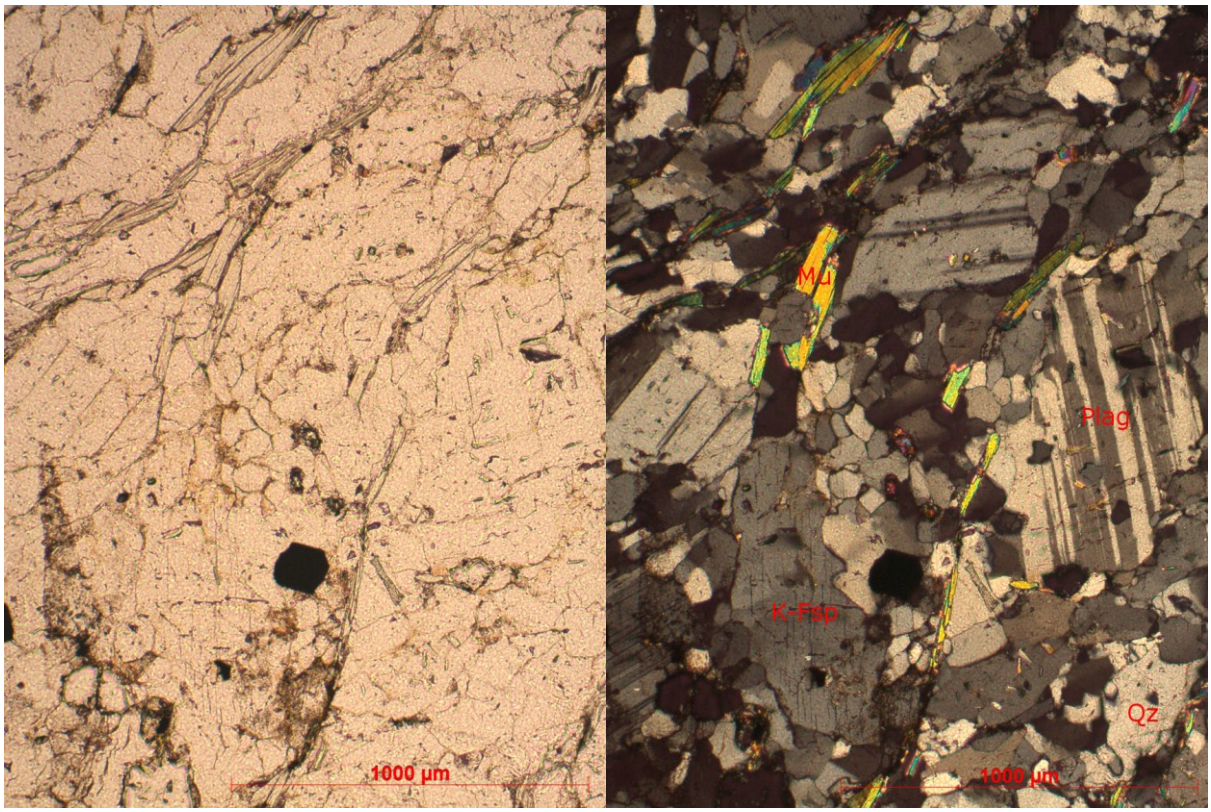

Fig. 43: Large feldspar (plagioclase and potassium feldspar) grains with muscovite and quartz. Sample 11Sch21; left uncrossed-, right crossed-nicols

Sample: 11Sch26

Petrographic name: Tourmaline-bearing orthogneiss

General remarks: This rock is from the orthogneiss unit (waypoint 142, Appendix B) in the southern Gollnerkuppe area. The field relations of this outcrop are documented in chapter 6.2.4.

Modal mineralogy:

An overview of the section is shown in Fig. 44. The alternation of dark tourmaline bearing and lighter quartz feldspar rich layers is diagnostic. The foliation is well developed.

Fig. 44: Overview of thin section 11Sch26

The major minerals are potassium feldspar, plagioclase, quartz and tourmaline. Accessory minerals are muscovite / sericite, zircon, apatite and magnetite.
Potassium feldspar and plagioclase occur as large relict crystals as well as ±recrystallized grains. Both feldspars show beginning sericitization. Quartz mainly recrystallized in the fine grained matrix and shows undulatory extinction. The tourmaline shows a layered distribution with quartz and muscovite (Fig. 45). Its habit is usually round shaped or xenomorphic.

Fabric: The fabric of the rock is granoblastic with larger feldspar and tourmaline porphyroclasts.

Metamorphism and alteration: The peak metamorphic assemblage of this section is potassium feldspar + plagioclase + quartz + tourmaline + muscovite.

Protolith: The protolith of this gneiss may have been a tourmaline-rich leucocratic igneous rock.

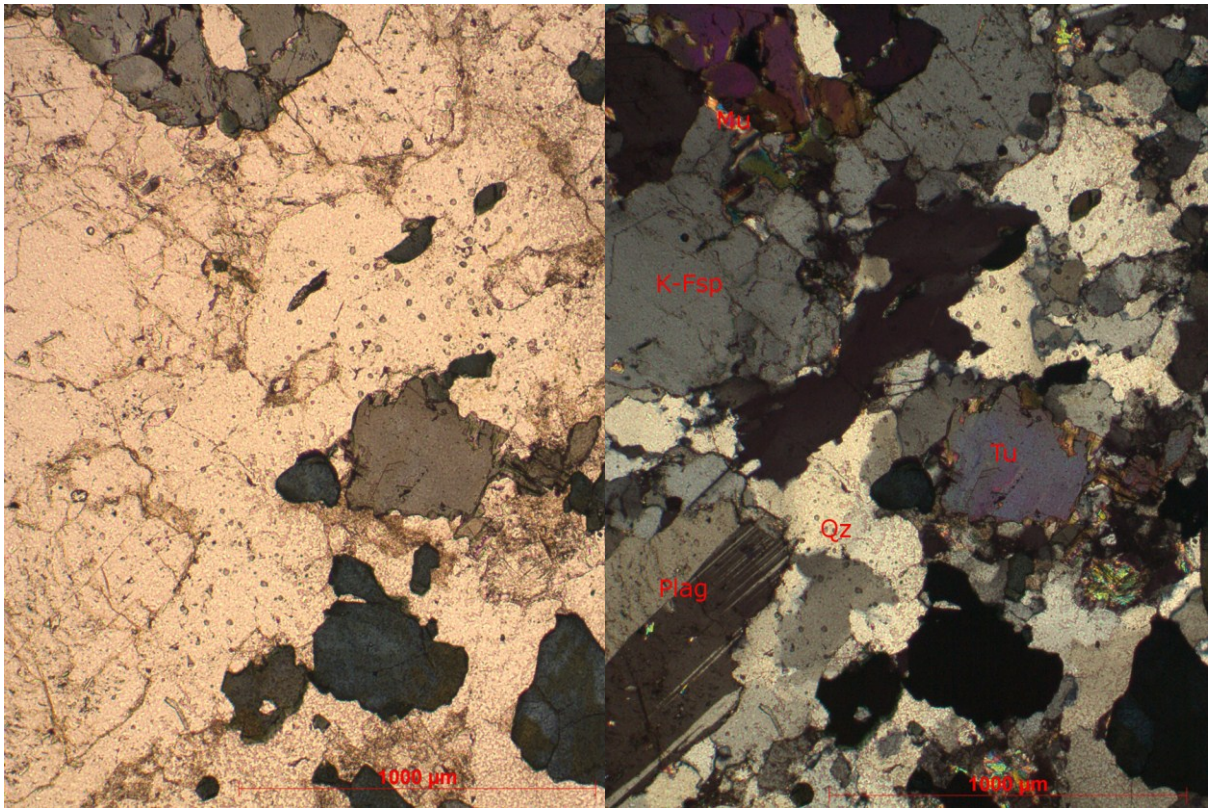

Fig. 45: Orthogneiss with strong pleochroic tourmaline, plagioclase and potassium feldspar with recrystallized quartz and minor muscovite. Sample 11Sch26; left uncrossed-, right crossed-nicols

8.1.4 Metaultramafite

Sample: 11Sch 24

Petrographic name: Magnetite-bearing olivine serpentinite

General remarks: This rock is from a single outcrop in the banded biotite gneiss unit (waypoint 189, Appendix B) in the eastern Adlerkuppe area. It represents a tectonic (?) relict of ultramafic rocks within this unit. The field relations of this outcrop are documented in chapter 6.2.6.

Modal mineralogy and fabric:

An overview of the section is shown on Fig. 46. There, it can be seen large opaque phases in a matrix of serpentine minerals and olivine. The variation in coloring is caused by the variable degree of serpentinization of this rock.

The major minerals in this section are serpentine, olivine and magnetite. Carbonates and pyrite are minor phases. Accessory phases include chalcopyrite, bornite, covellite, millerite and clay minerals (weathered sericite?).

Different domains are to be seen in this section. Strongly serpentinized as well as micro-areas with still preserved relict-texture can be distinguished. Fine-grained serpentine-group minerals are dominant in the first. These micro-areas are well foliated. The foliation is defined by serpentine minerals and by discontinuous bands, which are rich in opaque phases (mostly magnetite). This foliation is weakly refolded. Large grains of carbonate, magnetite, olivine up to 2mm in size and small grains of pyrite are visible in this part. The carbonates are partly replaced by serpentine.

Fig. 46: Overview of thin section 11Sch24

Olivine is main mineral in the micro-area preserving the relict texture. The fabric there is granoblastic grading to mesh structure with progressive serpentinization. The foliation is much weaker in these zones and mostly defined by magnetite. The sulfide assemblage developed in the micro-area includes larger pyrite grains associated with covellite, bornite, chalcopyrite and millerite. Millerite is slightly brighter then pyrite and shows a strong anisotropy with distinct colors from bright to slate blue-grey.

Metamorphism and alteration: The metamorphic mineral assemblage is dominated by serpentine-minerals + carbonates + magnetite. Olivine could be part of the metamorphic assemblage but it is affected to variable degree by lower temperature serpentinization.

Protolith: The protolith of this rock is an ultramafic rock, rich in olivine (e.g. dunite) comparable to ultramafic rocks in the Speik complex.

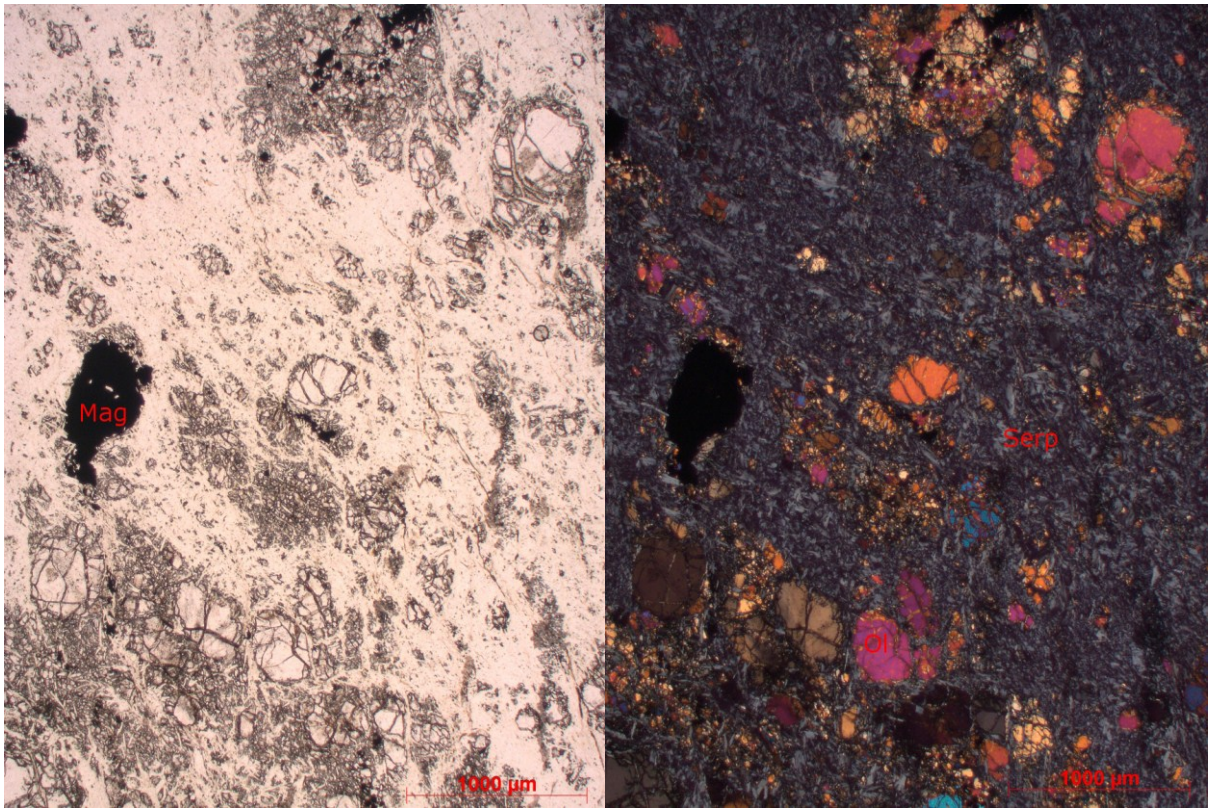

Fig. 47: Larger magnetite (opaque) and olivine (colorless, high relief on left photograph) in a matrix of serpentine group minerals. The serpentine minerals are well foliated. Sample: 11Sch24, left uncrossed-, right crossed-nicols

8.1.5 Vein rocks

Sample: 11Sch22a

Petrographic name: Altered amphibolite with chlorite-calcite veinlets

General remarks: This rock is from the banded ampbibolite gneiss unit (waypoint 118, Appendix B) in the Kropfgraben area. The field relations of this outcrop are documented in chapter 6.2.7. The thin section documents alteration related to formation of chlorite-calcite filled veinlets in an amphibolite.

Modal mineralogy:

An overview of the section is shown on Fig. 48. There, it can be seen that the metamorphic host rock is crosscut by thin veinlets. Accordingly, the mineralogical composition of the two different domains they are described separately.

Fig. 48: Overview of thin section 11Sch22a

Altered host rock: Plagioclase, quartz, calcic amphiboles (hornblende, tremolite), chlorite are the major minerals. Calcite, sericite are minor, rutile, ilmenite and titanite are accessory phases.

Plagioclase and *quartz* form a fine-grained (~0.1-0.3 mm) matrix. Twinning in plagioclase is rarely to be seen. Distinction of the two phases is furthermore hampered by the ubiquitous moderate to strong sericite alteration.

Calcic amphiboles are present in two types. Larger (up to 1 mm) xenoblastic *hornblende* porphyroblasts show stronger pleochroism (colorless to pale greenish), low 1st order interfernce colors and amphibole-diagnostic cleavage. They may show patchy extinction and in some parts of the porphyrolasts lots of tiny mineral inclusions (high birefringence). The second amphibole likely is *tremolite*. It is characterized by subhedral elongate crystal morphology showing distinct oblique extinction. It is colorless to very weakly pleochroitic and has higher interference colors (2nd order). These amphiboles are weakly oriented. *Chlorite* has pale greenish colors and pleochroism and shows anomalous interference colours (brown-grey). It is randomly oriented especially within polycrystalline aggregates in nests. There it may occur together with calcite. *Calcite* in the host rocks occurs in irregular nests and often contains inclusions of other minerals like tremolite. The Ti-phases *rutile*, *ilmenite* and *titanite* occur as polyphase aggregate grains. Rutile often forms the cores of larger aggregate grains and is intergrown with ilmenite. Titanite commonly forms reaction rims (coronas) around rutile/ilmenite. *Fe-hydroxides* are present along cracks and some foliation planes.

Veinlets: Three mm-thick veinlets crosscutting the altered host rock are to be seen in the thin section (Fig. 48, Fig. 49). The contacts between the veinlets and the host rock are sharp and straight. The two major minerals in the veinlets are *calcite* and *chlorite*. The mineral assemblage in individual veinlets is mostly monomineralic; i.e. either filled with chlorite or calcite. In places it can be observed that calcite-filled veinlets crosscut the chlorite masses; this indicates a poly-phase formation. Calcite is coarse-grained and develops a granoblastic structure. Very large grains show deformation twinning and bending of the twinning lamellae (Fig. 49). *Ilmenite* with elongate tabular morphology is an accessory phase in the veinlets. It is fresh and often monocrystalline and often grows at steep angles to the vein contact. A few tiny grains of Fe-sulfides (pyrite, pyrrhotite) were observed. Interestingly, quartz is missing in these veinlets.

Fabric: The heterogeneous planar distribution of light (quartz, plagioclase) and dark minerals (amphiboles, chlorite) and the alignment of some amphiboles allow the recognition of a weak foliation in the host rock despite its intense alteration. Alteration certainly postdates this early planar fabric and was post-kinematic with respect to the penetrative foliation. The veinlets, now filled with chlorite and calcite, formed during a later brittle deformation event. Brittle deformation and filling with vein minerals was polyphase as indicated by the crosscutting relationship of calcite veinlets within chlorite veinlets.

Alteration: The thin section records intense alteration. The dominant alteration minerals are chlorite and calcite. The alteration assemblages in the host rock and in the assemblage in the veinlets are comparable, except that quartz is only present in the host rock. Hence, it is unclear if quartz was part of the alteration assemblage. Sericitzation of plagioclase and quartz in the altered host rock could be related to the same alteration event. The alteration is classified as being of the chlorite-carbonate±quartz (?) type. The rock is slightly weathered, as indicated by the presence of Fe-hydroxides.

Protolith*:* A mafic protolith is assumed from the modal mineralogy and the bulk composition estimated thereof.

Interpretation: The pervasive alteration in this rock seems to be coeval with the formation of chlorite-calcite veinlets in this rock; i.e. the same fluids precipitating calcite and chlorite in the veinlets infiltrated the adjacent host rock and caused pervasive alteration in vicinity of the veinlets.
There is no mineralization associated with this veinlets. The orientation of the veinlets (see chapter 7, Structural geology) is also not consistent with the orientation of the mineralized vein structures in the Schönberg area. Hence, it is concluded that these veinlets and the related alteration are *not* related to Cu-Au mineralization but rather reflect local fluid flow along late- to post-metamorphic small-scale brittle structures.
It is also unclear how tremolite fits into the metamorphic evolution of this rock. Its weak alignment in the foliation and wrapping around the pre-existing hornblende porphyroblasts would indicate that it is not related to the alteration processes but that it belongs to the regional metamorphic paragenesis. Hornblende, plagioclase ± quartz could have been the stable minerals at peak conditions of the amphibolite facies.

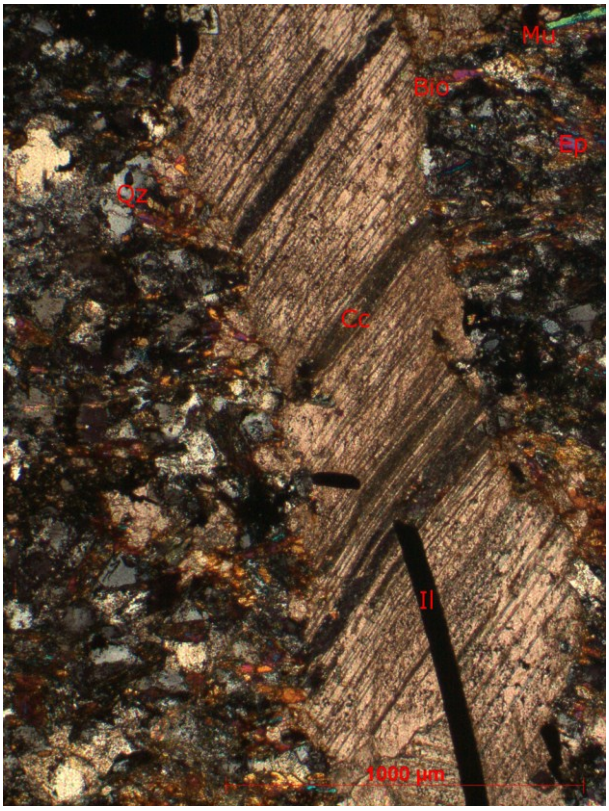

Fig. 49: Veinlets filled with calcite (showing deformation twinning) in altered host rock. The latter contains quartz, calcite, epidote, tremolite(?) as alteration minerals. Sample: 11Sch22a; crossed-nicols

8.1.6 Altered host rock with copper mineralization

Sample T.03

Petrographic name: Altered host rock, Cu-mineralization

General remarks: This sample was taken at Barbara dump. It is from a larger block containing sulfide mineralization in the form of sulfide-quartz-carbonate veinlets (Fig. 50). This section allows studying the relation between hydrothermal veinlets containing the Cu-Fe sulfide and gangue assemblage and the alteration type developed in the adjacent host rock.

Modal mineralogy:

The major minerals in the vein are quartz, calcite and the sulfides chalcopyrite, arsenopyrite and pyrite. Quartz is intergrown with the sulfides and forms perfectly euhedral crystals, what seems to be a peculiar feature of this type of vein quartz. The co-existing coarse grained carbonate is calcite. Euhedral rutile also occurs in the veinlet.

Alteration: The host rock is affected by intense wall rock alteration (Fig. 50 and Fig. 51). The alteration assemblage contains sericite, carbonate and quartz. Rutile and other Ti-minerals

(titanite (?), anatase (?)) likely also belong to the alteration assemblage. From the primary host rock mineralogy only quartz, and to some extent, muscovite but no feldspars are preserved. Locally, muscovite defines a ghost-like relict metamorphic foliation. This sample represents sericite-carbonate alteration that affected a quartz-mica-(feldspar?)-rich protolith.

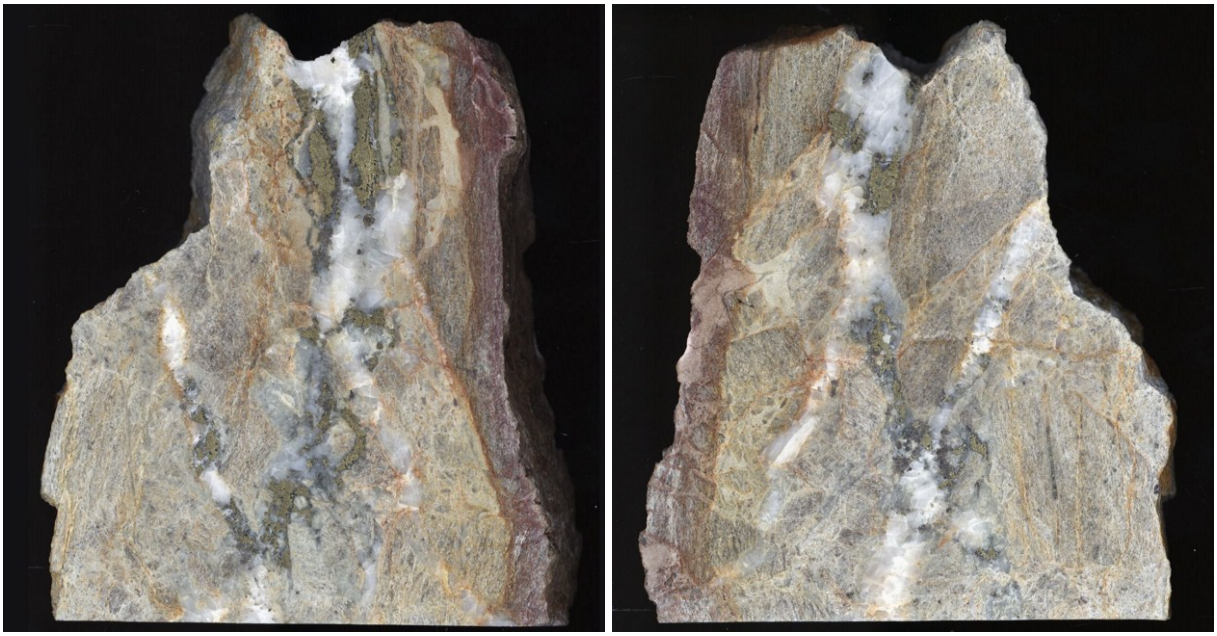

Fig. 50: Ore sample (slabs) from the Barbara dump. Carbonate-quartz-sulfide veinlets crosscut the strongly altered host rock. Frame width 9.5cm

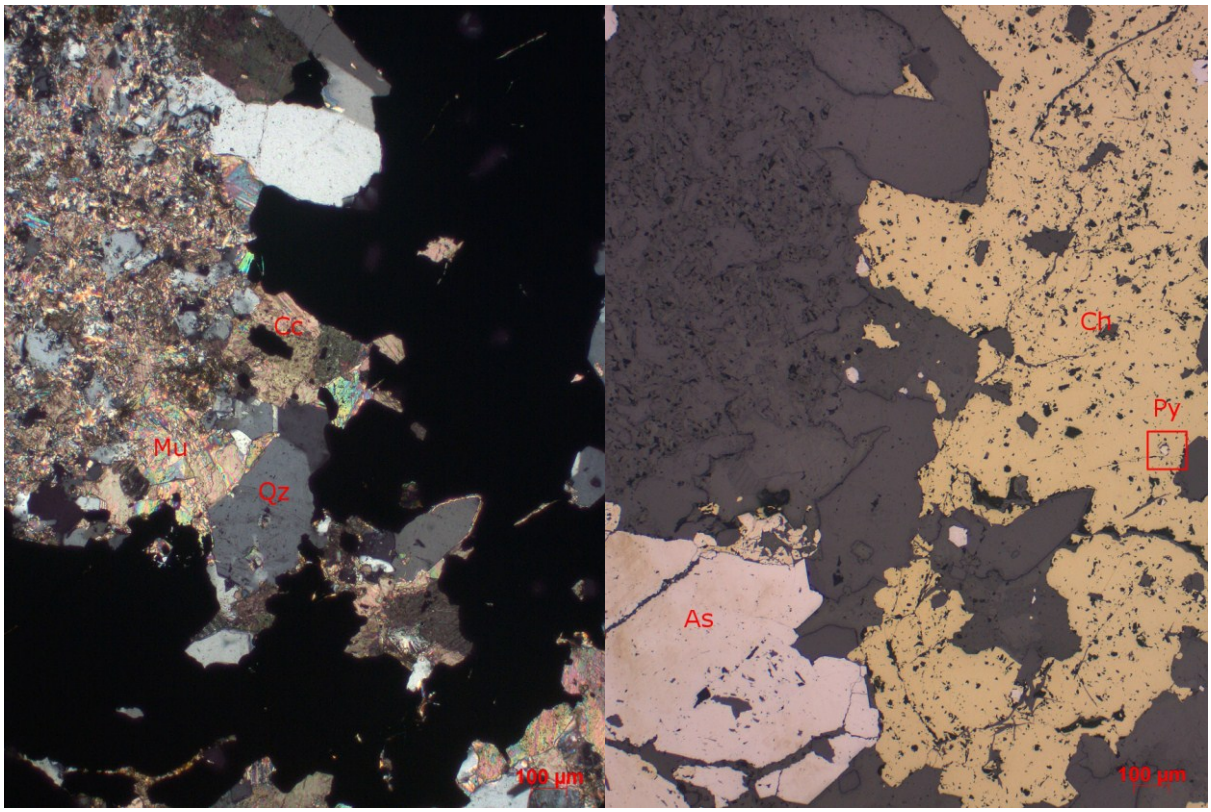

Fig. 51: Contact of chalcopyrite-arsenopyrite-quartz veinlet with host rock. Feldspar is altered to a fine mixture of muscovite / sericite and calcite. Sample: T.03; left crossed-nicols, right reflected light microscopy

8.2 Ore microscopy

The studied samples are from all three mining districts in the Schönberg / Flatschach area i.e. Weissenbach, Brunngraben and Adlitzgraben (Table 7, Table 8). The sample set provided by Prof. W. Paar mainly represents material from Weissenbach and there is a dominance of samples from Brandegger vein in this district. Samples P.14 to P.22 have already been investigated by Paar and Meixner (1979), although no mineral chemical data were given in this study. The samples 78560 to 78581 (Table 8) are the original polished blocks from the PhD thesis of Jarlowsky (1951), that were archived at Universalmuseum Joanneum (UMJ). Sample J.01 to J.05 are also from UMJ but new polished sections were prepared from hand specimens. Samples T.01 to T.03 are new samples collected from the Barbara dumpsite in spring 2012.

Table 7: Location of samples, paragenetic Stage and gold occurrence, sample set Prof. Paar

Sample no.	Mining district	Location / Adit	Paragenetic Stage	Gold present
P.1	Weissenbach	n/a	2	
P.2	Weissenbach	n/a	2	
P.3	Weissenbach	n/a	2	
P.4	Weissenbach	n/a	2	
P.5	Weissenbach	n/a	2	
P.6	Weissenbach	n/a	2	
P.7	Weissenbach	n/a	2	x
P.8	Brunngraben	Fuchsstollen 1	3	
P.9-1	Brunngraben	Fuchsstollen	3	
P.9-2	Brunngraben	Fuchsstollen	3	
P.10	Weissenbach	n/a	2	x
P.11	n/a	n/a	3	
P.12	Weissenbach	Brandegger	2	x
P.13	Weissenbach	Brandegger	2	
P.14	Weissenbach	Brandegger	2	
P.15	Weissenbach	Brandegger	2	x
P.16	Weissenbach	Brandegger	2	
P.17	Weissenbach	Brandegger	2	
P.18	Weissenbach	Brandegger	2	x
P.19	Weissenbach	Brandegger	1	
P.20	Weissenbach	Brandegger	3	
P.21	Weissenbach	Brandegger	3	
P.22	Weissenbach	Brandegger	3	x

n/a … unknown

Table 8: Location of samples, paragenetic Stage and gold occurrence, sample set from (Jarlowsky, 1951) and self-collected samples.

Sample no.	Mining district	Location / Adit	Paragenetic Stage	Gold present
78560	Brunngraben	Fuchsstollen 6	none	
78561	Weissenbach	Barbarastollen adit	1	
78562	Weissenbach	Barbarastollen	1	x
78563	Adlitzgraben	Adlitzgraben	1	
78564	Adlitzgraben	Urbani - Unterbau	1	
78565	Weissenbach	n/a	4	
78566	Weissenbach	Annastollen dump site	1	
78567	Weissenbach	Annastollen dump site	1	
78568	Weissenbach	Annastollen dump site	1	x
78569	Weissenbach	Dreifaltigkeit dump site	1	x
78570	Weissenbach	Dreifaltigkeit dump site	1	
78571	Weissenbach	Dreifaltigkeit dump site	2	
78572	Brunngraben	Ludwigstollen dump site	1	
78573	Brunngraben	Ludwigstollen dump site	1	x
78574	Brunngraben	Fuchsstollen1 dump site	2	
78575	Brunngraben	Fuchsstollen 1 dump site	1	
78576	Brunngraben	Fuchsstollen 1 dump site	1	
78577	Brunngraben	Fuchsstollen 1 dump site	1	
78578	Brunngraben	Fuchsstollen 3, dump site	2	
78579	Brunngraben	Fuchsstollen 3, dump site	2	
78580	Brunngraben	Fuchsstollen 3, dump site	2	
78581	Brunngraben	between Fuchsstollen and Flatschach	1	
J.01	Weissenbach	between Bischof and Mesner	none	
J.02	Adlitzgraben	Adlitzgraben	1	
J.03	Weissenbach	Dreifaltigkeit dump site	1	
J.04	Weissenbach	Barbarastollen dump site	1	x
J.05	Adlitzgraben	Urbani - Unterbau	1	x
T.01	Weissenbach	Barbarastollen dump site	1	
T.02	Weissenbach	Barbarastollen dump site	1	
T.03	Weissenbach	Barbarastollen dump site	1	

8.2.1 Paragenetic Stages - a short summery

Based on microscopy and EMPA analyses three paragenetic Stages can be distinguished in the ore samples from Flatschach. The detailed microscopic descriptions of the minerals are given in the following chapters. The distribution of the main ore and gangue minerals is shown in Fig. 52.

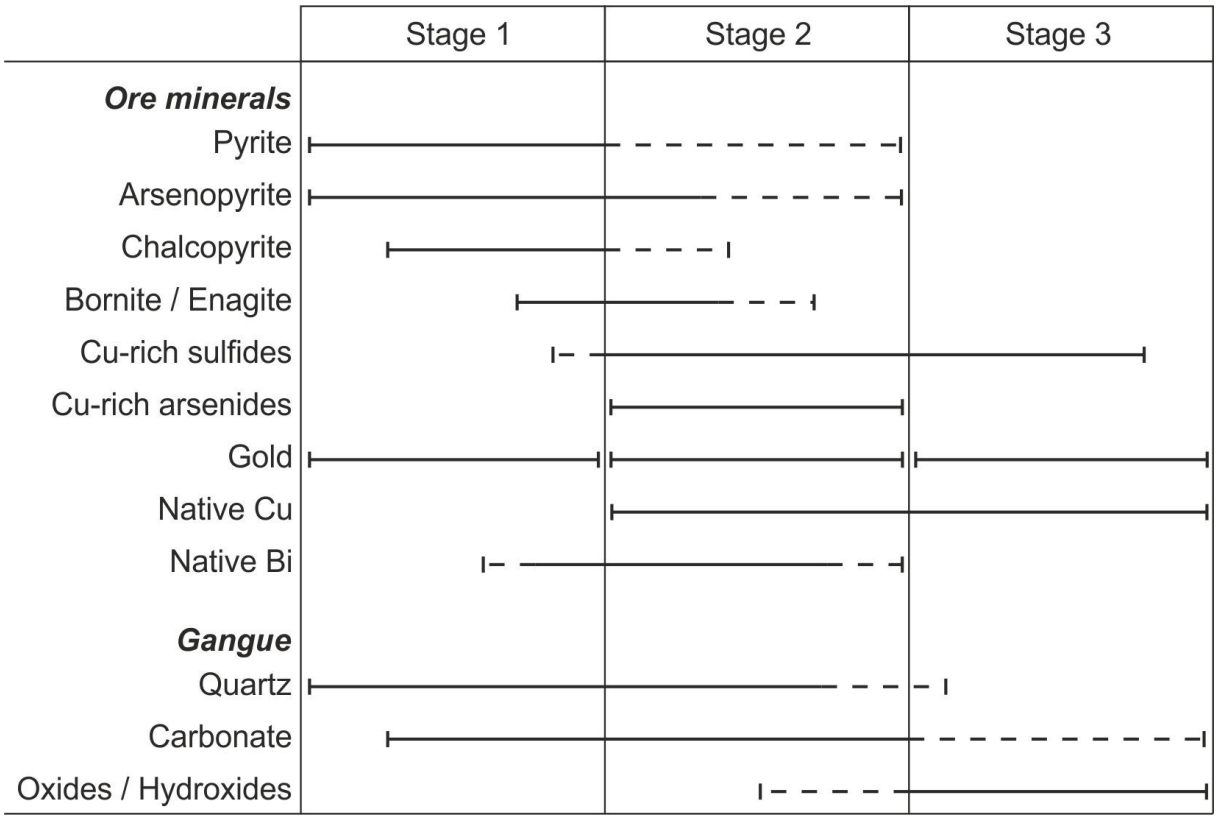

Fig. 52: Distribution of the main ore and gangue minerals in the three paragenetic Stages. Note that gold is present in all three Stages.

Stage 1

The main samples of this type are those from the sample set of Jarlowsky (1951), plus one section from Prof. Paar's sample set.

Stage 1 includes the relatively oldest sulfides, which are often replaced by the younger Stage 2 Cu sulfides; e.g. replacement of chalcopyrite by digenite. Main ore minerals of this Stage are arsenopyrite, pyrite and chalcopyrite. Associated minerals are enargite, sphalerite, galena, bornite, alloclasite, native bismuth and matildite. The associated gangue minerals are quartz and calcite.

Stage 2

Stage 2 includes Cu-rich sulfides (digenite, anilite, yarrowite etc.) and arsenides (domeykite, koutekite) as well as native bismuth plus native copper. The common gangue minerals are calcite, dolomite / ankerite and a younger generation of quartz. Gold is part of this paragenetic Stage too. It is associated with the Cu sulfides and native bismuth but is mostly inter-grown with the carbonate gangue. Though domeykite and koutekite occur in the same samples, they have not been observed in direct contact with gold. Chalcopyrite is only a relict phase.

Two types of gold can be distinguished: larger gold grains with >Au/Ag and smaller ones with <Au/Ag. The second type also forms rims or overgrowths on the first one but it also occurs as small isolated grains in adjacent digenite

Stage 3

Stage 3 includes Fe- and Cu- oxides, -hydroxides and -carbonates formed during a late oxidation event, likely during supergene weathering. The following minerals are assigned to this Stage: hematite, cuprite, goethite, malachite. These minerals often form fine grained and poorly crystallized polyphase aggregates. There are certainly more phases present in this Stage. However, these were not studied in detail.

It is important to note that gold is also part of this oxidized assemblage. It occurs as minute <10μm grains mostly in the Fe oxides / hydroxides. This type of gold is also chemically distinct (see chapter 9.5).

Table 9: Ore and gangue minerals identified in this study. The mineral name, the abbreviation and the ideal mineral formula are given.

Mineral	Abbreviation	Chemical composition
Digenite	Di	$Cu_{1.8+x}S$
Anilite	An	$Cu_{1.75}S$
Geerite	Ge	$Cu_{1.6}S$
Spinkopite (?) (bb. covellite) *	Cv	$Cu_{1.39}S$
Yarrowite (bb. covellite) *	Cv	$Cu_{1.13}S$
Domeykite	Do	$Cu_{3-x}As$, x = 0.02 – 0.4
Koutekite	Ko	Cu_5As_2
Arsenopyrite	As	FeAsS
Pyrite	Py	FeS_2
Chalcopyrite	Ch	$CuFeS_2$
Enargite	En	Cu_3AsS_4
Fahlore (?)	Fa	$Cu_{12}As_4S_{13}$ - $Cu_{12}Sb_4S_{13}$
Native copper	Cu	Cu
Native bismuth	Bi	Bi
Matildite	Mat	$AgBiS_2$
Bismuthinite	Bis	Bi_2S_3
Native gold	Au	Au; electrum (Ag, Hg)
Sphalerite	Sp	ZnS
Galena	Ge	PbS
Bornite	Bo	Cu_5FeS_4
Alloclasite ?	Al	$Co_{1-x}Fe_xAsS$ (low Ni content)
Safflorite	Sa	$(Co,Fe,Ni)As_2$
Xenotime	Xe	$Y(PO_4)$
Calcite	Ca	$CaCO_3$
Calcian siderite	Si	$(Fe,Ca)CO_3$
Dolomite	Dl	$(Mg,Ca)CO_3$
Malachite	Ma	$Cu_2(CO_3)(OH)_2$
Quartz	Qz	SiO_2
Hematite	He	Fe_2O_3
Magnetite	Mag	Fe_3O_4
Ilmenite	Il	$FeTiO_3$
Cuprite	Cp	Cu_2O
Fe - hydroxide (goethite, “limonite”)	Hy	FeO(OH)
Muscovite	Mu	$KAl_2((OH,F)_2\|AlSi_3O_{10})$
Chlorite	Cl	$(Fe,Mg,Al,Zn)_6(Si,Al)_4O_{10}(OH)_8$
Serpentine	Serp	$(Mg)_3(Si_2O_5)(OH)_4$
Rutile	Ru	TiO_2
Titanite	Ti	$CaTi(O\|SiO_4)$

* bb. covellite … “Blaubleibender covellite”, actually a mixture of spinkopite and yarrowite

The mineral compositions of the ore samples are listed in Table 10 and Table 11.

Table 10: Modal mineralogy of 23 polished sections, sample set W. Paar. For abbreviation of mineral names see Table 9.

	Fe-rich sulfides				Cu-rich sulfides					Native Elements			Gangue:				
Sample Nr.:	Py	As	Ch	Bo	general	Di	An	Cv	Do / Ko	Cu	Bi	Au	Carb	Qz	Oxides	Hydroxides	Other
P.01		x			x	x	xx	xxx	x	xx	x		x	x			
P.02	x	x			xx	x	x	x	x	x	x	x	x	x		x	
P.03	x	x	+/-		x	x	x	xx		xx	xx		x	x			
P.04	x	x	+/-	+/-	xx	x	x	x	x		x		x	x	x(Fe)	x	
P.05	x	x	+/-	+/-	xx	x	x	x					x	x			
P.06	xx	xxx	+/-	+/-	xx	x		xx				x	x	x		x	
P.07	x	x			xxx	xxx	x	x	xx	x	xx	x	x	x			
P.08					x	x	x	x	+/-	xx			x	x	x(Cu)	x	Ru
P.09-1	x	xx			x	x	x	x		x	xx		x	x		x	
P.09-2	x	xx			x	x	x	x	x	x	x		x	x		x	
P.10	x	x			xxx	xxx	x	x	x	x	xx	x	x	x	x	x	Cp
P.11									+/-	x			x	x	xxx	xxx	Cp
P.12	x	x			xx	x	x	x	x	x	x	x	x	x			
P.13	x				xx	x		x	x	x	xx	x	x	x		x	
P.14	x	x			xx	x	x	xxx		x	x	x	x	x	?	x	
P.15	x	x			xx	x	x	x	x	x	x		x	x			
P.16		+/-	+/-		xx	x	x	x	xxx	x+	xxx		x	x			
P.17	x	x			xx	x	x	x	x	x	x	x	x	x		x	
P.18	x	xx			xxx	x	x	x	xxx	x	xxx	x	x	x			Ru
P.19	x	x	x	x	x	x		x		x	x	x	x	x		x	En
P.20			x		xx	?		x	xx	x					x(Cu)	x	Al
P.21			x		xx		x	xx		xx			x	x	xxx	x	
P.22	x	+/-			xx	x	xx	xxx		x		x	x	x	xx	xx	

+/- ... very rare; x ... rare; xx ... common; xxx ... very common

Table 11: Modal mineralogy of 26 polished sections, sample set Jarlowsky (1951) plus 3 new polished sections. For abbreviation of mineral names see Table 9.

	Fe-rich sulfides				Cu-rich sulfides						Native Elements		Gangue:				
Sample Nr.:	Py	As	Ch	Bo	general	Di	An	Cv	Do / Ko	Cu	Bi	Au	Carb	Qz	Oxides	Hydroxides	Other
78560	xxx													x		x	Chl, Ti
78561	xxx	xx	+/-										x	x			Ru, Ti
78562	xxx	x	xxx									x	x	xxx			Ru
78563	x	x											x	xx			Ru, Ti
78564	x		xxx										xxx	+/-			Ru, Ti, Al
78565	x													xxx			Mu, K-Fsp, Plg
78566	x	x	xxx	x	x						x		x	x			Ru, Ti, Sa
78567	x	x	xxx										x	xxx			Ru
78568	x	x	xxx	x							x	x	x	x			Ru, Ti, En
78569	x	x	xxx									x	x	xxx			Ti, Mat, Bis
78570	x	xx	xxx										x	xx			Ru, Ti
78571	x	x	xx	x	xx	x		x			x		x	xx			Ru, Bis, Mat
78572	x	x											xxx	x			Bis
78573	xx	xxx	+/-								x	x	x	x		x	
78574	x	xxx	xx	x	xx	x	+/-	x	+/-				x	x		x	Ru, Ti, En
78575	x	x	xx	x	x	xx	+/-	x	+/-				x	x		x	Ru, Ti, En
78576	x	x	xxx	x	x	x	+/-	x	x				xx	x		x	
78577	x	x	xxx		xx	x	x	x	x				x	xxx		x	Ru
78578		+/-		x	xxx	xx	x	x			x		xxx		x	x	
78579			xxx	x	xx	xx		x					x	x			
78580					xxx	xx	x	x			x		xxx	x	x	x	
78581	x	x	xx	x	x		x	x					x	x			
J.01	x	x	xx		x	x		x					xx	x			
J.02	x	x	xxx								+/-		x	xx			Ru
J.03	x	x	xxx	+/-	x	+/-	+/-	x	x		x		xxx	x		x	Ru, En
J.04	x	x	x								x	x	xxx	x			Ru
J.05	xxx	xx	xx		x	+/-	+/-	+/-				x	x	xxx			Ru, Ti
T.01	x	x	xxx		x	+/-	+/-	+/-					xxx	x			Ti
T.02	x	x	xxx										x	x			Ti
T.03	x	xx	xx										x	x			Ti

+/- ... very rare; x ... rare; xx ... common; xxx ... very common

8.2.2 Arsenopyrite, pyrite, chalcopyrite and bornite

Arsenopyrite and pyrite are the most frequent ore minerals in the polished sections. Both show sub- to euhedral morphology with up to approximately 1 mm large crystals. The arsenopyrite shows a white color and its anisotropy with blue to yellowish brown colors is distinct. Two generations of pyrite are distinguishable. The first generation (Pyrite 1) is inclusion-free, often euhedral and intergrown with arsenopyrite. The larger pyrite and arsenopyrite grains often show cataclastic texture. Pyrite and arsenopyrite filling fractured chalcopyrite as well as, vice versa, chalcopyrite filling fractured arsenopyrite and pyrite was observed. The second pyrite generation (Pyrite 2) is intimately intergrown with the gangue minerals; partly it forms overgrowths on Pyrite 1 and arsenopyrite (Fig. 53). Pyrite 2 contains lots of inclusions of gangue minerals. Arsenopyrite and pyrite, especially the latter, also occur in the fraction <50 μm. In few sections pyrite shows a weak anisotropy with greenish tints.
Chalcopyrite occurs as large anhedral massive grains, often with inclusions of euhedral pyrite and arsenopyrite, or disseminated in carbonate gangue. The pure yellow color and the weak anisotropy are diagnostic for this mineral. Sometimes chalcopyrite overgrows euhedral gangue quartz, what indicates a later crystallization. Chalcopyrite is the main carries of gold mineralization in the paragenetic Stage 1 (Fig. 54).
In more altered sections of paragenetic Stage 2 and 3 (see chapter 8.2.1) chalcopyrite, pyrite and arsenopyrite occur as relicts. Arsenopyrite is more or less not replaced by the Cu-rich sulfides. In contrast pyrite and chalcopyrite are commonly transformed to Cu-rich sulfides (digenite etc.; Fig. 55).
In the oxidized Stage 3 assemblage chalcopyrite is only present as tiny rounded inclusion in euhedral quartz.

Bornite shows a light pink-brown color (fresh after polish) but it changes quickly to a red too violet tint, sometimes with a weak pleochroism. The anisotropy varies strongly but a weak anisotropy is always visible. Bornite occurs in thin coronas around chalcopyrite and in micro-fractures. Some of these coronas are poly-phase including digenite and covellite (Fig 56).

Other accessory ore minerals, which were observed as small inclusions in quartz include allocasite, galena and sphalerite.

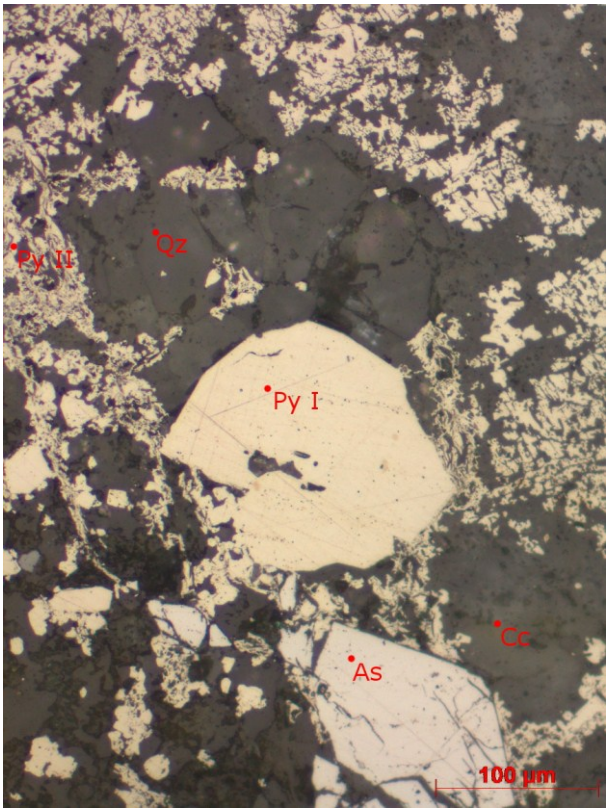

Fig. 53: Generation 1 and 2; pyrite generation 1 co-exists with arsenopyrite. Sample 78561

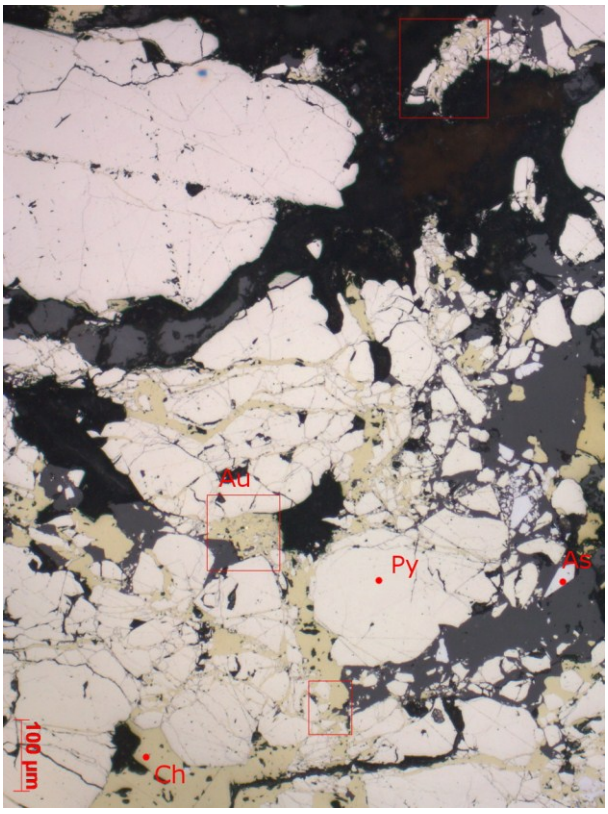

Fig. 54: Chalcopyrite filling fractured pyrite. Gold is mainly associated with chalcopyrite. Minor arsenopyrite is also present. Sample J.05; red boxes marks areas with gold grains.

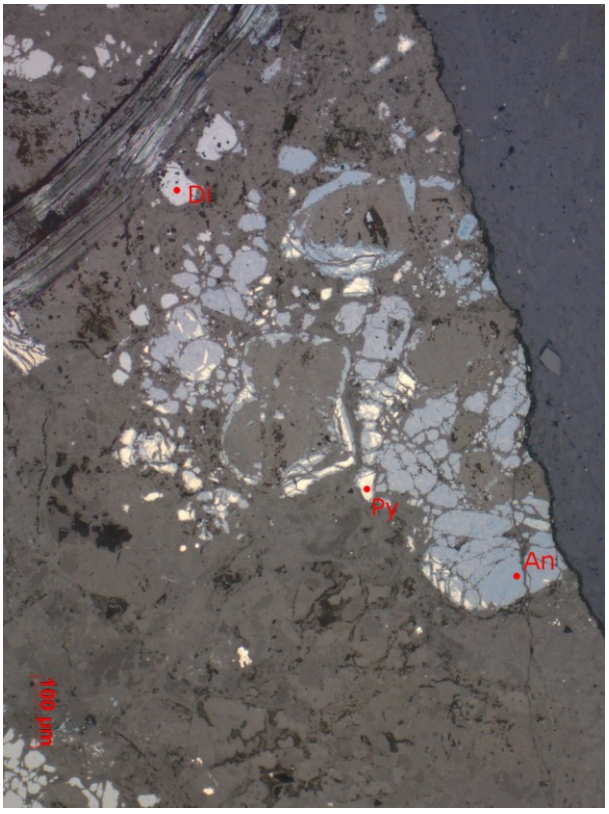

Fig. 55: Pyrite replaced by Cu-rich sulfides (digenite, anilite etc.) of Stage 2. Sample P.7

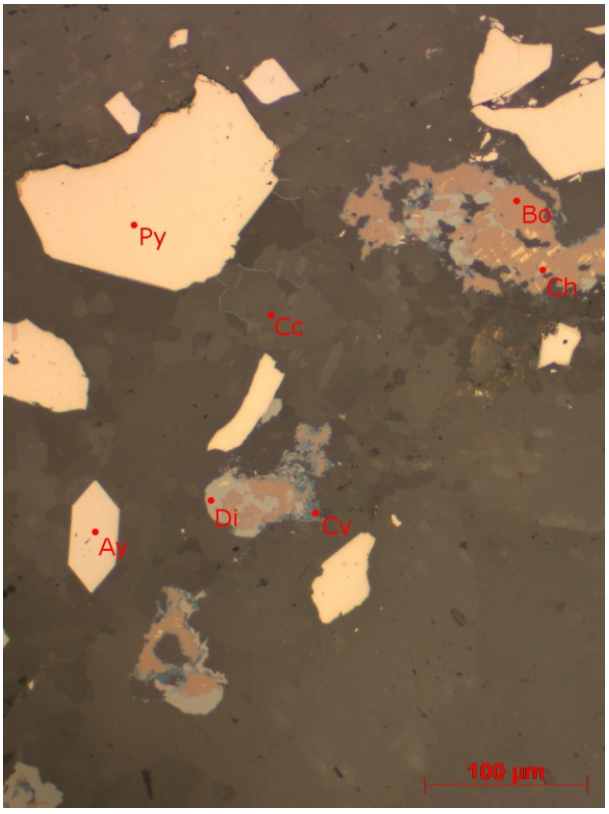

Fig 56: Chalcopyrite replaced by bornite, digenite and bb. covellite in a carbonate (calcite) matrix. Sample 78568

8.2.3 Cu-rich sulfides and native copper

Cu-rich sulfides include digenite, anilite, geerite (rare) and blaubleibender (bb.) covellite (actually a mixture of spinkopite and yarrowite). The microscopic distinction of these minerals is only possible in part. The distinction oft these minerals mostly results from analyses with the EMPA (see chapter 9.2).

With increasing Cu:S ratio these minerals get a more bluish tint (Fig. 57); i.e digenite shows a bluish grey color, anilite getting a stronger bluish to violet tint and bb. covellite showing a indigo blue to grayish blue pleochroism and color. Bb. covellite is strongly anisotropic. It shows extreme unusual by bright orange color under crossed nicols. All other Cu-rich phases are either isotropic (digenite) or weakly anisotropic.

The Cu-sulfides commonly exhibit a cataclastic or replacements textures; i.e. the larger grains are fractured and fragmented. The grains have mostly rounded shapes and they are commonly fractured and filled with carbonate gangue (Fig. 57).

The Cu-rich minerals mainly form by replacement of chalcopyrite and pyrite. The replacement of chalcopyrite starts with bornite, followed digenite, bb. covellite ± enargite (Fig. 58). Chalcocite is missing in the ore sections. Fine grained covellite also occurs in cloud-shaped micro-areas together with native bismuth. In sections with a higher amount of native bismuth minerals (i.e. sample P.15), digenite is intergrown with native bismuth. In sections with a high amounts of oxide/hydroxide gangue (Stage 3), digenite is manly absent and bb. covellite becomes the dominant Cu-sulfide (Fig. 59).

Native copper occurs in larger grains (>100μm). It shows skeletal / dendritic or fine “bloomy” morphology (Fig. 60) but it is also present as fine disseminated native copper in the carbonate or oxide/hydroxide (Stage 3) gangue. It shows a coppered color and a very high reflectance. Sometimes it is partly oxidized to cuprite. In few cases, native copper is intergrown with bb. covellite (Fig. 60).

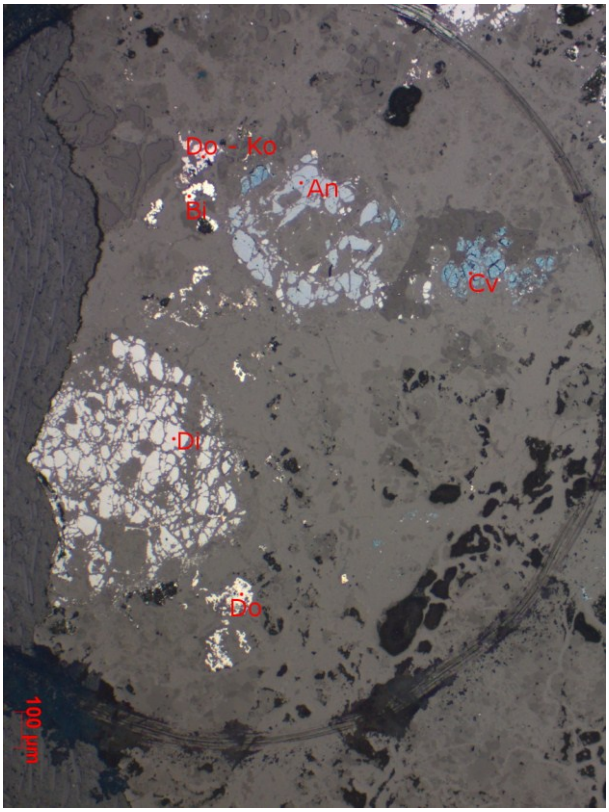

Fig. 57: Decrease in Cu in the Cu-sulfides form digenite, anilite to bb. covellite results in an increasing bluish tint of the minerals. Sample P.12

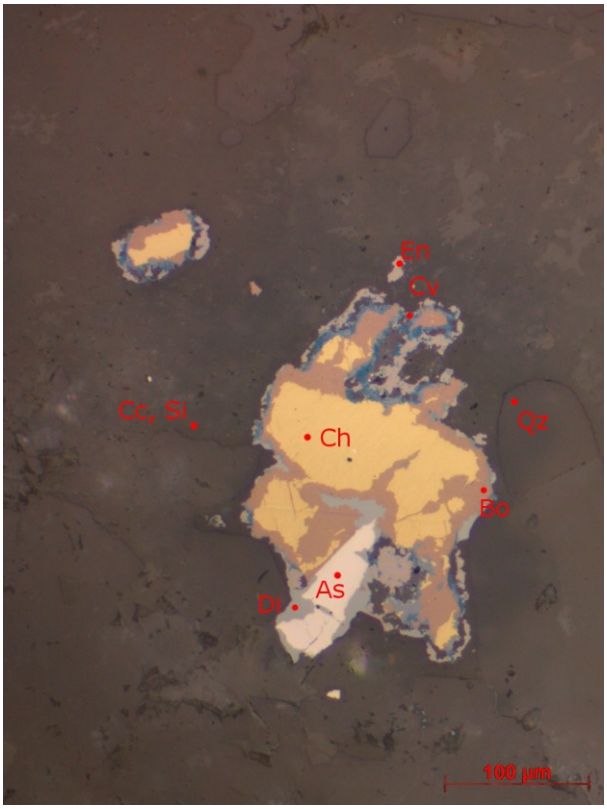

Fig. 58: Chalcopyrite and arsenopyrite replaced by bornite, digenite, bb. covellite and enargite. The matrix is calcite and quartz. Sample 78576

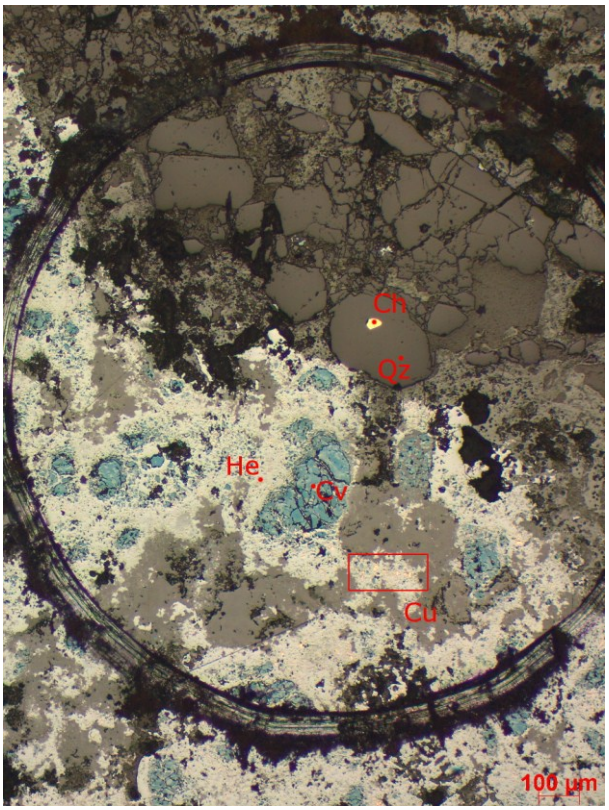

Fig. 59: Chalcopyrite inclusion in quartz crystal in association with hematite / Fe-hydroxides gangue native copper and bb. covellite. Sample P.21

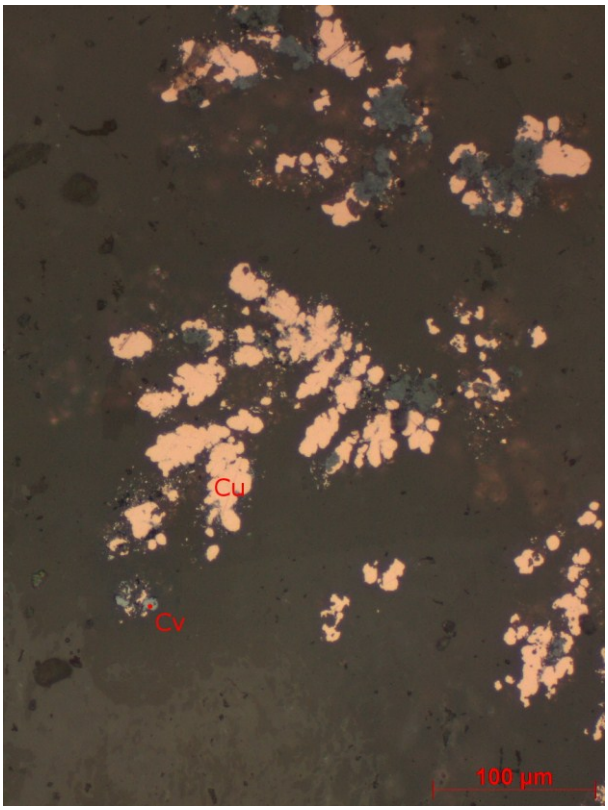

Fig. 60: Native copper with a skeletal / dendritic to fine “bloomy” morphology. Bb. covellite is intergrown with native copper. Sample P.1

8.2.4 Cu-rich arsenides, enargite and safflorite

Ore minerals briefly described in this chapter include domeykite, koutekite, enargite and safflorite. Two structural types of domeykite are known: The isotropic cubic (α-) and anisotropic hexagonal (β-) type. Another phase often intimately intergrown with domeykite is koutekite, an orthorhombic phase, which is also distinctly anisotropic. Moreover, the unequivocal microscopic discrimination of these phases is hampered by the quick staining of polished surfaces when exposed to air. For the clear distinction of these phases mineral chemical data (WDS analyses by EMPA) are therefore necessary (see chapter 9.3).

Domeykite and koutekite are typical for paragenetic Stage 2. They are commonly associated with carbonate gangue. Domeykite and koutekite form irregular aggregates of different shape. They occur in a reticulate network of micro-fractures or irregular “reef like” aggregates; there these phases are often porous (Fig. 61). In other sections they rather form irregular patches composed of anhedral domeykite/koutekite intergrowths. Both minerals show strong oxidation effects on the polished sections. The reflectance decreases and the color changes from light-yellow in fresh material to gray-bluish rapidly, within a few hours after (re)-polishing (compare Fig. 61, Fig. 62). In some samples domeykite/koutekite are associated with native bismuth (Fig. 61, Fig. 62).

Enargite is an (early?) alteration phase of Stage 1 chalcopyrite and arsenopyrite (Fig. 63). Enargite has a very light pink-brown color with a rather weak pleochroism and a moderate anisotropy. It occurs in thin coronas around chalcopyrite (Fig. 63) and in micro-fractures. Some of these coronas are poly-phase including bornite, digenite and covellite (Fig. 58) and eventually fahlores (Fig. 63).

Safflorite was only observed in sample 78566, where it is associated with chalcopyrite. Tiny eu- to subhedral safflorite crystals forms elongate aggregates. Locally star-shaped arrangements of safflorite crystals are visible (Fig. 64). Safflorite has a nearly pure white color and high reflectance with a distinct pleochroism under crossed polars. The color is whiter then that of arsenopyrite. The anisotropy is rather strong with colors varying from bluish-grey to dark brown.

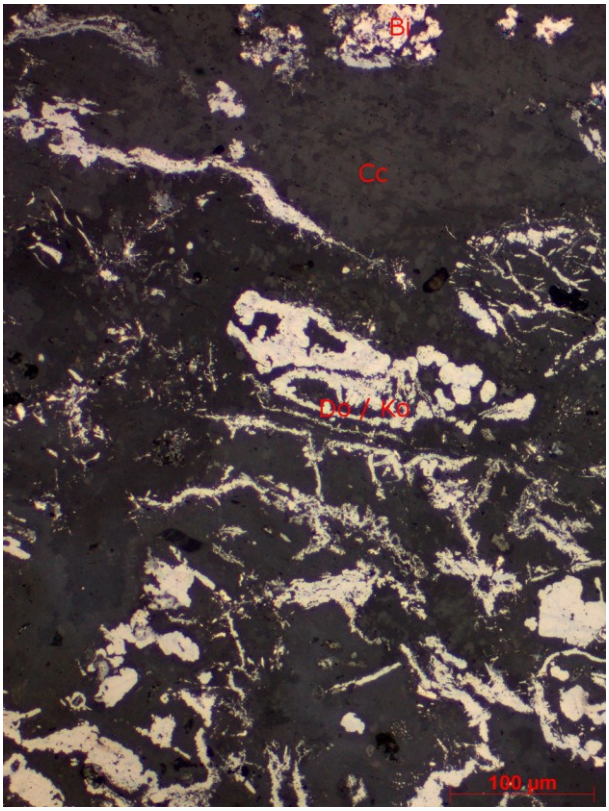

Fig. 61: Domeykite / koutekite with native bismuth in a reticulate network and “reef-like” forms in carbonate gangue. Sample P.18; freshly polished

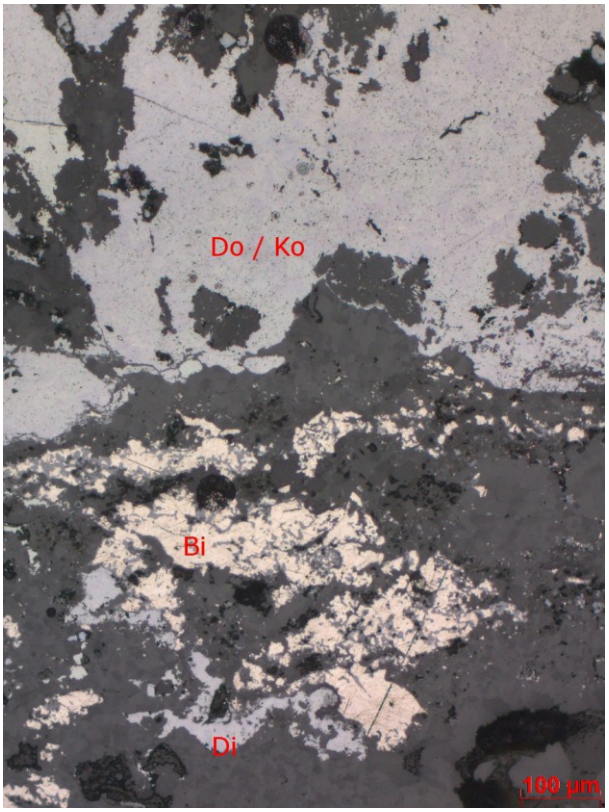

Fig. 62: Domeykite / koutekite intergrowth with native bismuth and digenite in carbonate gangue. Sample P.18, few days after polishing

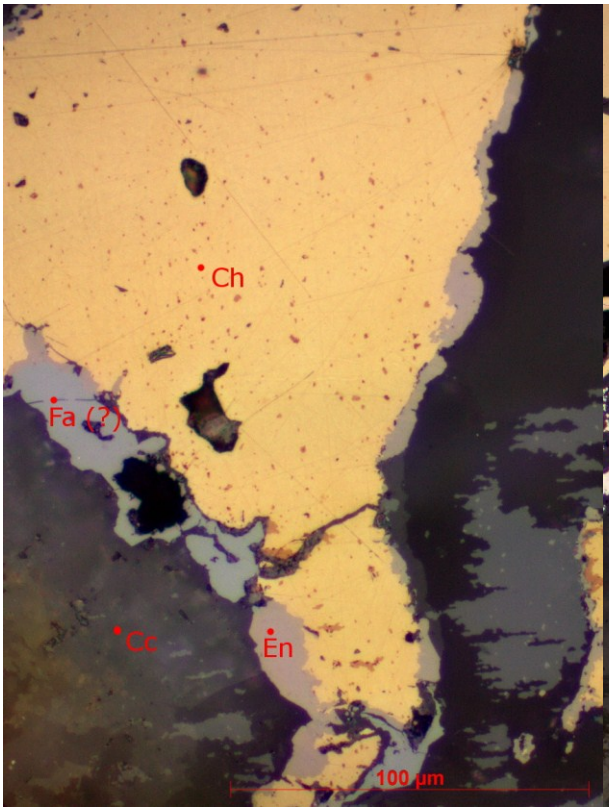

Fig. 63: Enargite and fahlore (?) forming a corona around chalcopyrite. Fa … possible fahlore, Sample J.03

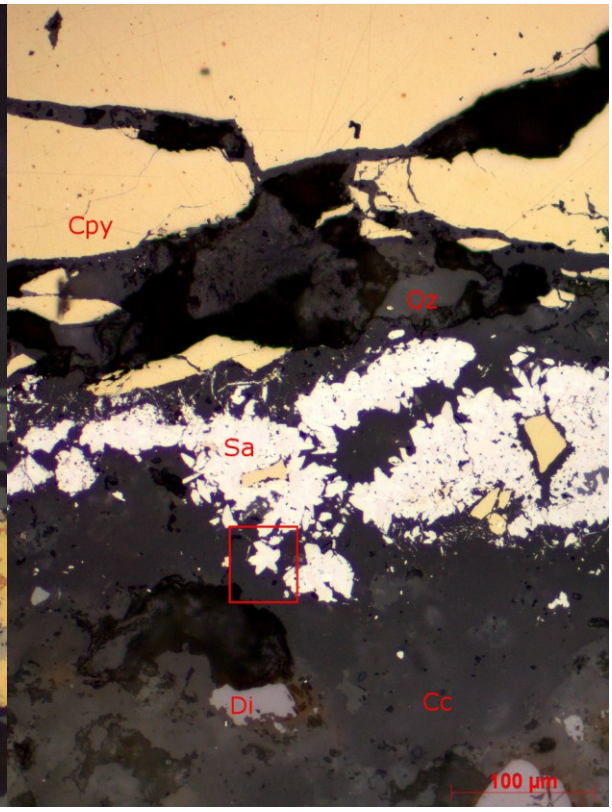

Fig. 64: Safflorite, chalcopyrite (partly cataclastic) and minor digenite in a carbonate-quartz matrix. The red box marks star-shaped euhedral safflorite intergrowths. Sample 78566

8.2.5 Native bismuth and bismuth sulfosalts

Bismuth minerals found in the samples include native bismuth, bismuthite and rare Bi-sulfosaltes like matildite. Native bismuth shows a creamy white color and high reflectance (Fig. 65). When exposed to air it quickly obtains a reddish tarnish. The anisotropy is distinct but often masked by polishing scratches because of its softness. Native bismuth was observed in all three paragenetic Stages, mainly in carbonate and oxides/hydroxides gangue, either finely disseminated or in larger (up to 1 x 6 mm) irregular micro-areas. It is quite common in sections containing the Stage 2 assemblage; i.e. associated with digenite, anilite and domeykite/koutekite (Figs. 57, 61, 62, 65). In few cases it is associated with native gold, matildite and bismuthinite and the primary (Stage 1) sulfides chalcopyrite, pyrite and arsenopyrite (Fig. 65).

Two bismuth sulfosalts are found in the sections; matildite and bismuthinite.
Matildite forms approximately 20μm polymineralic grains with native bismuth (Fig. 66). It shows a white color and a weak pleochroism, which is not always visible because of the small grain size and is intimate intergrowth with native bismuth. The identification of this phase was confirmed by WDS analyses on the EMPA (see chapter 9.4).
Bismuthinite shows a white color with a slight yellow shade, a strong pleochroism and a high reflectance. The anisotropy is strong (yellow-green to lighter green tints). In the two samples where it was observed it is always associated with native bismuth.

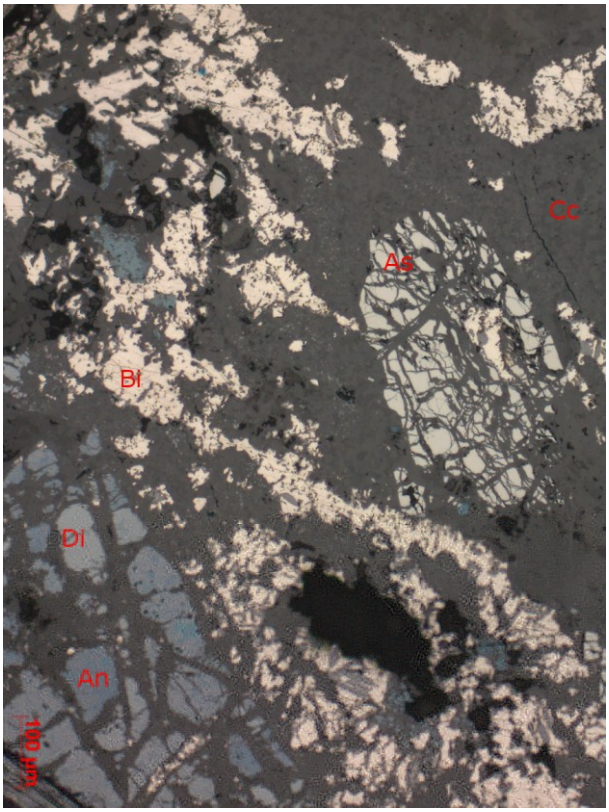

Fig. 65 Large aggregations of native bismuth intergrown with Cu-rich minerals and arsenopyrite in carbonate gangue. Sample P.18

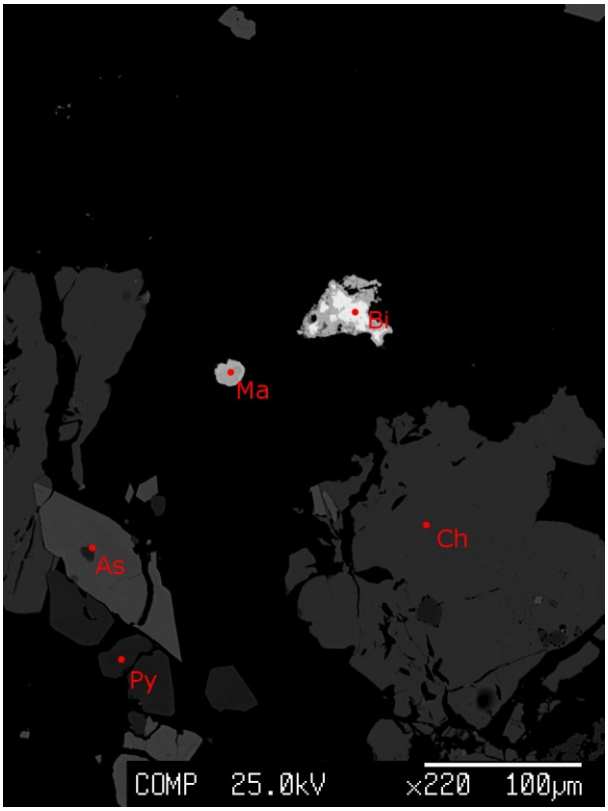

Fig. 66 Back-scatterd electron image of matildite (as single grain and intergrown with native bismuth) with primary sulfides in carbonate gangue (black). Sample 78568

8.2.6 Native gold

Mineral assemblage with gold

Gold occurs as bright yellow grains with diagnostic very high reflectance, color and softness. It is isotropic, but it never becomes completely dark under crossed nicols, commonly a greenish shade is observed. Larger gold grains always shows scratches on the polished surface because of its softness. These scratches may superimpose the isotropy and cause a sort of a pseudo-anisotropy.

Gold has been documented in all 3 paragenetic Stages.

In the Stage 1, gold occurs together with chalcopyrite and arsenopyrite, often found at the grain boundaries of these two minerals (Fig. 67, Fig. 68). It also occurs in fractures refilled with gangue. In some cases, gold occurs in clusters of grains of very variable grain size. The shapes are commonly irregular. Gold in this Stage shows composition of Au/Ag from nearly pure gold 95/5 to ~70-80/20-30 (see chapter 0). Silver-rich gold (electrum) is rare.

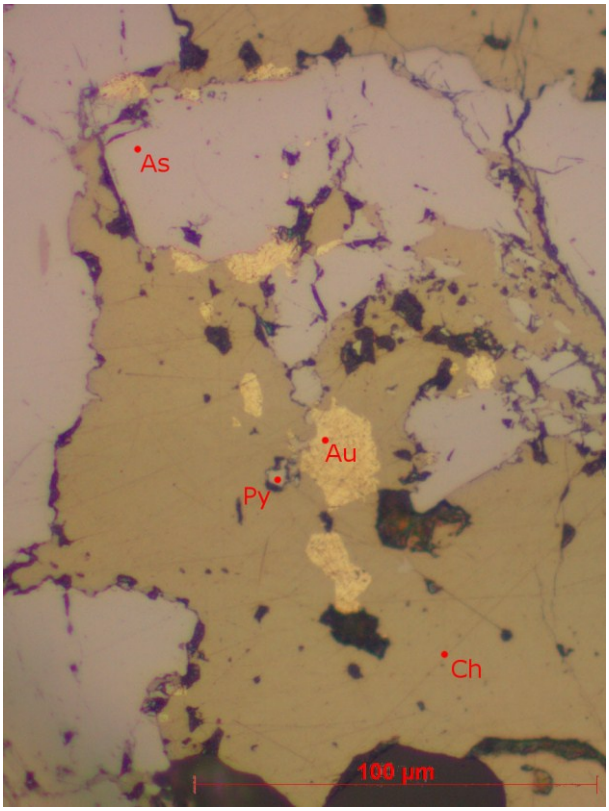

Fig. 68: Gold with chalcopyrite and arsenopyrite. Sample 78568

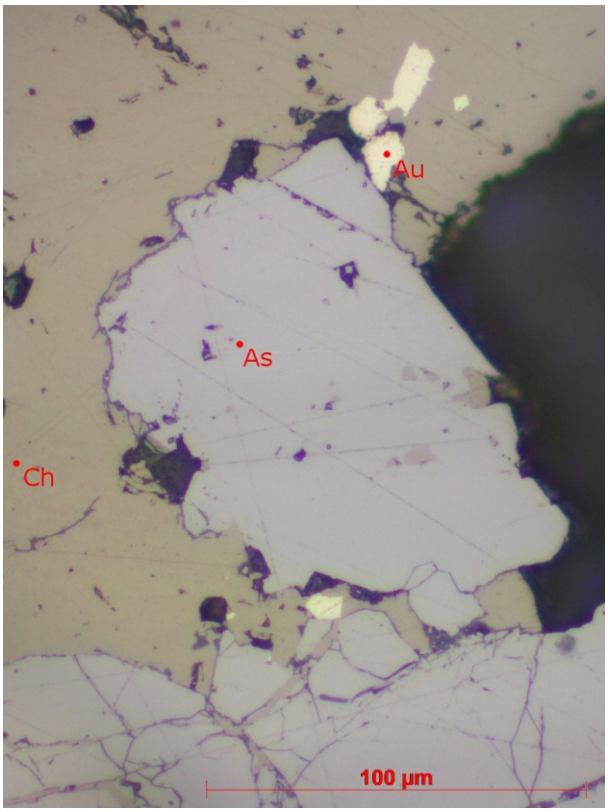

Fig. 67: Gold occurring at the grain boundaries between chalcopyrite and arsenopyrite and within chalcopyrite. Sample J.05

Gold in paragenetic Stage 2 occurs primarily in the carbonate gangue together with digenite (containing relicts of pyrite), domeykite/koutekite and native bismuth (Fig. 69). However, only in few cases it is observed in direct contact with the Cu-rich sulfides such as digenite (Fig. 70). Gold commonly is of rounded to angular shape. Two types of gold can be distinguished: larger gold grains with >Au/Ag and smaller ones with <Au/Ag (see chapter 0).

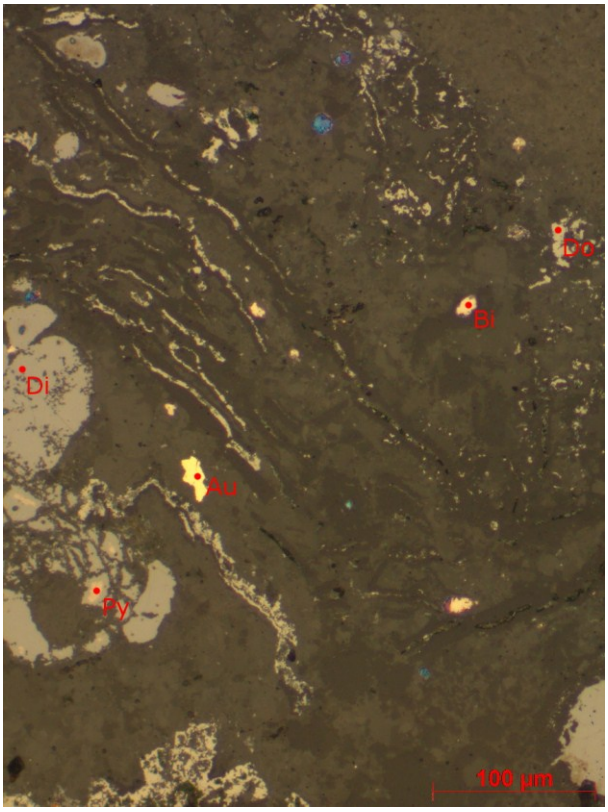

Fig. 69: Gold and native bismuth in carbonate gangue with Stage 2 Cu-sulfides and -arsenides. Gold is slightly brighter than native bismuth. Pyrite is replaced by digenite. Domeykite occurs in reef-like stringers. Sample P.10

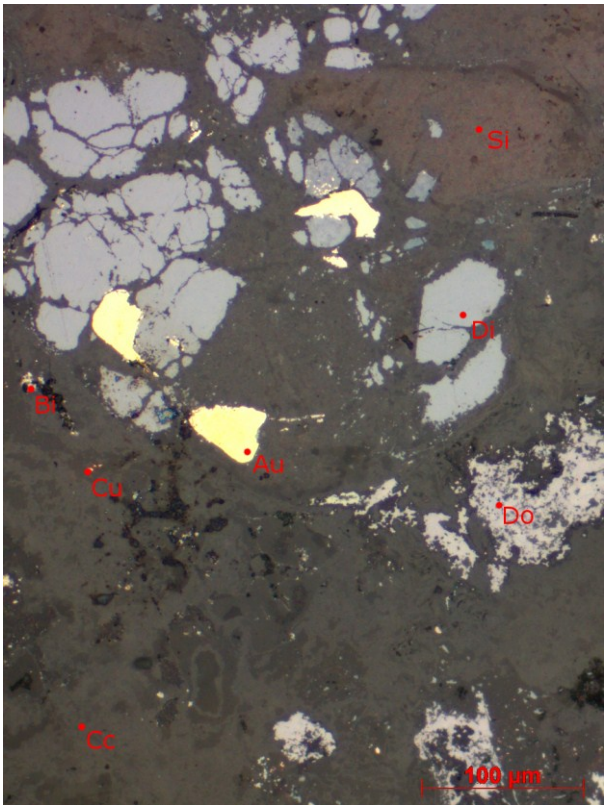

Fig. 70: Larger rounded to angular gold grains intergrown with digenite. Other phases present are domeykite, native bismuth, native copper and carbonate-quartz gangue. Sample P.07

In Stage 3, gold mainly occurs in patchy clusters to linear arrays consisting of multiple small grains in the oxide/hydroxide matrix. The assemblage includes various oxide-hydroxides, which have not been studied in detail. Hematite (confirmed by Laser-Raman spectroscopy) is a common mineral in this assemblage. In sample P.22 it can be documented that this oxide-hydroxide assemblage formed by replacement of Cu-sulfides. There, covellite which replaced another Cu-rich sulfide is partly preserved (Figs. 71, 72). Gold in this Stage is electrum and has higher Hg contents (see chapter 0).

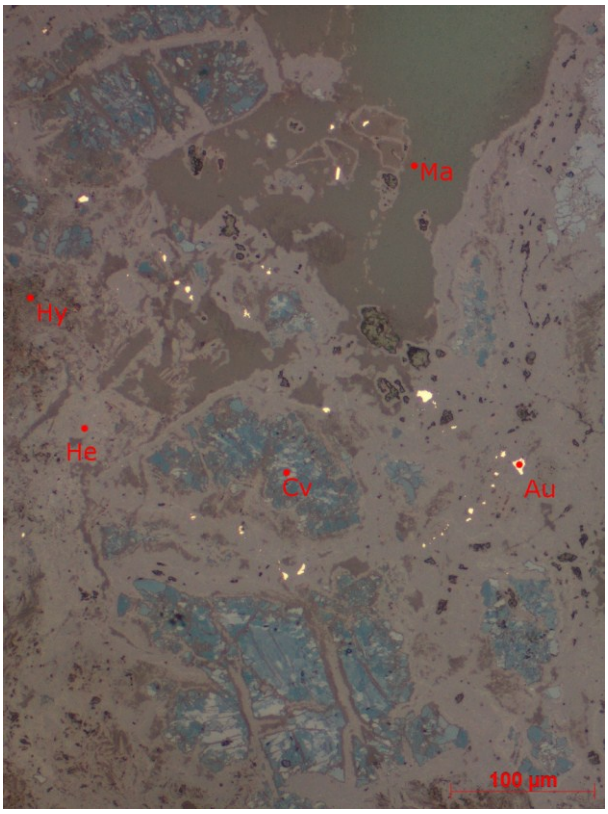

Fig. 71: Cluster of small gold grains in hematite / malachite matrix. Covellite forms pseudomorphs after a higher-temperature Cu-(Fe?)-sulfide and is itself replaced by the oxide assemblage. Sample P.22

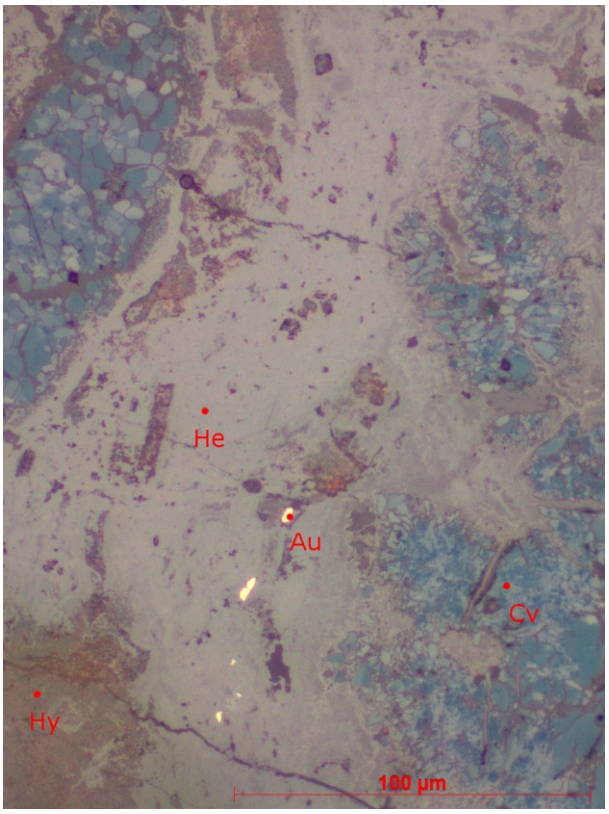

Fig. 72: Gold in hematite / Fe-hydroxide matrix. Gold occurs in the middle of the fracture filled with these phases, which replace covellite. Sample P.22

Gold grain size

The grain size distribution of gold from the three paragenetic Stages is shown in Fig. 73. In the box plot are plotted the maximum length measured for each grain under the microscope. Most grains are assigned to gold of Stage 1 (402 grains), followed by Stage 3 (74 grains) and Stage 2 (53 grains).

The median grain size of Stage 1 is 4.8 µm. It must be noted that there is a large number of grains plotting outside the box toward larger grain sizes. The lower quartile is 2.8 µm; the upper quartile is 10.6µm.

Gold from Stage 2 seems to be slightly coarser-grained; the median is 13.7 μm although because of the smaller number of measured grains the uncertainly is larger and there is a considerable overlap with Stage 1 gold. The lower quartile is 6.0 μm; the upper quartile is 23.9 μm. Gold of Stage 3 is on average finer grained. The median is 5.2 μm; the lower quartile is 2.5 μm; the upper quartile is 6.1 μm.

The maximum grain size of Stage 3 gold is 22 μm. In summary we can conclude that mean values of Stages 1 and 3 are comparable. Gold of Stage 2 is slightly coarser grained. Larger gold grains with sizes > ~20 μm are restricted to Stages 1 and 2.

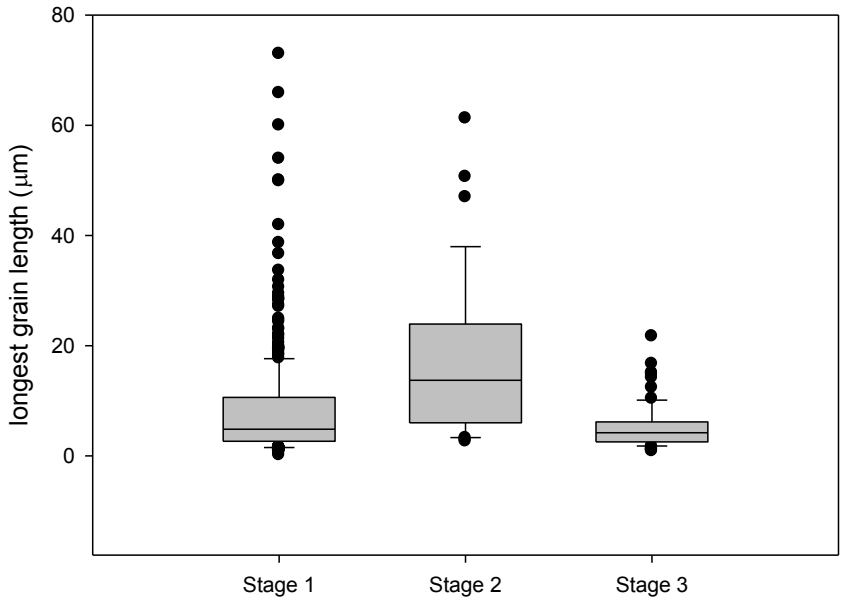

Fig. 73: Box plot of measured grain size of gold in the ore samples

8.2.7 Gangue minerals

The minerals with low reflectance in reflected light are referred to as gangue phases. These phases include various carbonates and quartz. The oxide/hydroxide assemblage of Stage 3 is also included in the description of the gangue phases, although it likely represents a supergene assemblage formed during weathering of the primary sulfide-rich ores.

Carbonate gangue

The following carbonate minerals were identified: Calcite, dolomite, Ca-Fe-(Mg) carbonate (ankerite?) and hydrated carbonates like malachite.

Calcite: Coarse-grained sparry calcite is the dominant carbonate in Stage 1 ores containing the primary Fe-rich sulfide – Au assemblage. It is commonly associated with variable

amounts of early hydrothermal quartz. Calcite gangue occurs in the paragenetic Stage 1 and as in fractures in Stage 2. Calcite is also present in healed (micro-) fractures, which crosscut pyrite, arsenopyrite and quartz.

Dolomite: Dolomite has been observed in association with the other carbonates in samples of the Stage 2. It forms anhedral relicts, which are replaced by a Ca-Fe-(Mg) carbonate.

Fe-Ca-(Mg) carbonate: The replacement of dolomite (Fe-poor) and calcite by a Ca-Fe-(Mg) phase is documented in several samples of Stage 2. The EDS spectra of this phase show a rather consistent Fe:Ca distribution and low Mg. Because the Ca content is significant and it looks rather homogeneous in BSE images we interpret this phase as a Ca-Fe-(Mg) carbonate phase. It could either be a calcian siderite or a Fe-dominated member of the dolomite series; i.e. ankerite. The name calcian siderite refers to siderite containing up to 20 mol% of calcite (http://www.mindat.org/min-7501.html). More detailed investigations would be necessary to fully characterize this phase.

Malachite is the most common carbonate in the paragenetic Stage 3. It shows the typical green color and occurs together with other carbonates (calcite, dolomite) and with oxide/hydroxides (see below).

Quartz gangue

Quartz is present in all three paragenetic Stages. A first type of hydrothermal vein quartz often forms anhedral to euhedral grains. It is in contact with the primary sulfides and calcite but it also may contain inclusions of chalcopyrite, allocasite, galena and sphalerite.

Very peculiar are euhedral quartz crystals, which are commonly associated with sparry calcite and ore minerals like chalcopyrite. The latter is also present as minute inclusions in this euhedral quartz (see chapter 8.1.6). From these observations we conclude that quartz formed coeval with the main primary sulfides pyrite, arsenopyrite, chalcopyrite etc., eventually even outlasting their crystallization.

In some samples, quartz is replaced by carbonates (Ca-Fe-(Mg) carbonate ?) belonging to paragenetic Stage 2. Preserved rims/coronas of ore minerals (pyrite, bb. covellite) outline the former shape of the replaced quartz grains that have been replaced by carbonate.

Oxides and hydroxides

The following oxides have been identified microscopically and were confirmed by other methods (EDS, Laser Raman spectroscopy): Hematite, magnetite, cuprite, rutile, titanite, and ilmenite. Rutile occurs as common accessory minerals in Stage 1 vein. Titanite is an accessory mineral in the carbonate-sericite alteration assemblage.

Hematite (confirmed by Raman) is one of the dominant minerals in the oxidized paragenetic Stage 3. It is associated with poorly characterized Fe-(Al) hydroxides (goethite, lepidokrokite, “limonite, ferrihydrite etc.) and commonly replaces Stage 2 Cu-rich sulfides and –arsenides (see above). Cuprite has also been confirmed by Raman. It is intergrown with or replaces native copper in paragenetic Stage 3.

9 Mineral chemical composition

9.1 Pyrite, arsenopyrite and chalcopyrite

Only few analyses were made from the Fe-richer sulfides pyrite, arsenopyrite (Table 12) and chalcopyrite (Table 13). Pyrite composition is non-stoichiometric with a small sulfur deficiency. It contains up to 4 mass% Cu and 2.4 mass% As. The higher As values could be incorporated in pyrite. The higher Cu values likely are due to beginning replacement of pyrite by Cu sulfides (see chapter 8.2). Arsenopyrite composition is also non-ideal; it contains more sulfur than arsenic.

Table 12: Mineral chemical composition of pyrite and arsenopyrite

Spot no.	P.12kr4-2	P.18kr4-a1	J.03-16	P.1kr4-a1	P.18kr4-a4	J.03-25
	$Fe_{1.01}S_2$ Pyrite	**$Fe_{1.05}S_2$ Pyrite**	**$Fe_{1.02}S_2$ Pyrite**	**$Fe_{0.95}As_{0.86}S_{1.14}$ Arsenopyrite**	**$Fe_{1.01}As_{0.89}S_{1.1}$ Arsenopyrite**	**$Fe_{1.01}As_{0.86}S_{1.14}$ Arsenopyrite**
Mass%						
Fe	45.32	44.24	46.90	33.39	36.11	34.91
Cu	2.01	4.01	1.21	0.77	0.21	0.00
S	51.25	48.54	52.88	22.99	22.70	22.37
As	1.93	2.40	bld	40.36	42.66	39.61
total	100.51	99.23	100.99	97.55	101.72	96.89
Ions calculated on the basis Σ of S = 2				**Ions calculated on the basis of Σ As+S = 2**		
Fe	1.015	1.046	1.018	0.952	1.012	1.019
Cu	0.040	0.083	0.023	0.019	0.005	0.000
S	2.000	2.000	2.000	1.142	1.109	1.138
As	0.032	0.042	0.000	0.858	0.891	0.862

bld … below limit of dedection

Chalcopyrite was only measured in the samples collected by Jarlowsky / Universalmuseum Joanneum. The chemical composition is nearly ideal (Table 13).

Table 13: Mineral chemical composition of chalcopyrite

Spot no.	J.03-1	J.03-4	J.03-14	J.03-20
	$Cu_{0.99}Fe_{0.99}S_2$ Chalcopyrite	**$CuFeS_2$ Chalcopyrite**	**$Cu_{0.98}FeS_2$ Chalcopyrite**	**$Cu_{0.99}FeS_2$ Chalcopyrite**
Mass%				
Fe	30.71	30.53	30.08	30.58
Cu	34.99	35.09	35.08	35.28
S	35.63	35.19	35.18	35.57
As	bld	bld	bld	bld
Total	101.33	100.82	100.35	101.43
Ions calculated on the basis of Σ S = 2				
Fe	0.990	0.996	0.982	0.987
Cu	0.991	1.006	1.006	1.001
S	2.000	2.000	2.000	2.000
As	0.000	0.000	0.000	0.000

bld … below limit of dedection

9.2 Cu_xS (2<x<1) minerals

Minerals: digenite, anilite, geerite, spinkopite and yarrowite (blaubleibender covelite)

In the Cu-S system, the main minerals distinguished on the basis of their Cu:S ratio are digenite, anilite and yarrowite (Fig. 74). Other less common Cu sulfides include djurleite, geerite (Table 14) and spinkopite(?).

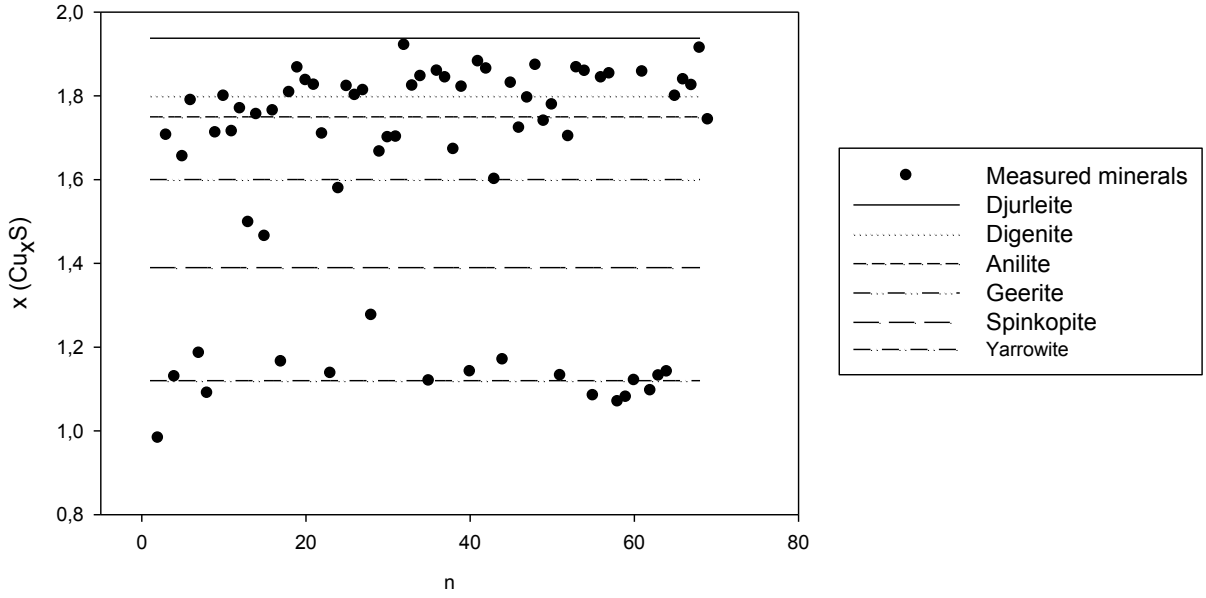

Fig. 74: Variation of Cu:S ratios in the analyzed Cu sulfides; normalized to one sulfur

Table 14: Chemical composition of djurleite and geerite

Spot no.	P.12kr1-10	P.1kr1-a1	P.7kr2-1	P.7kr4-7	P.12kr4-1
	$Cu_{1.91}S$	**$Cu_{1.92}S$**	**$Cu_{1.58}S$**	**$Cu_{1.65}S$**	**$Cu_{1.6}S$**
	Djurleite	**Djurleite**	**Geerite**	**Geerite**	**Geerite**
Mass%					
Fe	1.63	bld	0.54	0.81	3.71
Cu	77.77	79.56	76.81	76.97	73.25
S	20.50	20.90	24.55	23.47	23.09
As	0.38	bld	bld	bld	0.80
Total	100.28	100.58	102.05	101.39	100.85
Ions calculated on the basis of 1 S					
Fe	0.046	bld	0.013	0.020	0.092
Cu	1.914	1.921	1.578	1.655	1.601
S	1.000	1.000	1.000	1.000	1.000
As	0.008	bld	bld	bld	0.015

bld … below limit of dedection

Table 15: Chemical composition of digenite, anilite and yarrowite (bb. covelite)

Spot no.	P.12kr1-7	P.12kr1-18	P.12kr2-3	P.12kr2-4	P.12kr3-16	P.12kr4-7
	$Cu_{1.86}S$ Digenite	**$Cu_{1.8}S$ Digenite**	**$Cu_{1.85}S$ Digenite**	**$Cu_{1.84}S$ Digenite**	**$Cu_{1.78}S$ Digenite**	**$Cu_{1.82}S$ Digenite**
Mass%						
Fe	2.59	3.45	2.56	2.51	2.71	0.39
Cu	78.61	77.30	78.28	77.96	77.20	78.67
S	21.36	21.68	21.32	21.34	21.90	21.80
As	bld	bld	0.19	0.17	0.08	0.24
Total	102.56	102.43	102.35	101.98	101.89	101.10
Ions calculated on the basis of 1 S						
Fe	0.070	0.091	0.069	0.068	0.071	0.010
Cu	1.857	1.799	1.852	1.843	1.778	1.821
S	1.000	1.000	1.000	1.000	1.000	1.000
As	bld	bld	0.004	0.003	0.001	0.005

Spot no.	P.7kr2-3	P.7kr4-9	P.7kr3-7	P.12kr1-1	P.12kr3-5	P.12kr3-17
	$Cu_{1.71}S$ Anilite	**$Cu_{1.71}S$ Anilite**	**$Cu_{1.77}S$ Anilite**	**$Cu_{1.74}S$ Anilite**	**$Cu_{1.72}S$ Anilite**	**$Cu_{1.74}S$ Anilite**
Mass%						
Fe	1.05	1.51	1.67	2.39	1.17	2.67
Cu	77.40	77.57	77.82	75.62	77.48	76.57
S	22.85	22.94	22.19	21.89	22.69	22.21
As	0.07	bld	bld	0.09	bld	0.16
Total	101.37	102.02	101.68	99.99	101.34	101.61
Ions calculated on the basis of 1 S						
Fe	0.026	0.038	0.043	0.063	0.030	0.069
Cu	1.709	1.706	1.769	1.743	1.723	1.739
S	1.000	1.000	1.000	1.000	1.000	1.000
As	0.001	0.000	0.000	0.002	0.000	0.003

Spot no.	p7kr2-2	p7kr3-10	p12kr1-4	p12kr1-9	p12kr2-1	p12kr3-15
	$Cu_{1.14}S$ Yarrowite	**$Cu_{1.17}S$ Yarrowite**	**$Cu_{1.13}S$ Yarrowite**	**$Cu_{1.12}S$ Yarrowite**	**$Cu_{1.08}S$ Yarrowite**	**$Cu_{1.13}S$ Yarrowite**
Mass%						
Fe	2.28	1.32	1.49	0.65	0.86	1.86
Cu	68.56	69.88	68.94	69.30	68.45	68.99
S	30.42	30.26	30.75	31.21	31.97	30.75
As	bld	bld	0.07	0.13	0.09	bld
Total	101.26	101.49	101.25	101.30	101.37	101.60
Ions calculated on the basis of 1 S						
Fe	0.043	0.025	0.028	0.012	0.015	0.035
Cu	1.137	1.165	1.131	1.120	1.080	1.132
S	1.000	1.000	1.000	1.000	1.000	1.000
As	0.000	0.000	0.001	0.002	0.001	0.000

9.3 Domeykite, koutekite and enargite

The two Cu-arsenides identified in several samples are domeykite and koutekite (Table 16). These two minerals cannot be distinguished easily in the microscopie and also show a continuous variation of their Cu:As ratio. A threshold value of 2.6 was used to discriminate between these two phases; accordingly, analyses with Cu:As > 2.6 are referred to as domeykite, those with Cu:As < 2.6 as koutekite (Fig. 17). One must be aware that this likely is an arbitrary discrimination because there seems to exist a continuous series (Table 16). Both minerals may contain minor amounts of Fe but are S-free.

Table 16: Mineral chemical composition of koutekite and domeykite

Spot no.	P.18kr8-a3	P.18kr6-a1	P.12kr1-11	P.18kr6-a2	P.7kr2-7	P.12kr1-8
	$Cu_{5.04}As_2$ Koutekite	**Cu_5As_2 Koutekite**	**$Cu_{5.17}As_2$ Koutekite**	**$Cu_{2.73}As$ Domeykite**	**$Cu_{2.76}As$ Domeykite**	**$Cu_{2.89}As$ Domeykite**
Mass%						
Fe	2.48	bld	1.30	0.46	1.10	1.17
Cu	67.11	68.44	66.12	69.29	68.40	68.96
S	0.05	bld	0.03	0.00	0.01	0.01
As	31.42	32.29	30.15	29.92	29.26	28.17
Total	101.17	100.78	97.60	99.87	98.77	98.31
Calculation on the basis of 2As (koutekite) and 1As (domeykite), respectively						
Fe	0.212	0.000	0.116	0.020	0.050	0.056
Cu	5.027	4,998	5.171	2.730	2.756	2.886
S	0.007	0.000	0.004	0.000	0.001	0.001
As	2.000	2.000	2.000	1.000	1.000	1.000

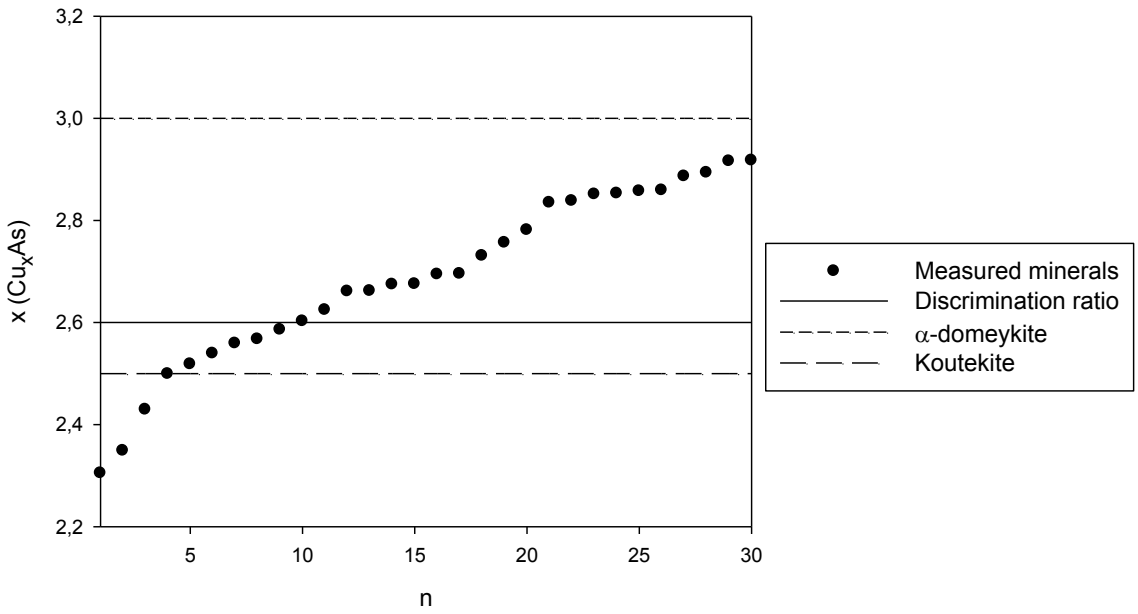

Fig. 75: Variation of the Cu:As ratio in the analyzed Cu-arsenides (domeykite and koutekite); normalized to one As. A threshold value of 2.6 was used for discriminating between these two phases. β-domeykite will be plot between 2.6 and 3.

Enargite was detected in the sample set of Jarlowsky / Universalmuseum Joanneum. The chemical composition is non ideal with a high Fe content. The ratio of Cu and S shows signification variation and is maybe influenced by near chalcopyrite.

Table 17: Mineral chemical composition of enargite; Pb was measured but was always below the limit of detection.

Spot no.	J.03-5	J.03-9	J.03-13	J.03-10
	$Cu_{3.14}As_{0.99}S_4$	**$Cu_{3.35}As_{1.07}S_4$**	**$Cu_{3.24}As_{0.99}S_4$**	**$Cu_{2.92}As_{0.89}S_4$**
	Enargite	**Enargite**	**Enargite**	**Enargite**
Mass%				
Fe	7.11	2.69	3.81	0.15
Cu	45.56	48.52	47.54	48.34
S	29.33	29.26	29.59	33.45
As	17.07	18.30	17.11	17.31
Total	99.07	98.77	98.05	99.25
Calculation on the basis of 4 S				
Fe	0.557	0.211	0.296	0.010
Cu	3.135	3.346	3.242	2.916
S	4.000	4.000	4.000	4.000
As	0.996	1.071	0.990	0.886

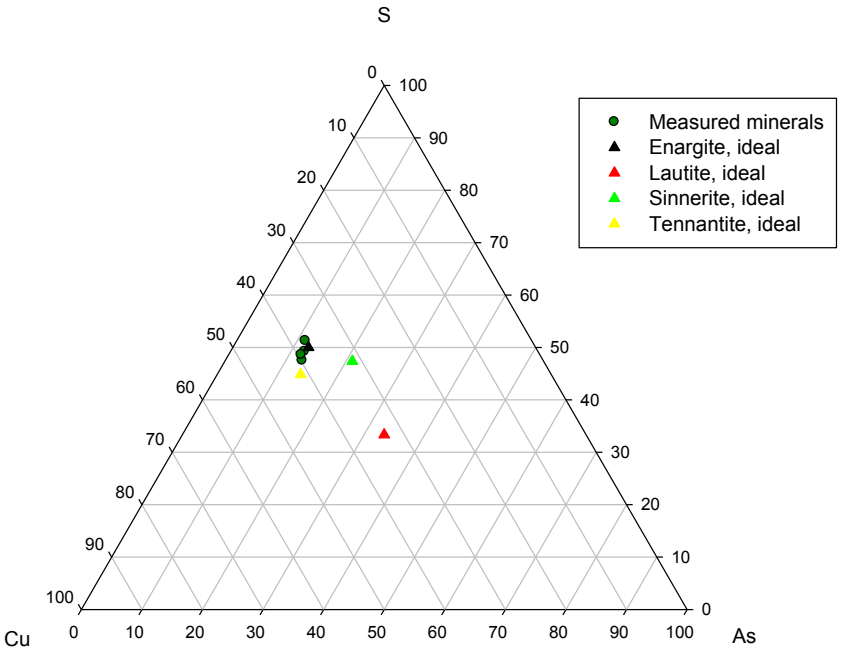

Fig. 76: Chemical composition of Cu-S-As phases. The analyses fit well with the ideal enargite composition.

9.4 Native bismuth, bismuthinite and matildite

Three bismuth phases can be distinguished by EMPA (Fig. 77, Table 18). There are: native bismuth, bismuthinite (Bi_2S_3) and matildite ($AgBiS_2$). The analyses of native bismuth are commonly close to 100 Mass% of Bi. The sulfur content in bismuthinite is slightly below the ideal stoichiometric values. Two analyses yielded 0.15 to 4.92 mass% of Sb.

The chemical composition of matildite is given in Table 18. The sulfur content is above the ideal formula. It contains 0.48 - 4.46 mass% Cu and 0.04 - 3.69 mass% Sb.

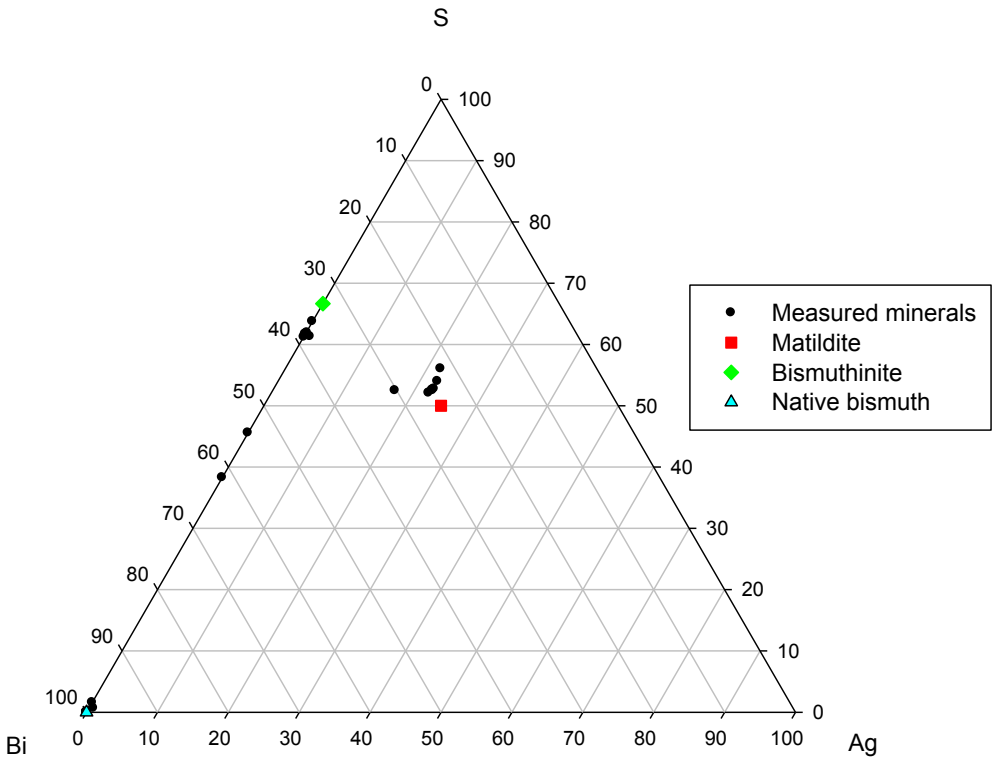

Fig. 77: Measured bismuth phases; green and red dots are the ideal composition of bismuthinite and matildite, respectively Pb was measured but not detected

Table 18: Chemical composition of native bismuth, bismuthinite and matildite.

Spot no.	P.18sulfo-20	78568sulfo-2	78568sulfo-6	78571sulfo-11	78568sulfo-1	78571sulfo-16
	Bi	**Bi**	**$Bi_{1.90}S_3$**	**$Bi_{1.84}S_3$**	**$Ag_{0.85}Bi_{0.95}S_2$**	**$Ag_{0.86}Bi_{0.95}S_2$**
	n. Bismuth	**n. Bismuth**	**Bismuthinite**	**Bismuthinite**	**Matildite**	**Matildite**
Mass(%)						
Pb	0.00	0.00	0.00	0.00	0.00	0.00
S	0.00	0.10	19.50	19.97	18.60	17.73
Fe	0.32	0.13	0.47	0.29	0.29	0.94
Sb	bld	bld	bld	0.39	3.69	bld
Cu	1.19	0.07	0.98	0.80	4.46	2.11
Ag	0.00	0.33	0.08	0.20	24.52	25.54
Bi	97.96	97.01	80.46	79.77	47.64	54.79
Total	99.47	97.66	101.64	101.42	99.20	101.11
Ions calculated on the basis of: n. bismuth 1 Bi, bismuthinite 3 S, Matildite 2 S						
Pb	0.000	0.000	0.000	0.000	0.000	0.000
S	0.000	0.007	3.000	3.000	2.000	2.000
Fe	0.012	0.005	0.041	0.025	0.018	0.061
Sb	0.000	0.000	0.006	0.015	0.104	0.000
Cu	0.040	0.002	0.076	0.061	0.242	0.120
Ag	0.000	0.007	0.004	0.009	0.784	0.856
Bi	1.000	1.000	1.899	1.838	0.786	0.948

9.5 Gold

Gold of the following samples has been analyzed with at the EMPA: P.7, P.10, P.12, P.15, P.18, P.22, 78562, 78568, 78569, 78573, J.04, J.05.

The mineral chemical composition of gold in the different samples is illustrated in Fig. 78; analyses are listed in Table 19 and Table 20. The analyses confirm the petrographic distinction of at least two generations of gold.

Table 19: Chemical composition of gold sample set Prof. W. Paar

Sample P.7

Spot no.	P.7KR4-1	P.7KR3-1	P.7KR3-2	P.7KR3-3	P.7KR3-4
Au	93.52	74.17	77.33	74.06	68.55
Hg	0.45	2.95	2.55	2.35	0.52
Ag	5.92	23.21	20.74	22.04	27.26
Cu	0.48	0.24	0.04	2.23	1.56
Total	100.37	100.57	100.66	100.68	97.89

Sample P.10

Spot no.	P.10KR1-1	P.10KR3-1	P.10KR4-1	P.10KR4-2	P.10-AU-BI
Au	94.94	73.45	75.90	72.85	72.91
Ag	5.37	23.86	22.59	23.08	23.60
Hg	0.85	2.41	1.18	2.57	2.00
Cu	0.78	0.55	bld*	0.02	0.14
Total	101.94	100.27	99.67	98.52	98.65

Sample P.12

Spot no.	P.12KR2	P.12KR2-1	P.12KR2-2
Au	74.36	73.45	69.55
Ag	23.37	23.25	25.36
Hg	2.07	2.27	2.22
Cu	bld*	0.05	0.21
Total	99.80	99.02	97.34

Sample P.15

Spot no.	P.15kr5-1	P.15kr5-2	P.15kr6-1	P.15kr4-1	P.15kr1-1	P.15kr2-1
Au	93.38	91.38	67.09	73.11	74.35	93.32
Ag	5.75	5.95	31.54	23.32	22.68	6.05
Hg	0.57	0.37	1.12	2.78	2.54	0.35
Cu	0.13	0.42	0.62	0.79	0.30	0.15
Total	99.83	98.12	100.37	100.00	99.87	99.87

Sample P.15

Spot no.	P.15kr3-1
Au	75.73
Ag	21.37
Hg	2.33
Cu	0.05
Total	99.48

Sample P.18

Spot no.	P.18KR5-1	P.18KA	P.18KA2
Au	71.32	66.47	73.30
Ag	24.65	29.26	23.81
Hg	3.62	1.75	2.63
Cu	0.98	0.06	0.17
Total	100.57	97.54	99.91

Sample P.22

Spot no.	P.22kr4-1	P.22kr4-2	P.22kr4-3n	P.22kr4-cl1	P.22kr4-cl2	P.22kr3-1
Au	37.77	38.93	39.46	38.69	47.00	51.22
Ag	42.40	43.06	44.75	48.11	38.67	36.40
Hg	12.49	9.00	7.19	8.54	10.18	7.00
Cu	0.19	0.22	0.12	0.44	0.70	7.27
Total	92.85	91.21	91.52	95.78	96.55	101.89

Spot no.	P.22kr3-2	P.22kr2-1	P.22kr5-1	P.22kr4 o	P.22kr4oB1	P.22kr4oB2
Au	38.67	44.22	38.86	43.38	33.91	34.63
Ag	46.34	44.33	42.65	39.71	44.24	41.99
Hg	6.08	5.91	11.38	12.02	15.13	13.68
Cu	2.10	0.61	0.22	0.17	2.31	3.86
Total	93.19	95.07	93.11	95.28	95.59	94.16

Table 20: Chemical composition of gold sample set Universalmuseum Joanneum / Jarlowsky

Sample 78562

Spot no.	78562-1	78562-2	78562-3	78562-4	78562-5	78562-6
Hg	3.40	0.26	3.39	3.38	3.89	2.66
Ag	20.48	5.48	21.93	24.30	22.96	26.04
Au	76.50	95.22	74.56	71.09	71.95	69.73
Cu	0.07	0.06	0.46	0.38	0.20	0.09
Total	100.45	101.01	100.34	99.15	99.00	98.52

Sample 78568

Spot no.	78568-1	78568-2
Hg	3.88	7.44
Ag	30.84	40.49
Au	64.13	45.86
Cu	1.03	0.66
Total	99.88	94.45

Sample 78569

Spot no.	78569-4
Hg	8.34
Ag	47.36
Au	35.01
Cu	1.46
Total	92.17

Sample 78573

Spot no.	78573-1	78573-2	78573-3	78573-4	78573-5	78573-6	78573-7
Hg	3.84	2.07	1.44	3.36	2.82	2.01	1.98
Ag	15.94	19.84	21.71	19.23	19.97	21.73	12.03
Au	81.63	79.30	74.92	76.44	75.77	76.75	87.32
Cu	bld*	bld*	0.00	bld*	0.00	bld*	bld*
Total	101.41	101.21	98.07	99.03	98.56	100.49	101.33

Sample J.04

Spot no.	J.04-1	J.04-2	J.04-3	J.04-4
Hg	14.29	2.44	7.72	5.96
Ag	39.02	29.23	28.07	34.73
Au	40.55	63.64	64.10	56.50
Cu	1.66**	1.81**	0.14	0.28
Total	95.52	97.12	100.03	97.47

Sample J.05

Spot no.	J.05-1	J.05-2	J.05-3	J.05-4	J.05-5	J.05-6	J.05-7
Hg	3.37	3.65	4.07	3.79	3.13	3.70	2.76
Ag	20.46	23.02	29.33	23.28	25.83	23.14	23.39
Au	77.52	73.80	64.37	72.38	68.53	73.05	70.57
Cu	0.15	0.94	0.39	0.57	0.42	0.60	0.47
Total	101.50	101.41	98.16	100.02	97.91	100.49	97.19

Spot no.	J.05-8	J.05-9	J.05-10	J.05-11	J.05-12	J.05-13	J.05-14
Hg	3.32	3.62	3.17	3.90	3.98	3.50	3.72
Ag	26.51	23.64	26.03	26.61	23.51	25.33	24.28
Au	67.96	72.90	69.76	69.30	71.04	71.21	70.99
Cu	0.64	0.71	0.00	0.05	0.02	0.02	0.80
Total	98.43	100.87	98.96	99.86	98.55	100.06	99.79

*totals are too low due to small grain size of gold

**higher Cu contents likely are from Cu-rich matrix because of the small grain size of analyzed grains

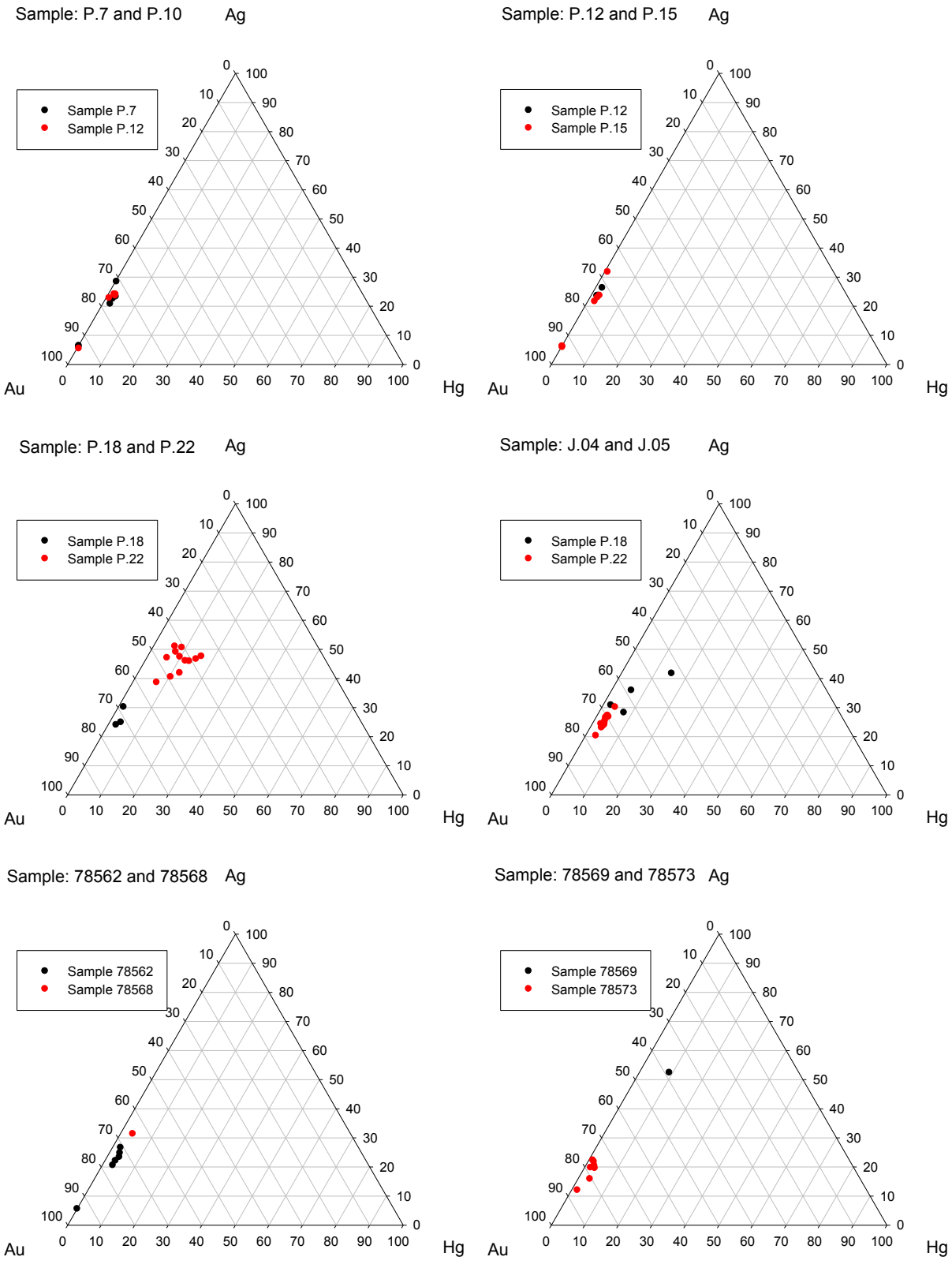

Fig. 78: Chemical composition of gold shown in Au-Ag-Hg triangular plots

Paragenetic Stages 1 and 2

In these two Stages 2 main gold compositions are found:

1. *Silver-rich gold to electrum, Hg-poor.* This group of analyses has a variable Au:Ag ratio with compositions ranging between $Au_{70-80}Ag_{20-30}$. A maximum of 7.6 mass% Hg was detected. This type of gold has been found in most samples. Mostly these grains are bigger (see chapter 8.2.6). The analyses of the sample 78573 show few analyses with a gold content up to 87 mass%.
2. *Pure gold*. A few analyses in samples P.7 and P.10 yielded high Au:Ag ratios ($Au_{95}Ag_5$). These analyses are very low in Hg

The chemical composition of both Stages is quite similar. Stage 1 gold grains show wider composition variation and sometimes a higher Hg content (Fig. 79). Data form Stage 2 overlap with those from Stage 1 (Fig. 80).

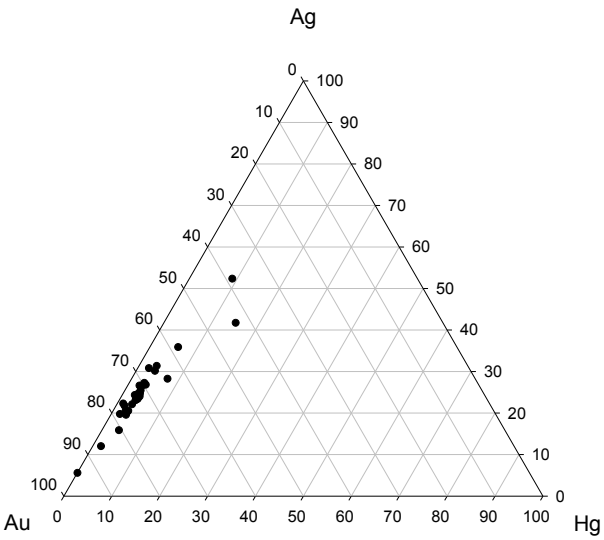

Fig. 79: Gold composition of Stage 1

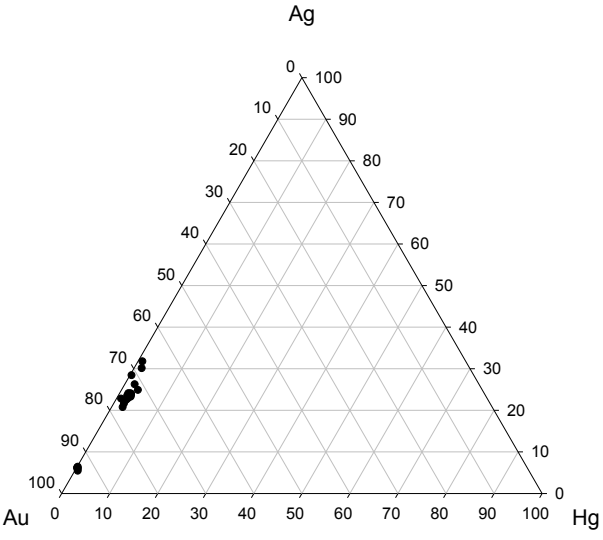

Fig. 80: Gold composition of Stage 2

Chemical composition of gold in Stage 3

Gold grains of this Stage were only found in sample P.22. The compositional variation is illustrated in Fig. 81. Generally, gold of Stage 3 can be described as Hg-rich electrum.

Gold contains up to 18 mass% Hg with a Au:Ag ratio of approximately 1:1. Most of these gold grains are very small (see chapter 8.2.6 Gold grain size). Only few grains were big enough for high quality measurements. Therefore the totals of many analyses are well below 100 mass%.

In contrast to gold of Stages 1 and 2 the Hg- and Ag content is significantly increased.

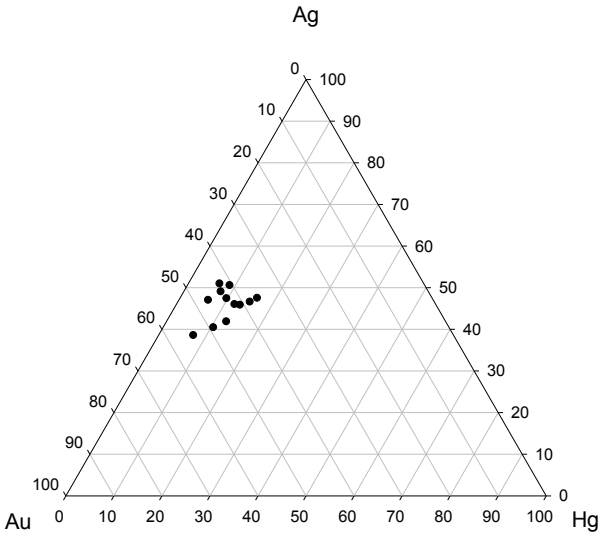

Fig. 81: Gold composition of Stage 3

9.6 Element mapping

Sample P.7

In Fig. 82 and Fig. 83 the results of element mapping of sample P.7 are shown. It demonstrates the elemental distribution within a gold-bearing micro-area (~1600μm²) and illustrates the complex micro-texture on this scale.

Several gold grains are present (white on CP image / back scattered electron image). The gold distribution shows a decrease of gold concentrations towards the rims of the grains (Fig. 82; corresponding to an increase in Ag, not shown).

Cu sulfides (digenite etc.) are characterized by medium gray color in the back scattered image and high combined Cu and S signals. The Cu arsenides domeykite and koutekite are characterized by combined high Cu and As contents. The different gangue phases (dolomite, calcite and calcian siderite) of the gangue matrix have variable concentrations of Ca, Mg, Fe, Si, O and C.

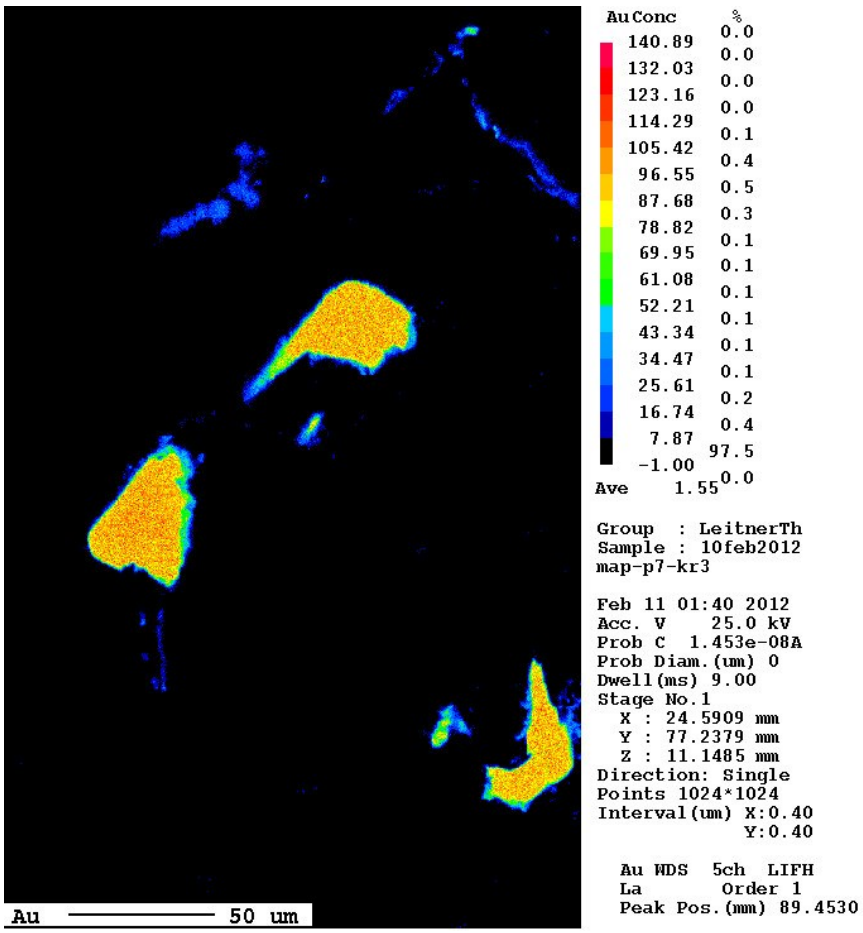

Fig. 82: Gold distribution in gold grains. Ag rich rims(blue-green) form around Ag-poor gold (yellow-red). Sample P.7

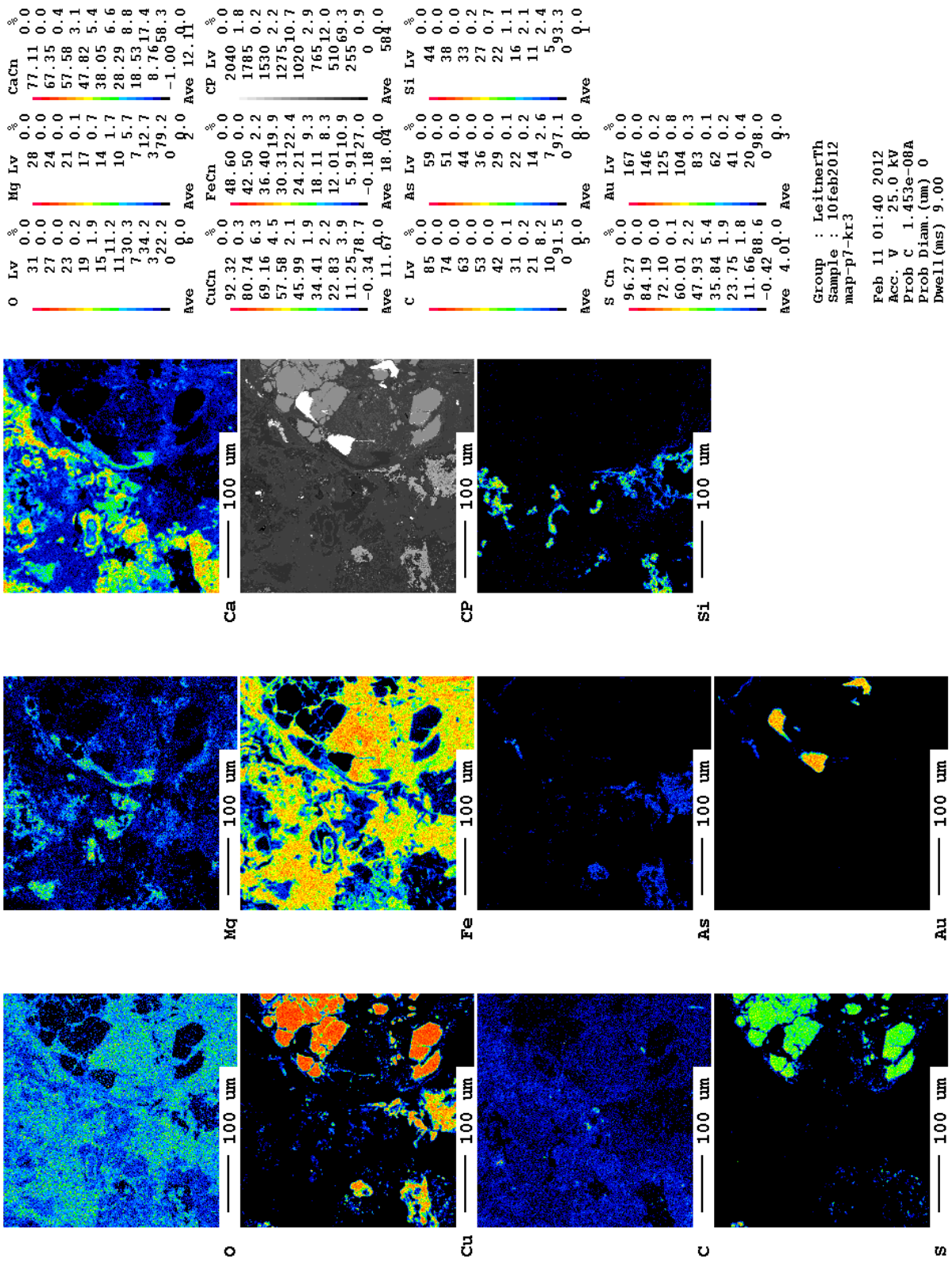

Fig. 83: Element map of a micro-area in sample P.7; Elements analyzed: O, Mg, Ca, Fe, Cu, C, As, Si, Au, S; CP back scattered electron image

Sample 78568

Results of the element mapping of a micro-area in sample 78568 are shown in Fig. 84 (compare with back scatter electron image Fig. 66). It illustrates the elemental distribution within a gold-bearing micro-area and illustrates the complex micro-texture. The variable concentrations of Cu, Fe, As and S reflect the distribution of the main sulfides chalcopyrite, pyrite and arsenopyrite. In addition to two tiny grains of native gold (just outside EMPA mapping area) two small (< 50 µm) grains were detected in which Ag and Au correlate with Bi and S.

These poly-phase grains were identified with WDS measurement as matildite with a low Sb content (see chapter 9.4, Table 18).

The distribution of Ca, Mg and Si reflects the gangue minerals dolomite, calcite and quartz. On the Ca and Mg images the complex intergrowth textures of the two carbonates become visible. In addition to quartz (red-yellow colors on Si image) another silicate phase (blue) might be present; the latter is characterized by very low grey values on the CP (backscattered image) and poor polishing in the microscopic image.

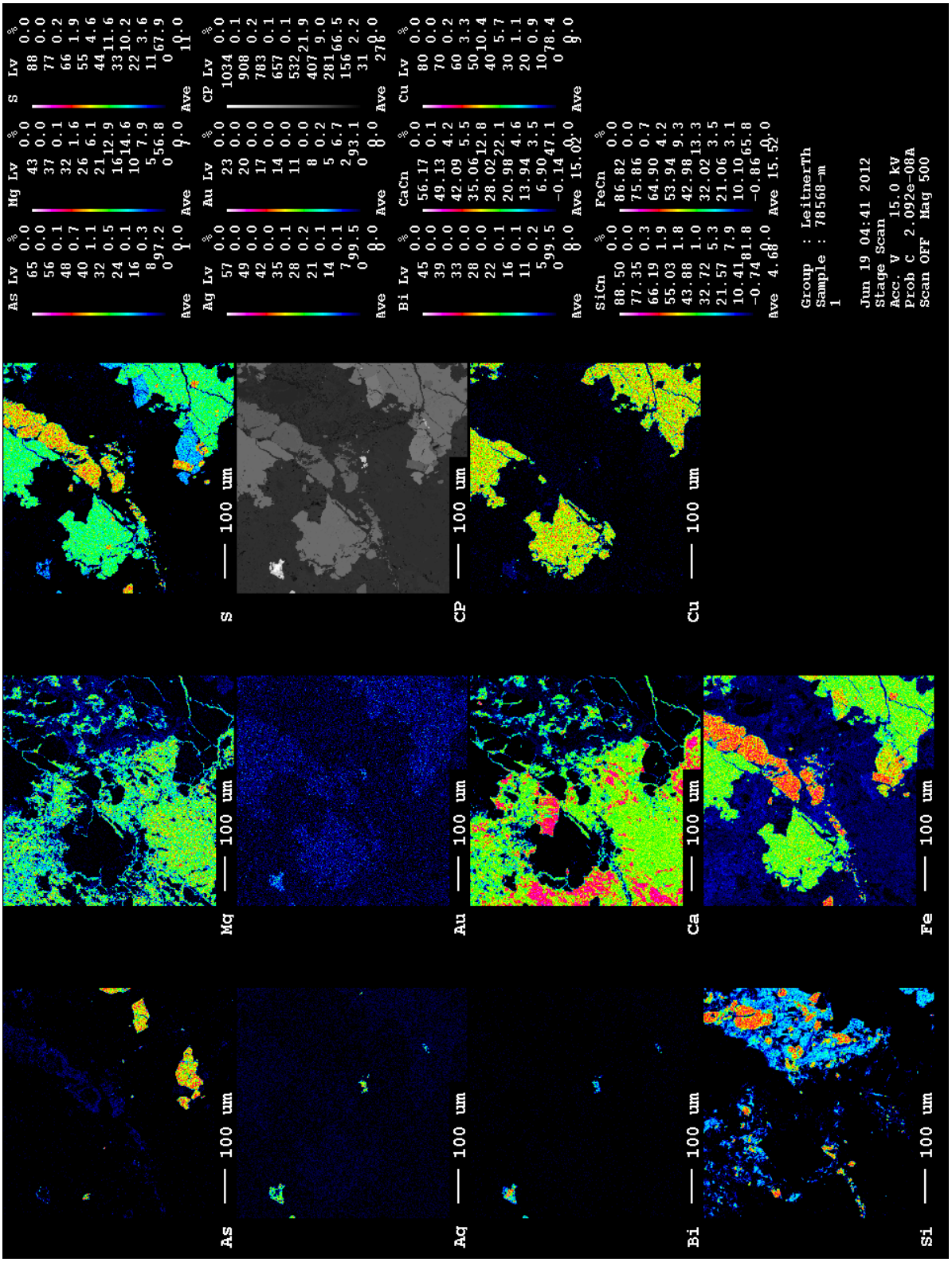

Fig. 84: Element map of a micro-area in sample 78568; Elements analyzed: Mg, Ca, Fe, Si, Cu, Ag, Au, Bi, As, S; CP back scattered image; for explanation see text

10 Raman spectroscopy

This analytical method was mainly used before EMPA measurements for a first quick phase identification. It was also used for the discrimination of optically and chemically similar Cu-rich sulfides and oxides. The spectra of sulfides are of limited value; because these phases are easily damaged by the high energy laser beam strong filters must be used. This has, however the disadvantage that the Raman bands are often too weak and undiagnostic to be useful. An example of a poor spectrum is shown in Fig. 85 for digenite. This phase only has shown a broad peak at ~300 cm^{-1}. The comparison spectrum from the RRUFF database is of the same poor quality. In contrast anilite revealed a spectrum of much better quality. Its major peak at 474.9 cm^{-1}. , but also smaller ones fit very well with the RRUFF data confirming the microscopic and chemical identification of this phase in sample P.7 (Fig. 86).
Phases in strongly oxidized sample P.22 were also measured. The optical identification of these minerals in reflected light was hampered by the small grain size of these minerals. Raman spectroscopy confirmed that hematite and cuprite are important phases in this sample. The major peaks of the cuprite spectra are: 216.9 cm^{-1}, 294.5 cm^{-1}, 414.4 cm^{-1} and 638.4 (Fig. 87). The major peaks of the hematite spectra are: 220.8cm^{-1}, 290.6 cm^{-1}, 403.1 cm^{-1}, 607.3 cm^{-1}, 652.6 cm^{-1} and 1318.4 cm^{-1} (Fig. 88).

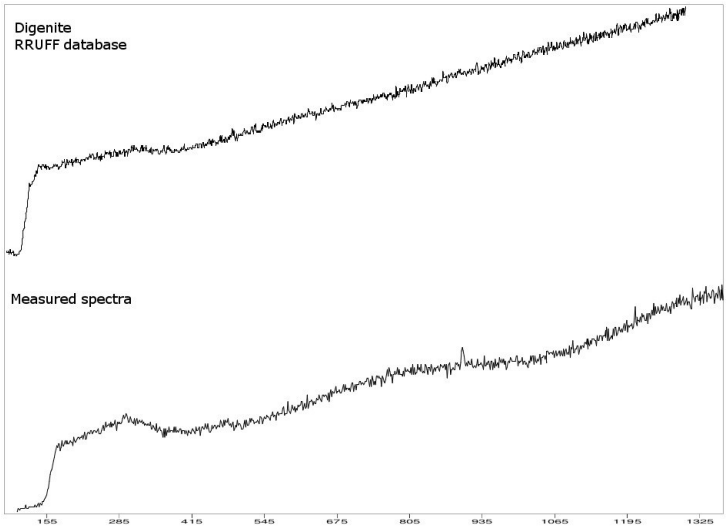

Fig. 85: Laser Raman spectra of digenite´, top: RRUFF database; bottom: measured spectra. Sample P.7

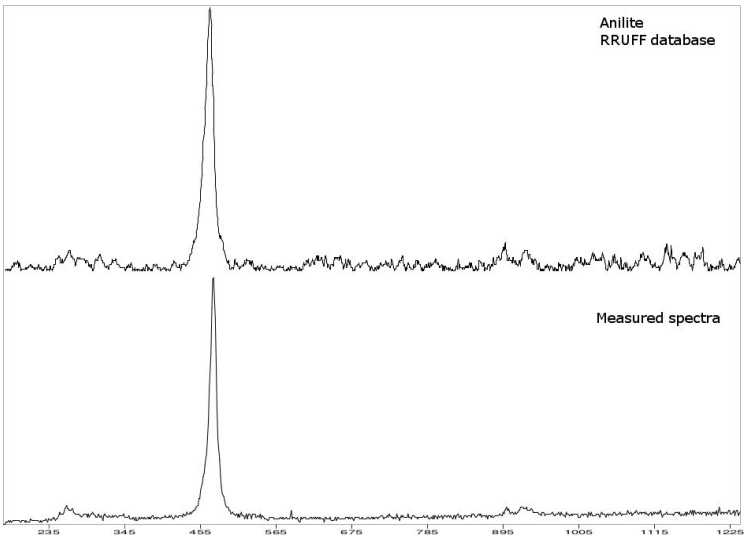

Fig. 86: Laser Raman spectra of anilite, top: RRUFF database; bottom: measured spectra. Sample P.7

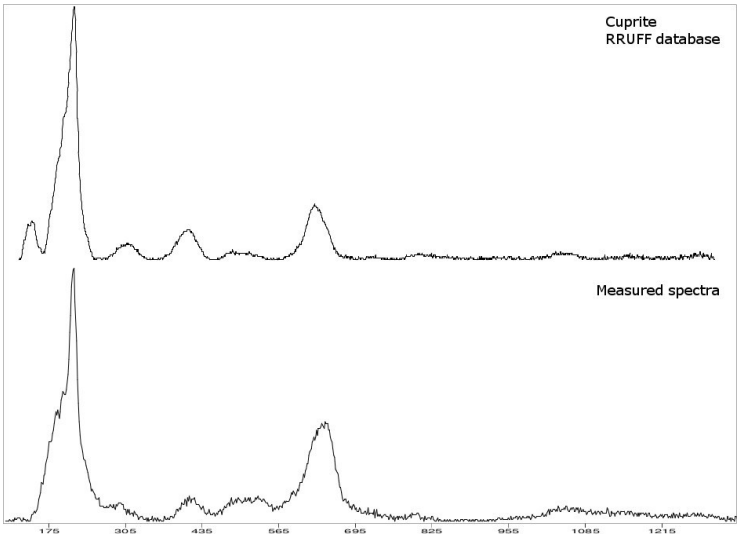

Fig. 87: Laser Raman spectra of cuprite, top: RRUFF database; bottom: measured spectra. Sample P.22

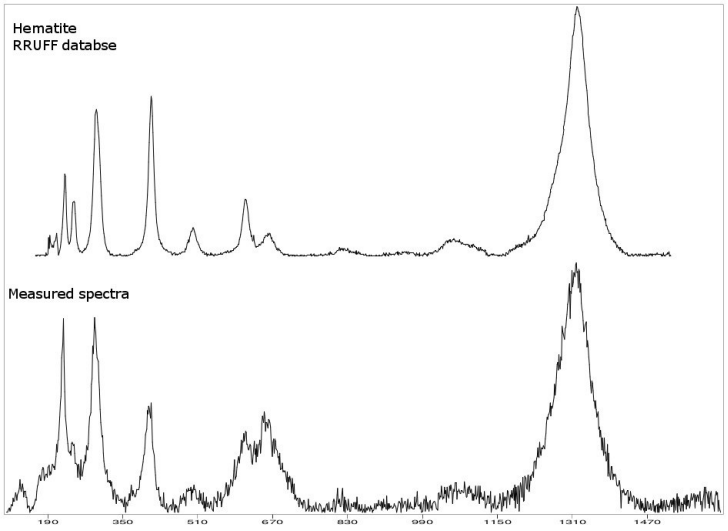

Fig. 88: Laser Raman spectra of hematite, top: RRUFF database; bottom: measured spectra. Sample P.22

11 Discussions

11.1 Deposit type classification

Gold deposits can be subdivided into primary and secondary deposits. Primary gold deposits are genetically related to metamorphic or magmatic hydrothermal fluid systems. Geotectonically, most of these gold deposits are related to convergent plate margins. Secondary gold deposits are formed by weathering and soil formation or as a result of erosion, transport and sedimentation in placers.

The follwing deposit types are distinguished (Pohl, 2011):
Primary deposits:

- Orthomagmatic deposits (with gold as by-product)
- Magmatic-hydrothermal deposits
- Volcanogenic epithermal and hot spring deposits
- Volcanogenic massive sulfide (VMS) and sedex deposits (with gold as by-product)
- Metamorphogenic hyrothermal deposits (including local metamorphic redistribution, concentration, and recrystallization of gold)

Secondary deposits:

- Lateritic gold deposits
- Residual placer deposits
- Colluvial, alluvial and coastal placer deposits

From the geological, mineralogical and chemical characteristics of the studied deposits in the Flatschach area, they are best compared with gold deposits in metamorphic settings, such as orogenic lode gold deposits. According to (Kerrich et al., 2000) the general characteristics of this type of gold deposits are:

- The host rocks are metamorphosed mafic to ultramafic volcanic rocks, intrusive rocks, banded iron formations and greywackes
- The deposits are structurally controlled occurring in ductile to brittle-ductile deformation zones, e.g. strike-slip faults, oblique-slip faults, anticlinal domes
- The mineralization is typically late tectonic and syn- to post-peak metamorphic occurring in veins, breccia zones or of disseminated type
- These deposits are distributed in orogenic belts of great geological complexity and reflect the orogenic evolution
- The alteration assemblages are dominated by quartz, Ca-Fe-Mg carbonates, muscovite, albite, pyrite and tourmaline

- The element associations are characterized by Au, Ag (±As, Sb, Te, W, Mo, Bi, and B) with minor Cu, Pb, Zn and Hg. Antimony and Hg are more common in low temperature deposits. The ratio of Au:Ag is on average 5:1.
- The temperature-pressure conditions of ore formation are between 220 - 500°C and 0.5 - 4kbar. The heat source is either the crust or the mantle.

The ore forming fluids are aqueous - carbonic with low salinity and small contents of H_2S, CH_4, CO_2 and N_2.

Several of these characteristics are in accordance with those documented from the Flatschach area. The host rocks of Cu-Au mineralization are metamorphosed volcano-sedimentary units of the western continuation (Galler Schuppenzone) of the Speik complex and include a sequence of banded biotite gneisses and amphibolites. These rocks derived from intermediate to mafic volcanics, the intercalated garnet-bearing biotite-(muscovite) gneisses and schists from clastic sediments. The historic mining sites are commonly located in areas where banded amphibolites predominate. Strongly serpentinized ultramafic rocks occur as small tectonic relicts within this zone. They can be correlated with the restitic mantle fragments of meta-ophiolites on the Late Proterozoic to Early Palaeozoic (?) Speik complex. Other major lithologies include orthogneisses and granite gneisses. Due to the texture (e.g. coarse-grained feldspar porphyroclasts) and reworked intrusive contacts that can be rarely observed in the field these rocks are interpreted a metagranitoids intruding the older volcano-sedimentary unit. The emplacement age of these metagranitoids is unclear. Some of them are certainly of Variscan age being possible equivalents of widespread Variscan metagranitoids in the Seckau complex. It cannot be excluded, however, that other undated orthogneisses are even older and related to the pre-Variscan orogenic processes.

The Cu-Au mineralization in the Flatschach area is strictly structurally controlled. It is bound to steep dipping NE-SW to NNE-SSW trending quartz-carbonate veins that formed in a brittle to semi-ductile deformation regime (see chapter 5, Fig. 8). The veins are discordant and crosscut the major lithological boundaries and foliations. The mineralized veins show evidence of poly-phase brittle deformation. Cataclastic deformation of sulfides has often been observed in the polished sections; e.g. sulfide grains are rounded and cataclastically fractured and brecciated. Due to the inaccessibility and poor exposure of the mineralized veins in the field the exact nature of the deformation causing these structures is still unknown.

From regional studies it is known that the peak metamorphism reaching amphibolite facies conditions in the study area and the associated ductile deformations are of Eoalpine (Late Cretaceous) age (e.g. see Schuster (2011a)). On the other hand the age of the ore veins

must be older than the coal-bearing sediments of the Neogene Fohnsdorf basin. A Neogene (Late Karpatian to Early Badenian) age has been documented for the sediments of the Fohnsdorf and Ingering formations (Strauss et al., 2001), which overlay the ore veins at the Fortuna Unterbau addit (Jarlowsky, 1951). Hence, these observations constrain the age of the Cu-Au-bearing structures to post-Late Cretaceous and pre-Late Karpatian/Early Badenian. Because the ore veins have not been dated yet, the exact age of the Cu-Au mineralization is, however, still unknown.

Considering the orientation of the ore veins it cannot be excluded that they are related to the Neogene sinistral WSW-ENE Mur-Mürz strike-slip fault system. The mineralized NE-SW oriented veins could be Riedl shear planes to the main fault. However, such a young Neogene age of the mineralization is unlikely because the temperatures in the basin (max. ~ 70°C, sub-bituminous coal) were too low for gold-transporting fluids but also because of the pre-Neogene age of the mineralized structures. Thus, the formation of the Cu-Au veins is more likely related to late orogenic processes; i.e. to structures and metamorpic hydrothermal fluids focused in britte-semiductile structures during the retrograde cooling Stage of Eoalpine metamorphism.

Further arguments for this interpretation come from alteration and element associations. The observed wall-rock alteration is well comparable with that of orogenic type gold deposits. Sericitization and carbonatization are the alteration types observed around the ore veins at Flatschach. In addition to quartz carbonates (calcite, dolomite/ankerite) are also frequent gangue minerals in the veins. The studied element association includes S, As, Cu, Fe, Au, Ag, Bi, ±Hg, ±Co ±Zn, ±Pb. These elements are fixed in various phases depending on the paragenetic Stage. The ratio of Au:Ag of gold from the primary (Stage 1) ore is ~4:1 to 5:1 and is also similar to orogenic lode gold deposits. The common assemblage of native gold with chalcopyrite, arsenopyrite and pyrite, as documented for Stage 1, is quite common in mesothermal deposits.

There are, however, also significant differences to classic orogenic lode gold deposits. In contrast to this group of gold deposits, the mines in the Flatschach area are Cu-dominated. Copper was the main commodity produced during several centuries of historic mining. Though the occurrence of gold and silver has been known for a while, they were to the author's knowledge never mined as by-products. Also the presence of unusual Cu-arsenides like domeykite and associated minerals of Stage 2 is atypical for orogenic gold deposits (see discussion below).

11.2 Mineral Phases and alterations

11.2.1 Temperature constraints and alteration of the Stage 1 assemblage

Stage 1 is deemed as the nearly unaltered primary ore. The main ore minerals of this Stage are arsenopyrite, pyrite and chalcopyrite. Associated minerals are enargite, sphalerite, galena, bornite, alloclasite, native bismuth, matildite and native gold. Stage 1 sulfides are to a variable extent replaced by the younger Stage 2 Cu sulfides; e.g. replacement of chalcopyrite by digenite etc. Enargite and bornite replacing chalcopyrite might mark the beginning of this replacement processes. The gangue minerals in Stage 1 are quartz and calcite. Quartz of Stage 1 often has euhedral morphology and calcite forms large crystals with perfect rhomohedral cleavage. Crystallization of calcite outlasted that of quartz.

Temperature constraints

Only few minerals allow constraining the temperatures of ore formation. The solidification point of native bismuth is ~269°C and it decreases with pressure. Native bismuth crystallizing from a melt phase is characterized by drop-shaped morphology and, when included in other sulfides by concentric radial micro-fracture patterns (Ramdohr, 1960). Unfortunately, bismuth in the samples studied exclusively occurs in the carbonate gangue (formed after quartz) and is not in direct contact with the other ore sulfide phases.

A better temperature constraint comes from the known stability field of matildite (Fig. 89). Matildite is stable below the congruent melting point of 801°C in two modifications (Craig, 1967; Ramdohr, 1960): the cubic high temperature (α), and the hexagonal low temperature (β) modification. α - matildite is stable above of 195°C and coexists with β - matildite between 182°C and 195°C. β - matildite is stable below 183°C. With decreasing temperature α - matildite decomposes to acanthite and β - matildite. The matildite in the studied samples is small in size (~10μm), which makes difficult to find out optically which modification is present. The backscatter electron images do not show exsolution of galena or acanthite and camacitic texture, features which would be typical for the transformation of α to β - matildite (Ramdohr, 1960). This suggests that α - matildite is present in the sample studied and that formation temperatures of matildite plus the associated gold were above 195°C.

Fluid inclusion data, which would allow better constraining the P-T-X conditions of ore formation are not yet available.

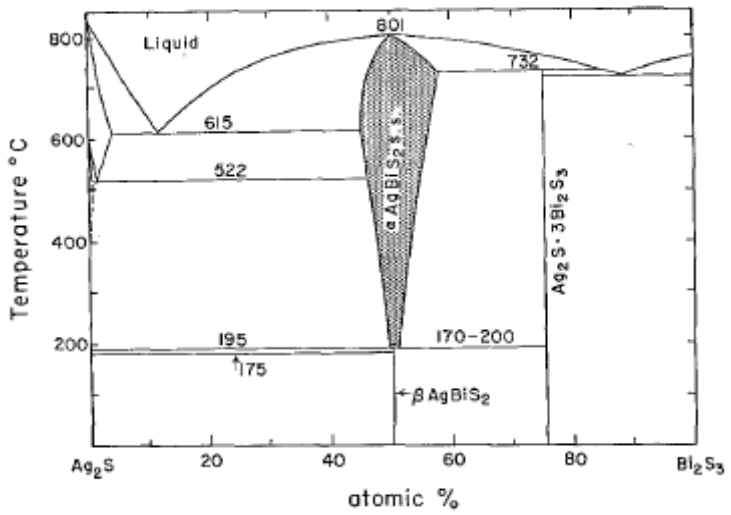

Fig. 89: Temperature - composition diagram of Ag_2S - Bi_2S_3 (after (Craig, 1967))

Wall rock alteration of Stage 1

Most samples studied are polished ore blocks of archive material; they are less suitable for obtaining information on the type of wall rock alteration. The study of alteration was furthermore hampered by the poor outcrop situation in the field and the inaccessibility of mineralization at the historic mine workings.

However, during sampling of the old dumps for an assay on gold contents a larger rather unweathered mineralized block was collected on the dump at Barbarastollen. The petrographic study of a polished thin section of this material allows getting some insight into the alteration related with Stage 1 Cu-(Au)[3] mineralization (see chapter 8.2). Wall rock alteration is characterized by sericite-carbonate-quartz. This is a common alteration assemblage of mesothermal gold deposits and one of the characteristics of orogenic vein-type gold deposits of Phanerozoic age (Kerrich et al., 2000).

11.2.2 Temperature constraints of the Stage 2 assemblage

Stage 2 includes Cu-rich sulfides (digenite, anilite, yarrowite etc.) and arsenides (domeykite, koutekite) as well as native bismuth plus native copper. The common gangue minerals are calcite, dolomite/ankerite and a younger generation of quartz. Gold is part of this paragenetic Stage too. It is associated with the Cu sulfides and native bismuth but mostly inter-grown with the carbonate gangue. Domeykite and koutekite occurring in the same samples with gold have *not* been observed in direct contact with gold. Chalcopyrite and pyrite are relicts of Stage 1 phases. Chalcopyrite is often completely and pyrite is commonly altered to Cu-rich

[3] Gold was not observed in this specific sample; gold values oft the bulk sample were also low, i.e. 3.5 ppm

minerals. Alteration of rare arsenopyrite is not visible. Bismuth sulfosalts become rare in Stage 2 but larger native bismuth aggregates are common. Enargite a rare arsenide in Stage 1 is gone. Domeykite and koutekite become the main Cu-arsenides in Stage 2. The dominant gangue minerals of Stage 2 are carbonates; quartz becomes less important. Partly quartz grains become replaced by carbonates, which is indicated by pseudomorphs of carbonates preserving the euhedral quartz morphology.

The chemical composition of Stage 2 is dominated by the elements Cu-(Fe)-Bi-Au-Ag-(Hg)-As-S. During the transformation of Stage 1 to Stage 2 assemblages ferrous iron, which was fixed in the sulfides pyrite, chalcopyrite and arsenopyrite, becomes oxidized and is incorporated the gangue minerals; i.e. Fe-bearing carbonates and oxides/hydroxides. The gangue carbonates of Stage 2 become richer in Mg and Fe. Because Mg-bearing phases are less common in Stage 1 magnesium could have been transported in the hydrothermal fluid.

The P-T-X conditions at which the Stage 2 assemblages formed are hard to define. It is obvious that Stage 2 assemblages overprint Stage 1 and are therefore relatively younger. However, the formation of the Fe-poor Cu-sulfides and Cu-arsenides could either be the result of low-temperature hydrothermal processes *or* of supergene weathering. Some constraints can be deduced from the experimentally determined stability of Cu-sulfides in the Cu-S system. The corresponding stability diagram after Barton (1973) is shown in Fig. 90. Following this diagram blaubleibender (bb.) covellite is only stable below 157°C. The low-temperature stability limit of digenite + bb. covellite is 76°C, whereas anilite and bb. covellite are stable below 70°C. At higher Cu:S ratio djurleite + anilite are stable at the same temperature.

In the samples studied digenite + bb. covellite but also anilite + bb. covellite were observed as coexisting phases. Djurleite is also present in some samples. The coexistence of digenite + bb. covellite constrains the temperature between 76°C and 157°C. In contrast, the occurrence of djurleite and anilite limit the maximum formation temperature of these assemblage to 70°C. To conclude: Digenite and bb. covellite formed at higher temperatures, whereas anilite + bb. covellite or anilite + djurleite formed later at lower temperatures. A possible interpretation is that these phases are not in equilibrium but rather represent a paragenetic sequence developed during cooling of the hydrothermal system. Alternatively, it could be two distinct Stages, the lower one related to Stage 3 weathering processes.

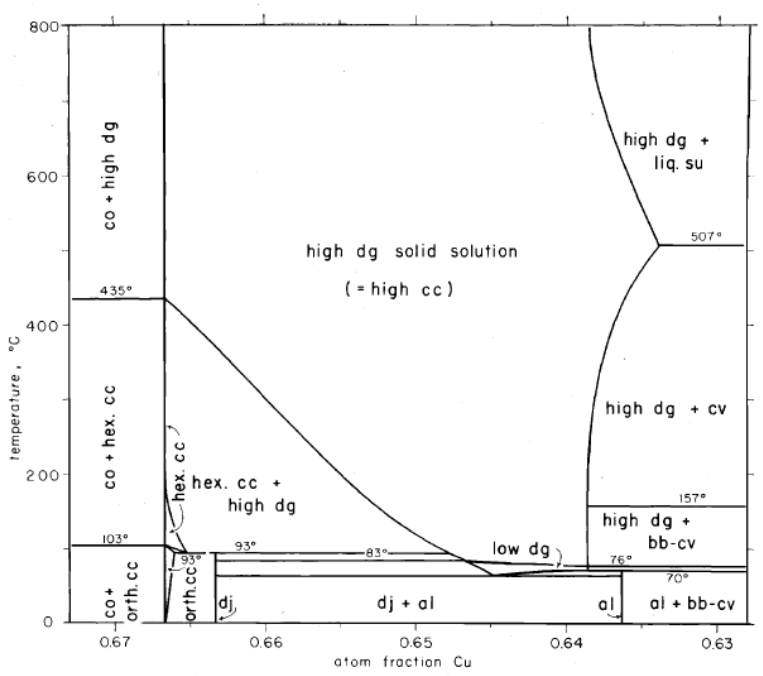

Fig. 90: Temperature - composition diagram of the Cu -S system. al .. anilite, bb-cv … blaubleibender covellite, cc … chalcocite, cv … covellite, co .. copper, dg … digenite, dj … djurleite, su … sulfur; (Barton, 1973)

Skinner and Luce (1971) described the breakdown of α-domeykite to β-domeykite and algodonite at a temperature of 90±10°C. But neither α-domeykite nor algodonite could be confirmed in the studied samples. The chemical composition of the analyzed Cu-arsenides vary between koutekite and β-domeykite with Cu_xAs <3 (Fig. 75).

Domeykite is a quite rare ore mineral. It was reported as an hydrothermal replacement mineral in Cu-ores (Ramdohr, 1960). Other localities for domeykite and koutekite are Langban (Värmland / Sweden) and Lake Superior (Canada).

11.2.3 Temperature constraints of the Stage 3 assemblage

Stage 3 includes Fe- and Cu- oxides, -hydroxides and -carbonates formed during a late lo-temperature oxidation event, likely during supergene weathering. The following minerals are assigned to this Stage: hematite, cuprite, goethite, malachite. These minerals often form fine-grained and poorly crystallized polyphase aggregates. Disequilibrium and reaction textures are commin. There are certainly other not-determined phases present related to this Stage. The following (secondary?) Cu-, Ni- carbonates, sulfates and arsenates were reported from Flatschach area (see mindat.org): annabergite, aragonite (variety) flos flori, azurite, brochantite, devilline, erythrite, malachite, olivenite, posnjakite and tyrolite.

The important processes in Stage 3 are combined strong oxidation and cementation. The matrix of Stage 3 mainly consists of hematite, Fe-hydroxides and less common malachite.

The amount of copper sulfides decreases and bb. covellite is more common. Native Cu is also present in the matrix. The common carbonates of the Stage 2 are mainly gone. Also the Cu-arsenides domeykite and koutekite disappear. Gold is still present in Stage 3 assemblages.

The chemical changes of Stage 3 are marked by a significant increase of ferric iron. The dominant elements in the ore minerals are Fe^{3+}-Cu-Au-Ag-Hg-S. The mineralogy (malachite , Fe-hydroxides etc.) indicate that Stage 3 assemblages formed at low temperatures and we interpret them as products of supergene weathering. The progressive transformation of copper sulfides formed at higher temperatures to lower temperature phases like bb. covellite, anilite, djurleite, native copper etc. can be explained with supergene leaching and cementation processes in the critical zone as schematically illustrated in Fig. 91 (Pohl, 2011)

After (Whiteside and Goble, 1986) chalcocite is a common Cu-sulfide formed in the cementation zone. It reacts to djurleite when affected by highly concentrated leachates such as ferric sulfate $Fe_2(SO_4)_3*H_2O$. At lower concentrations ($<10^{-2}$ mol) isometric chalcocite first transforms into its tetragonal structural type and then into digenite. In the Flatschach samples chalcocite was neither detected microscopically nor by EMPA analyses. Djurleite occurs rarely. The lack of chalcocite and pre-dominance of digenite could therefore indicate an advanced supergene alteration; i.e. nearly complete transformation to digenite The stability of phases like chalcocite will, however, also be influenced by other factors; e.g. presence of additional elements like As in the system, pH value etc.

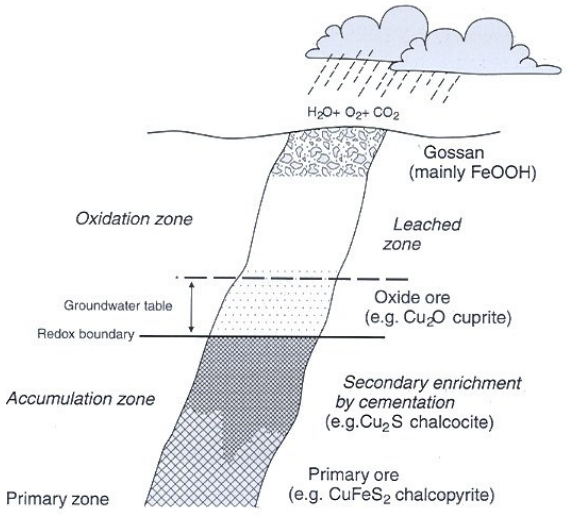

Fig. 91: Schematic illustration of the supergene alteration zones (from (Pohl, 2011)

11.2.4 Sequence of mineralization events

The following sequence of mineralizing events is proposed.

- Stage 1 represents the primary hydrothermal assemblage that formed in metamorphic vein structures at higher (mesothermal?) temperatures above ~200°C. Importantly gold was already part of this assemblage.
- Stage 2 assemblages clearly overprint Stage 1 minerals. Cu-rich sulfides and Cu-arsenides like domeykite and koutekite formed during this Stage. Coexistence of digenite + bb. covellite indicates that *at least part* of this assemblage still formed at temperature conditions (c. 70-160°C) comparable to the lower T range of epithermal deposits. Gold is still present in this Stage.
- Finally, Stage 1 and 2 assemblages are progressively overprinted by low-T assemblages (T<70°C), which are thought to be related to supergene weathering processes. Stage 3 resulted in combined oxidation and cementation processes. Gold is also present in Stage 3.

11.2.5 Characteristics of gold in the three paragenetic Stages

Gold has been reported from all three paragenetic Stages. Stages 1 and 2 are similar regarding grain size and composition of gold. Only minor deviation in Au:Ag values and Hg concentrations are documented. The larger variation in composition and grain size of gold in Stage 1 can be explained with the much larger data set of Stage 1 (more gold grains were found). A possible interpretation for this similarity is that gold found in Stage 2 was “inherited” from Stage 1. Whereas gold in Stage 1 is commonly associated with the sulfides chalcopyrite, arsenopyrite and occasionally pyrite (along grain boundaries, as inclusions, less common in gangue matrix), gold seems to become liberated during transformation of Stage 1 into Stage 2 assemblages. In Stage 2 gold is rather associated with the carbonate gangue phases.

In one case crystallization of Ag-richer rims (electrum) around Ag-poor gold grains was observed in a sample dominated by the Stage 2 assemblage. At present it is unclear at which Stage this Ag-rich gold overgrowths formed.

Stage 3 gold clearly differs from the two other types of gold. It is finer grained (<10 µm) (Fig. 81, Fig. 82) and it is characterized by lower Au:Ag ratios (approximately 1) as well as higher Hg contents. Gold in Stage 3 is interpreted as remobilized gold. During remobilization of gold

under strongly oxidized conditions – likely during supergene weathering – gold obviously became enriched in silver and especially in mercury.

12 Conclusion

- The Cu-(Au) veins in Flatschach area are hosted in metamorphic rocks of the Austroalpine crystalline basement. Formation of discordant minerealized veins post-dates Late Cretaceous peak metamorphism but was prior to the deposition of the coal-bearing Neogene sediments in the Fohnsdorf pull apart basin.
- Three different paragenetic Stages are distinguished. (a) Stage 1 includes Cu-Fe sulfides and arsenides like chalcopyrite, arsenopyrite, pyrite etc. with quartz and calcite as gangue minerals. (b) Stage 2 is rich in Cu-rich sulfides (digenite, bb. covellite) and arsenides (domeykite, koutekite). The gangue phases of this Stage are mainly carbonates (calcite, dolomite/ankerite). (c) Stage 3 includes secondary Fe-(Cu) oxides, -hydroxides, -carbonates etc., which formed during supergene weathering.
- The three Stages correspond to distinct mineralization events starting with metamorphic-hydrothermal ore formation (Stage 1) at mesothermal (?) temperatures above ~200°C. Stage 2 assemblages partly formed during an epithermal overprint (70-160°C) but also include lower temperature (<70°C) assemblages. The latter and the oxidized Stage 3 assemblages are related to supergene processes.
- Gold occurs in all three paragenetic Stages. Gold of Stage 1 and 2 is similar in size and composition but has different liberation characteristics. Gold from Stage 3 is finer-grained and has higher Ag and Hg concentrations. It is interpreted as remobilized gold from the primary ores.
- The historic copper deposits at Flatschach show some similarities to orogenic lode gold deposits in metamorphic terranes elsewhere, but have a predominance of Cu. A further difference is the development of mineralogically unusual Cu-As-S sulfide/arsenide assemblages developped during lower temperature hydrothermal as well as weathering processes.

13 References

Barton, P. B., 1973, Solid solutions in the system Cu-Fe-S, Part I; The Cu-S and Cu-Fe-S joins: Economic Geology, v. 68, p. 455-465.

Becker, P. L., 1979, Geologische Karte der Republik Österreich 1:5000 Erläuterung zu Blatt 162 Köflach: Wien, Geologische Bundesanstalt, 60 p.

Bestel, M., Gawronski, T., Abart, R., and Rhede, D., 2009, Compositional zoning of garnet porphyroblasts from the polymetamorphic Wölz Complex, Eastern Alps: Mineralogy and Petrology, v. 97, p. 173-188.

Boos, R., and Spannraft, H., 1949, Erzgänge Flatschach bei Knittelfeld: Unpublished Staatsprüfungsarbeit thesis, Montanuniversitaet Leoben.

Craig, J., 1967, Phase relations and mineral assemblages in the Ag-Bi-Pb-S system: Mineralium Deposita, v. 1, p. 278-306.

Dal Piaz, G. V., Bistacchi, A., and Massironi, M., 2003, Geological outline of the Alps: Episodes, v. 26, p. 175-180.

Faryad, S. W., Melcher, F., Hoinkes, G., Puhl, J., Meisel, T., and Frank, W., 2002, Relics of eclogite facies metamorphism in the Austroalpine basement, Hochgrössen (Speik complex), Austria: Mineralogy and Petrology, v. 74, p. 49-73.

Flügel, H. W., and Neubauer, F., 1984, Steiermark; Erläuterungen zur Geologischen Karte der Steiermark, 1:200 000: Wien, Geologische Bundesanstalt, 127 p.

Frank, W., Frey, I., and Jung, G., 1981, Strukturgeologische und geochronologische Neuergebnisse aus Stub- und Koralpe., Jahrbuch 1980 Hochschulschwerpunkt, 2: Leoben, p. 11-18.

Friedrich, O. M., 1964, Die Kupfererzgänge von Flatschach bei Knittelfeld: Archiv für Lagerstättenforschung in den Ostalpen, v. 2, p. 34-75.

Jarlowsky, W., 1951, Die Kupfererzgänge von Flatschach bei Knittelfeld: Unpublished doctoral thesis, Montanuniversitaet Leoben, 34 p.

Kerrich, R., Goldfarb, R., Groves, D., Garwin, S., and Jia, Y., 2000, The characteristics, origins, and geodynamic settings of supergiant gold metallogenic provinces: Science in China Series D (Earth Sciences), v. 43, p. 1-68.

Leitner, T., 2011, Geology of the Schönberg and Tremmelberg area: Unpublished report for Noricum Gold Ltd., Montanuniversitaet Leoben, 13 p., Leoben

Leitner, T. and Raith J. G., 2012a, Ore microscopy and microprobe analyses on samples from the Flatschach Cu-(Au) mine - project Schönberg, Austria: Unpublished report for Noricum Gold Ltd., Montanuniversitaet Leoben, 13 p., Leoben

Leitner, T. and Raith J. G., 2012b, Ore microscopy and microprobe analyses of the Jarlowsky (1951) samples - project Schönberg, Austria: Unpublished report for Noricum Gold Ltd., Montanuniversitaet Leoben, 13 p., Leoben

Melcher, F., Meisel, T., Puhl, J., and Koller, F., 2002, Petrogenesis and geotectonic setting of ultramafic rocks in the Eastern Alps: constraints from geochemistry: Lithos, v. 65, p. 69-112.

Neubauer, F., 1988, Bau und Entwicklungsgeschichte des Rennfeld-Mugel- und des Gleinalm-Kristallins (Ostalpen): Unpub. doctural thesis, Universitaet Graz, 137 p.

Neubauer, F., Frisch, W., Schmerold, R., and Schloser, H., 1989, Metamorphosed and dismembred ophiolite suites in the basement units of the Eastern Alps: Tectonophysics, v. 164, p. 49-62.

Paar, W. H., and Meixner, H., 1979, Neues aus den Kupfererz-Gängen des Flatschacher Bergbau-Reviers in Knittelfeld, Steiermark: Der Karinthin, p. 148-150.

Petroff, W., 1943, Wiedergewältigung der alten Kupfererzbaue in Flatschach bei Knittelfeld: Unpublished doctural thesis, Montanuniversitaet Leoben, 41 p.

Pohl, W. L., 2011, Economic Geology, Principles and Practice: Oxford, Wiley-Blackwell, 663 p.

Punzengruber, K., Polegeg, S., and Scherer, J., 1977, Geochemische Untersuchung von Bachsedimenten im Kristallin nördlich von Knittelfeld und ihre Bedeutung für die Lagerstättensuche: Berg- und Hüttenmännische Monatshefte, v. 122, p. 5.

Ramdohr, P., 1960, Die Erzmineralien und ihre Verwachsungen: Berlin, Akademie Verlag, 1277 p.

Rücker, A., 1906, Gutachten über die Bergbaue Zeiring und Flatschach in Obersteiermark: Unpublished report, Vienna, p. 21.

Scharbert, S., 1981, Untersuchungen zum Alter des Seckauer Kristallins: Mitteilungen der Gesellschaft der Geologie- und Bergbaustudenten in Österreich, v. 27, p. 173-188.

Schermaier, A., Haunschmid, B., and Finger, F., 1997, Distribution of Variscan I- and S-type granites in the Eastern Alps: a possible clue to unravel pre-Alpine basement structures: Tectonophysics, v. 272, p. 315-333.

Schmid, S. M., Fügenschuh, B., Kissling, E., and Schuster, R., 2004, Tectonic map and overall architecture of the Alpine orogen: Eclogae Geologicae Helvetiae, v. 97, p. 93-117.

Schuster, R., 2011a, Silvretta - Seckau - Deckensystem, In: Rupp 2011 (Ed.) Erläuterungen - Geologische Karte von Oberösterreich 1:200.000: Wien, Geologische Bundesanstalt, p. 61 - 64.

Schuster, R., 2011b, Koralm-Wölz Deckensystem, In: Rupp 2011 (Ed.) Erläuterungen - Geologische Karte von Oberösterreich 1:200.000: Wien, Geologische Bundesanstalt, p. 64 - 67.

Schuster, R., Scharbert, S., Abart, R., and Frank, W., 2001, Permo-Triassic extension and related HT/LP metamorphism in the Austroalpine -Southalpine realm, Mitteilungen der Gesellschaft der Geologie- und Bergbaustudenten in Österreich, 44: Wien, p. 111-141.

Skinner, B. J., and Luce, F. D., 1971, Stabilities and compositions of alpha-domeykite and algodonite: Economic Geology, v. 66, p. 133-139.

Strauss, P., Wagreich, M., Decker, K., and Sachsenhofer, R., 2001, Tectonics and sedimentation in the Fohnsdorf-Seckau Basin (Miocene, Austria): from a pull-apart basin to a half-graben: International Journal of Earth Sciences, v. 90, p. 549-559.

Tollmann, A., 1977, Geologie von Österreich - Die Zentralalpen Wien, Deuticke, 766 p.

Whiteside, L. S., and Goble, R. J., 1986, Structural and compositional changes in copper sulfide during leaching and dissolution: The Canadian Mineralogist, v. 24, p. 247-258.

14 Acknowledgements

The author acknowledges financial support by Noricum Gold Ltd. and is grateful for the opportunity to have performed this master thesis within the framework of an ongoing exploration project. He especially thanks Univ.Prof. Dr. Werner Paar for providing sample material and polished sections from his collection. Special thanks are also given to members of the Chair of Resource Mineralogy; to my supervisor Univ.Prof. Dr. Johann Raith for his valuable advice and input in writing this thesis, to Ao.Univ.Prof. Dr. Ronald Bakker for his assistance with Laser Raman spectroscopy and to Helmut Mühlhans for sample preparation and his assistance with EMPA analyses. Dr. Bernd Moser and Dr. Hans-Peter Bojar, Universalmuseum Joanneum Graz, are thanked for providing historic sample material from the museum collections. Dr. Ralf Schuster, GBA Vienna, is thanked for his interest and visit to the field area. Ass.Prof. Dr. Heinrich Mali and Dr. Alexander Schmiderer are thanked for the joint visits to the old mining sites in the beginning of the project.

15 Appendix

The appendix are attached as digital data on dvd

A Geological map (map and pdf file)

B Map of chemical analyzes Minerex 1985 (pdf file)

C Outcrop data (pdf file)

D Mineral chemical data (pdf file)